EUROPEAN ORGANISATION FOR NUCLEAR RESEARCH (CERN)

Submitted to: PRD

CERN-EP-2021-249
January 18, 2022

Search for single production of a vector-like T quark decaying into a Higgs boson and top quark with fully hadronic final states using the ATLAS detector

The ATLAS Collaboration

A search is made for a vector-like T quark decaying into a Higgs boson and a top quark in 13 TeV proton–proton collisions using the ATLAS detector at the Large Hadron Collider with a data sample corresponding to an integrated luminosity of 139 fb^{-1}. The Higgs-boson and top-quark candidates are identified in the all-hadronic decay mode, where $H \to b\bar{b}$ and $t \to bW \to bq\bar{q}'$ are reconstructed as large-radius jets. The candidate Higgs boson, top quark, and associated B-hadrons are identified using tagging algorithms. No significant excess is observed above the background, so limits are set on the production cross-section of a singlet T quark at 95% confidence level, depending on the mass, m_T, and coupling, κ_T, of the vector-like T quark to Standard Model particles. In the considered mass range between 1.0 and 2.3 TeV, the upper limit on the allowed coupling values increases with m_T from a minimum value of 0.35 for $1.07 < m_T < 1.4$ TeV to 1.6 for $m_T = 2.3$ TeV.

Contents

1 Introduction

The discovery of the Higgs boson [1, 2] and measurements of the Higgs-boson couplings [3–6] by the ATLAS and CMS collaborations confirm that the Standard Model of particle physics (SM) is an accurate description of nature at currently accessible energy scales. However, the SM still leaves many questions unanswered and is therefore not a complete theory. For example, radiative corrections to the Higgs-boson propagator from top-quark loops lead to a quadratic divergence in the mass of the Higgs boson [7]. The mechanism to cancel out the contribution from the top quark requires an unreasonable degree of fine-tuning to produce the observed 125 GeV Higgs boson. This so-called hierarchy problem is often considered to indicate that new physics naturally cancels out the divergent contributions to the Higgs-boson mass.

Vector-like quarks are hypothetical spin-1/2 particles that arise in various models that address problems in the SM such as the hierarchy problem. Vector-like quarks are color-triplets whose left- and right-handed chiralities transform in the same way under weak-isospin [8, 9]. In Little Higgs [10, 11] and Composite Higgs [12, 13] models, the Higgs boson is naturally light because it is a pseudo Nambu–Goldstone boson arising from a spontaneously broken global symmetry [14]. Vector-like quarks arise naturally in such models. Unlike the chiral current of SM quarks, vector-like quarks have a pure vector current in the Lagrangian. In addition, vector-like quarks do not acquire mass by interacting with the Higgs field, so they are not excluded by measurements of Higgs-boson properties.

In these models, vector-like quarks are expected to couple preferentially to third-generation quarks [8, 15] and can have both neutral-current and charged-current decays. An up-type vector-like T quark with charge $+2/3$ can decay into Wb, Zt, or Ht, while a down-type B quark with charge $-1/3$ can decay into Wt, Zb, or Hb (and the charge conjugate states). To be consistent with results from precision electroweak measurements, the mass-splitting between vector-like quarks belonging to the same SU(2) multiplet should be small [16], preventing cascade decays such as $T \to WB$. Couplings between the vector-like quarks and the first- and second-generation quarks are not excluded [17, 18], but they are expected to be small.

Vector-like quarks can be produced singly or in pairs in proton–proton (pp) collisions. There have been numerous searches for the pair production of vector-like quarks [19–36] that have excluded T-quark masses below 1.37 TeV at 95% confidence level (CL) for a variety of decay modes. For T-quark masses above ∼1 TeV, vector-like quarks would mainly be produced singly if the couplings to SM particles were sufficiently large. Searches for single production of T quarks have placed limits on T-quark production cross-sections for T-quark masses between 1 and 2 TeV at 95% CL for various SM couplings [37–46]. For these higher masses, where single vector-like quark production is expected to dominate [16], the cross-section depends on the vector-like quark mass scale as well as the couplings to SM particles.

This paper reports a search for single production of a singlet vector-like T quark in 13 TeV pp collisions produced at the Large Hadron Collider (LHC) and recorded by the ATLAS detector in a 139 fb^{-1} data sample. The search targets T quarks decaying into a SM Higgs boson and a top quark, $T \to Ht$, where both the Higgs boson and top quark decay hadronically and are reconstructed as jets of particles. A Feynman diagram for this process is shown in Figure 1. The mass, m_T, of the T quark and the overall coupling factor, κ_T, to the SM W boson, Z boson, and Higgs boson [47] are unknown parameters. There are also three additional parameters, ξ_W, ξ_Z, and ξ_H, that determine the T-quark branching ratios. In this analysis, the asymptotic limit of these parameters – as m_T goes to infinity – is assumed, leading to branching ratios of $1/2$, $1/4$, and $1/4$ for $T \to Wb$, $T \to Ht$, and $T \to Zt$, respectively. In this model, the unknown parameters m_T and κ_T define the expected T-quark cross-section and resonance lineshape. The search assumes this signal model in the interpretation of the data.

The T quark is assumed to be a weak singlet state in this analysis; if additional multiplets of vector-like quarks are assumed, the possible final states and branching ratios require an approach involving simultaneous consideration of several final states [16], which is beyond the scope of this paper.

The results reported here significantly extend the sensitivity to events in which a singly produced T quark decays to Ht followed by the hadronic decays $H \to b\bar{b}$ and $t \to bW$. The use of fully hadronic decays allows the direct reconstruction of the T-quark final state, increasing the expected signal-to-background ratio in the signal region defined for the search. The sensitivity is further improved by the larger integrated luminosity used in this search, by using tagging techniques with greater background rejection, and by the development of a data-driven multijet background estimate that reduces the uncertainty in the background modeling.

This fully hadronic final state is of particular interest for vector-like quark masses above 1 TeV. The resulting high-p_{T} jets from the top-quark and Higgs-boson are "boosted", so that the decay products of the top quark and Higgs boson are collimated and captured in two large-radius (large-R) jets. This final state has the largest branching fraction of all the potential Ht decay modes and the large-R jets can be identified as either Higgs-boson or top-quark candidates through tagging algorithms that use the substructure within the jet [48, 49]. In addition, bottom-quark jet identification (b-tagging) provides high background rejection with high efficiency given the three bottom-quark jets coming from the $H \to b\bar{b}$ and $t \to Wb$ decays. Assuming the existence of single T-quark production, the signal would appear as an excess of events with

Ht invariant masses around the T-quark mass for values of $\kappa_T \lesssim 0.5$. Above this κ_T, the Ht invariant mass distribution broadens to masses below the T-quark mass as κ_T increases due to the convolution of increasing width and partonic densities.

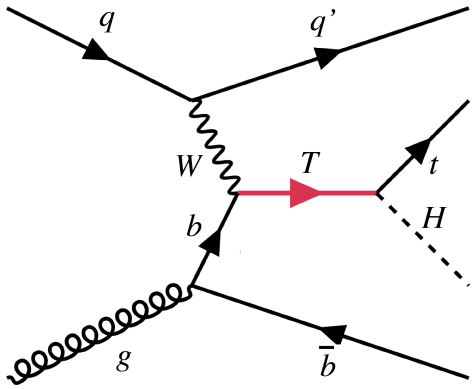

Figure 1: A Feynman diagram illustrating the W-mediated production of a single T quark, shown in red, decaying into a top quark and Higgs boson.

The largest backgrounds come from boosted top-quark pair production and multijet events arising from the production of lighter high-p_{T} quarks (u, d, s, c, and b) and/or gluons. The ATLAS [50–58] and CMS [59–69] collaborations have published measurements of the $t\bar{t}$ differential cross-sections at center-of-mass energies of $\sqrt{s}$ = 7 TeV, 8 TeV, and 13 TeV in pp collisions. The measured cross-section for the production of top quarks with $p_{\mathrm{T}} > 300$ GeV is ~20% lower than predicted by perturbative quantum chromodynamics (QCD) calculations performed at next-to-leading-order (NLO) in the strong coupling constant α_{s}. A control sample of fully reconstructed high-p_{T} top-quark pairs is used with Monte Carlo (MC) models to normalize the expected background from top-quark pairs in the Ht candidate sample. The multijet background is estimated using data-driven techniques developed for studies of events containing boosted top quarks [57].

This paper is organized as follows. Section 2 describes the ATLAS detector and Section 3 describes the datasets and MC samples that are used in this analysis. Section 4 describes the object definition and event selection, while Section 5 summarizes the estimation of SM backgrounds to the T-quark signal. The systematic uncertainties are presented in Section 6 and Section 7 presents the results of the search. Conclusions are drawn in Section 8.

2 ATLAS detector

The ATLAS detector [70] at the LHC is centered on the pp collision point and covers nearly the whole 4π solid angle.[1] It consists of an inner tracking detector surrounded by a 2 T superconducting

[1] ATLAS uses a right-handed coordinate system with its origin at the nominal interaction point (IP) in the center of the detector and the z-axis along the beam pipe. The x-axis points from the IP to the center of the LHC ring, and the y-axis points upwards. Cylindrical coordinates (r, ϕ) are used in the transverse plane, ϕ being the azimuthal angle around the z-axis. The pseudorapidity is defined in terms of the polar angle θ as $\eta = -\ln\tan(\theta/2)$. Angular distance is measured in units of $\Delta R \equiv \sqrt{(\Delta\eta)^2 + (\Delta\phi)^2}$.

solenoid, electromagnetic and hadronic calorimeters, and a muon spectrometer incorporating three large superconducting toroid magnets.

The inner detector, including the insertable B-layer added as a new innermost layer in 2014 [71, 72], provides charged-particle tracking information from a pixel detector and silicon microstrip detector in the pseudorapidity range $|\eta| < 2.5$ and a transition radiation tracker covering $|\eta| < 2.0$.

The calorimeter system covers the pseudorapidity range $|\eta| < 4.9$ and measures the positions and energies of electrons, photons, and charged and neutral hadrons. Within the region $|\eta| < 3.2$, electromagnetic calorimetry is provided by barrel and endcap high-granularity lead and liquid-argon sampling calorimeters. The hadronic sampling calorimeter uses either scintillator tiles or liquid argon as active material and steel, copper or tungsten as absorber.

The muon spectrometer comprises separate trigger and high-precision tracking chambers measuring the tracks of muons in a magnetic field generated by superconducting air-core toroid magnets. The precision chamber system covers the region $|\eta| < 2.7$, while the muon trigger system covers the range $|\eta| < 2.4$.

A two-level trigger system is used to select which events to save for offline analysis [73]. The first level is implemented in hardware/firmware and uses a subset of the detector information to reduce the event rate from the 40 MHz proton bunch crossings to less than 100 kHz. This is followed by a software-based high-level trigger that reduces the event rate to approximately 1 kHz. An extensive software suite [74] is used in the reconstruction and analysis of real and simulated data, in detector operations, and in the trigger and data acquisition systems of the experiment.

3 Data and simulated samples

This analysis studies pp collisions with a center-of-mass energy of $\sqrt{s} = 13$ TeV recorded by the ATLAS detector between 2015 and 2018. Only data-taking periods in which all the subdetectors were operational are considered. The dataset corresponds to an integrated luminosity of 139 fb^{-1} [75], measured using the LUCID-2 detector [76]. The events used in this analysis were collected by a set of triggers requiring at least one anti-k_t jet [77, 78] with a jet radius parameter of $R = 1.0$ [73]. The maximum p_{T} threshold value of these triggers was 480 GeV, which was found to be fully efficient when requiring the offline reconstruction of at least one large-R jet with $p_{\text{T}} > 500$ GeV and $|\eta| < 2.0$, as described in Section 4.

The main backgrounds for this search are from $t\bar{t}$ and multijet events. There are also small contributions from single-top-quark and $t\bar{t}$ + X ($X = W, Z, H$) events. The multijet background is estimated using a data-driven method described in Section 5, while the other backgrounds, as well as the T-quark signal events, are estimated with MC simulations as described below. The multijet background estimate also includes backgrounds arising from electroweak and QCD processes such as W/Z + jets production.

The T-quark signal samples were produced at leading order, using the MadGraph5_aMC@NLO MC generator [79] to generate the hard interaction and the Pythia 8 generator for parton showering and hadronization. The parton distribution function (PDF) set used is NNPDF3.0nlo [80]. Both W-mediated and Z-mediated production contribute to single T-quark production and were included in the MC event generation, with the Z-mediated process having a cross-section five times smaller than the W-mediated process and comprising less than 1% of the total yield after the event selection described in Section 4. The matrix elements were calculated using the phenomenological model given in Ref. [47]. These include all tree-level processes, ensuring the inclusion of both resonant and nonresonant single T-quark

production modes. The decay channel considered is $T \to Ht$, with m_T and κ_T as unknown parameters. The three additional parameters, ξ_W, ξ_Z, and ξ_H, that determine the T-quark branching ratios are set to the asymptotic limit in m_T, leading to branching ratios of 1/2, 1/4, and 1/4 for $T \to Wb$, $T \to Ht$, and $T \to Zt$, respectively. In order to accurately model the change in cross-section and lineshape as m_T and κ_T are varied, MC samples were created for a variety of mass and coupling values, with m_T ranging from 1.0 to 2.3 TeV in steps of 0.1 TeV and κ_T ranging from 0.1 to 1.6 in steps of 0.05 for $\kappa_T < 0.5$ and 0.1 for larger κ_T. All signal samples are normalized to cross-sections that have been calculated at NLO in QCD [81]. These cross-sections are computed in a T-quark narrow-width approximation and a correction factor is applied [82] to account for finite-width effects.

For all MC samples, the masses of the top quark (m_{top}) and Higgs boson were set to 172.5 GeV and 125.0 GeV, respectively. The production of $t\bar{t}$ events was modeled using the POWHEG BOX v2 [83–86] generator. This provides matrix elements at NLO with the NNPDF3.0NLO PDF. In addition, the h_{damp} parameter, which controls the matching of the matrix element to the parton shower in POWHEG and effectively regulates the high-p_{T} radiation against which the $t\bar{t}$ system recoils, was set to $1.5 \times m_{\text{top}}$ [87]. The functional form of the renormalization and factorization scales was set to the default scale $\sqrt{m^2_{\text{top}} + p^2_{T,\text{top}}}$. The PYTHIA 8.230 [88] parton-shower and hadronization models were employed, using a set of tuned parameter values called the A14 tune [89], and the NNPDF2.3LO set of PDFs [90]. The decays of bottom and charm hadrons were simulated using the EVTGEN 1.6.0 program [91].

The $t\bar{t}$ sample is normalized to the cross-section prediction at next-to-next-to-leading order (NNLO) in QCD including the resummation of next-to-next-to-leading logarithmic (NNLL) soft-gluon terms calculated using TOP++ 2.0 [92–98]. For pp collisions at a center-of-mass energy of $\sqrt{s} = 13$ TeV, this cross-section is $\sigma(t\bar{t})_{\text{NNLO+NNLL}} = 832 \pm 51$ fb. The cross-section uncertainties due to the PDF and α_{s} are calculated using the PDF4LHC prescription [99] with the MSTW2008NNLO 68% CL [100, 101], CT10NNLO [102, 103] and NNPDF2.3LO 5f FFN [90] PDF sets, and are added in quadrature to the effect of the scale uncertainty.

The uncertainty due to initial-state radiation (ISR) was estimated by varying the Var3c A14 tune, renormalization scale μ_{r}, factorization scale μ_{f}, and the h_{damp} parameter independently. The Var3c A14 tune variation corresponds to the variation of α_{s} for ISR in the A14 tune. The renormalization scale and factorization scales were varied by factors of 0.5 and 2.0 corresponding to an increase and decrease in ISR, respectively. The h_{damp} uncertainty is measured by comparing the nominal $t\bar{t}$ sample with a sample using $h_{damp} = 3m_{top}$. The impact of final-state radiation (FSR) uncertainties was evaluated by increasing and decreasing the renormalization scale for emissions from the parton shower by a factor of two.

The impact of using a different parton-shower and hadronization model was evaluated by comparing the nominal $t\bar{t}$ sample with a sample that was also generated by POWHEG BOX v2 but used HERWIG 7.1.3 [104, 105] instead of PYTHIA 8.230 for parton showering and hadronization. The HERWIG 7.1 default set of tuned parameters [105, 106] and the MMHT2014LO PDF set [107] were employed.

To assess the uncertainty in the matching of NLO matrix elements to the parton shower, the POWHEG $t\bar{t}$ sample was compared with a sample of events generated with MADGRAPH5_AMC@NLO 2.6.0 but retaining the PYTHIA 8.230 parton-shower and hadronization models. The MADGRAPH5_AMC@NLO calculation used the NNPDF3.0NLO set of PDFs, as in the POWHEG sample, and PYTHIA 8 again used the A14 tune and the NNPDF2.3LO set of PDFs.

The production of a single top quark in association with a W boson (tW) was modeled using the POWHEG BOX v2 generator [84–86, 108] at NLO in QCD with the five-flavor scheme and the NNPDF3.0NLO

set of PDFs. The diagram removal scheme [109] was used to remove interference and overlap with $t\bar{t}$ production.

The Pythia 8.230 parton-shower and hadronization models were employed, using the A14 tune and the NNPDF2.3lo set of PDFs. The inclusive cross-section for tW production was corrected to the theory prediction calculated at NLO in QCD with NNLL soft-gluon corrections [110, 111].

Single-top-quark t-channel production was modeled using the Powheg Box v2 [84–86, 112] generator at NLO in QCD using the four-flavor scheme and the corresponding NNPDF3.0nlo set of PDFs. Parton showering and hadronization were performed with Pythia 8.230, using the A14 tune and the NNPDF2.3lo set of PDFs. The inclusive cross-section was corrected to the theory prediction calculated at NLO in QCD with the Hathor 2.1 generator [113, 114]. Single-top-quark s-channel MC events were not generated because the cross-section for this process is much smaller than that for tW production and the t-channel processes. However, the s-channel process makes a small contribution to the data-driven multijet background estimate and is therefore partially accounted for. The production of SM tH is treated in a similar manner, as the background yield is negligible due to a combination of small cross-section and low yield in the high-p_{T} region.

The production of $t\bar{t}$ in association with a Higgs boson ($t\bar{t}+H$) was modeled by the Powheg Box v2 [83–86, 115] generator at NLO. The production of $t\bar{t}$ in association with a W or Z boson was modeled using the MadGraph5_aMC@NLO 2.3.3 generator at NLO. Parton showering and hadronization for these processes was performed by Pythia 8.210 and the decays of bottom and charm hadrons were simulated using EvtGen 1.2.0. The cross-sections for the $t\bar{t}+W/Z/H$ processes were calculated using MadGraph5_aMC@NLO at NLO QCD and NLO EW accuracies using Ref. [116]. The $t\bar{t}+Z$ cross-section was corrected to take into account contributions from off-shell Z bosons with masses down to 5 GeV. The predicted values of the cross-sections at 13 TeV are $0.88^{+0.09}_{-0.11}$ pb, $0.60^{+0.08}_{-0.07}$ pb, $0.51^{+0.04}_{-0.05}$ pb for $t\bar{t}+Z$, $t\bar{t}+W$, and $t\bar{t}+H$, respectively, where the uncertainties reflect QCD scale variations.

The effect of multiple interactions in the same and neighboring bunch crossings (pileup) was modeled by overlaying the simulated hard-scattering event with inelastic pp events generated with the Pythia 8.186 MC generator [117] using the NNPDF2.3lo set of PDFs and the A3 set of tuned parameters [118].

The detector response was simulated using the Geant4 framework [119, 120], and the data and MC events are reconstructed with the same software algorithms.

4 Object reconstruction and event selection

4.1 Object definition

This analysis makes use of jets, electrons, muons, and event-based quantities formed from their combinations.

Electron candidates are identified from high-quality inner-detector tracks matched to calorimeter energy deposits consistent with an electromagnetic shower [121]. The calorimeter deposits must form a cluster with $E_{\mathrm{T}} > 25$ GeV $|\eta| < 2.47$ and be outside the transition region $1.37 \leq |\eta| \leq 1.52$ between the barrel and endcap calorimeters. A likelihood-based requirement is used to suppress misidentified jets, and calorimeter- and track-based isolation requirements are imposed using the gradient working point [121].

Muon candidates are reconstructed using high-quality inner-detector tracks combined with tracks reconstructed in the muon spectrometer [122]. Only muon candidates with $p_{\mathrm{T}} > 25$ GeV and $|\eta| < 2.5$ are considered. Isolation criteria similar to those used for electrons are used [123]. To reduce the impact of nonprompt leptons, muons within $\Delta R = \sqrt{(\Delta\eta)^2 + (\Delta\phi)^2} = 0.4$ of a jet are removed.

The anti-k_t algorithm implemented in the FastJet package [77, 78] is used to define three types of jets for this analysis: (1) VRTrack jets with a variable-radius parameter with values between $R = 0.02$ and $R = 0.4$ [124], (2) small-R jets with $R = 0.4$, and (3) large-R jets with $R = 1.0$. These are reconstructed independently of each other. The VRTrack jets make use of tracking information from the inner detector, the large-R jets use information from topological clusters [125] in the calorimeter, and the small-R jets use both tracking information and topological clusters [126].

Only jets that have $p_{\mathrm{T}} > 25$ GeV and $|\eta| < 2.5$ are considered. To reduce pileup effects, the jet-vertex tagger (JVT) algorithm [127] is used to reject small-R jets that do not originate from the primary interaction vertex. The primary vertex is selected as the one with the largest Σp_{T}^2, where the sum is over all tracks with transverse momentum $p_{\mathrm{T}} > 0.5$ GeV that are associated with the vertex. This JVT algorithm is applied only to small-R jets with $p_{\mathrm{T}} < 60$ GeV and $|\eta| < 2.4$.

The topological clusters used as input to the small-R and large-R jet reconstruction are calibrated using the local calibration method [128]. The jet energy scale is energy- and η-dependent with calibration factors derived from simulation and in situ measurements [125, 129, 130]. The large-R jet candidates are required to have $|\eta| < 2.0$ and $p_{\mathrm{T}} > 350$ GeV. The η requirement is imposed to optimize the T-quark signal-to-background ratio and to select jets in a kinematic regime where the object tagging is efficient and well-understood. The p_{T} requirement ensures that the large-R jets are sufficiently collimated to contain most of the decay products of the top quark or Higgs boson. A trimming algorithm [131] with parameters $R_{\mathrm{sub}} = 0.2$ and $f_{\mathrm{cut}} = 0.05$ is applied to suppress gluon radiation and further mitigate pileup effects. The small-R jets are used to validate the modeling of large-R jets arising from the $t\bar{t}$ and multijet backgrounds and are not used directly in the event selection. Only small-R jets with $p_{\mathrm{T}} > 25$ GeV and $|\eta| < 2.5$ are considered, so as to match the VRTrack jet candidates.

4.2 Higgs boson, top quark, and b-jet tagging

This analysis searches for Higgs bosons, top quarks, and b-hadron jets (b-jets) to identify T-quark candidates that undergo a $T \to Ht$ decay, followed by $H \to b\bar{b}$, $t \to Wb$, and $W \to q\bar{q}'$ decays. Distinct tagging algorithms are employed to identify these three objects.

Higgs-boson candidates are identified by requiring the large-R jet mass [128] to be between 100 and 140 GeV, along with an upper bound on the jet-substructure variable τ_{21} [132, 133], which is a relative measure of whether the jet has a two-body or one-body structure. The upper bound on τ_{21} is chosen as a function of the jet p_{T} in order to achieve a tagging efficiency of 70% for Higgs bosons, independent of their p_{T}. The tagger provides a rejection factor between five and ten for light-quark and gluon jets.

The top-quark-tagging algorithm uses a deep-neural-network (DNN) scheme [48]. It makes use of jet-substructure variables to discriminate between top-quark jets and jets arising from W, Z, Higgs bosons, gluons, and lighter quarks. An 80% efficiency working point is used, which is defined for all top-quark jets whose decay products are clustered together into the large-R jet. In addition, only jets with a reconstructed mass between 140 and 225 GeV are considered. The orthogonal mass window requirements for tagging

Higgs bosons and top quarks ensure that a jet can only be identified as either a top-quark or Higgs-boson candidate.

The b-tagging algorithm used is known as DL1, a DNN-based tagging scheme that uses the secondary vertex information and the impact parameters of the charged tracks in a VRTrack jet [49]. The working point chosen for this algorithm results in 70% tagging efficiency for b-jets in $t\bar{t}$ events, with a rejection of ~10 and ~400 for charm and light quarks, respectively. This algorithm is applied to all VRTrack jets that have been geometrically matched to the large-R jets by requiring that the jet axes have an $\eta-\phi$ distance $\Delta R < 1.0$.

4.3 Event preselection

A preselection is performed to obtain a sample of candidate signal and background events. Each event is required to have a primary vertex with five or more associated tracks with $p_{\mathrm{T}} > 0.5$ GeV [134].

To identify the fully hadronic Ht decay topology, events must have at least two large-R jets with $p_{\mathrm{T}} > 350$ GeV and $|\eta| < 2.0$. The highest-p_{T} jet is required to have $p_{\mathrm{T}} > 500$ GeV to ensure that the inclusive jet trigger used to record the events has 100% efficiency. The two highest-p_{T} large-R jets are referred to as the leading and second-leading jets. All other large-R jets are ignored. The large-R jets must have a mass between 100 and 225 GeV.

To remove candidates where a $t\bar{t}$ event has resulted in a lepton+jet or dilepton final state, events are rejected if they have an identified electron or muon candidate, as described in Section 4.1.

This preselection defines the data sample used in the T-quark search, which comprises about 4 million events.

4.4 Event classification by tagging states

The leading and second-leading large-R jet candidates are examined to determine if either jet satisfies the Higgs-boson-tagging or top-quark-tagging criteria. In addition, each VRTrack jet contained within a large-R jet is examined to determine if it is b-tagged. In what follows, a b-tagged VRTrack jet associated with a large-R jet is referred to as a b-tag.

With these tagging definitions, the events are classified according to the tagging states of each large-R jet: the jet could be neither Higgs-boson-tagged nor top-quark-tagged, be Higgs-boson-tagged, or be top-quark-tagged. The jet also could have no b-tags, 1 b-tag, or $\geq$2 b-tags. Altogether, a large-R jet could be in one of nine different tagging states, so a 9×9 matrix is defined as shown in Figure 2 to categorize all possible tagging states of the two jets in an event.

Three sets of regions are defined: a signal region SR, a $t\bar{t}$ normalization region NR, and eight validation regions, as illustrated in Figure 2. The signal region consists of those events where one jet is Higgs-boson-tagged with $\geq$2 b-tags and the other jet is top-quark-tagged with $\geq$1 b-tag, and comprises four event-tagging states as illustrated in Figure 2.

The $t\bar{t}$ normalization region is designed to contain the highest-purity sample of $t\bar{t}$ pair events. The four event-tagging states that define this region are those with both large-R jets being top-quark-tagged and each having at least 1 b-tag. Top-quark-tagged jets with $\geq$2 b-tags are included, as these typically result from

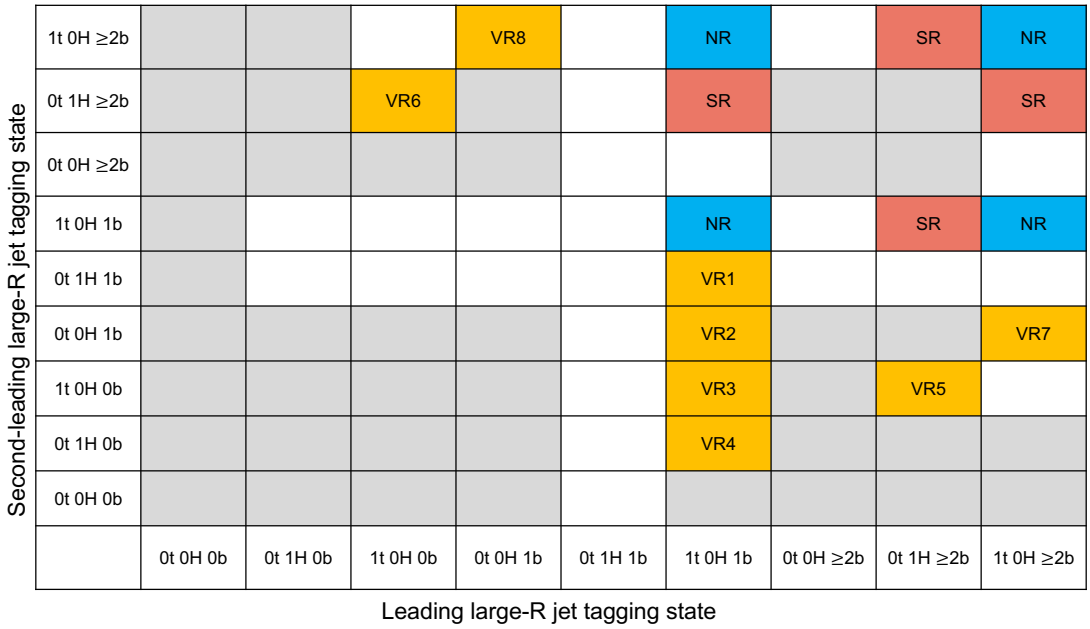

Figure 2: The 9×9 matrix that represents the 81 exclusive event-tagging states defined by the 9 possible tagging states of each large-R jet. Each event can be in only one of the 81 event-tagging states. The red event-tagging states comprise the events in the signal region (*SR*), the blue event-tagging states comprise the $t\bar{t}$ normalization region (*NR*), and the yellow event-tagging states are validation regions labeled *VR*1 through *VR*8. The gray event-tagging states are regions used to estimate the multijet background, as described in Section 5.1.

mistagging a charm-quark jet arising from a $W \rightarrow c\bar{s}$ decay. This region is used to study top-quark-tagging performance and to validate the top-quark acceptance and background estimates.

The validation regions are used to validate the background estimation techniques used in the *SR* and *NR*. The regions with a leading large-R jet top-quark-tagged with 1 b-tag and the second-leading large-R jet not being top-quark-tagged with 1 b-tag (*VR*1 and *VR*2) or the second-leading large-R jet being either Higgs-boson-tagged or top-quark-tagged with no b-jets (*VR*3 and *VR*4) validate the multijet and non-all-hadronic $t\bar{t}$ background estimates. The validation regions defined by the event-tagging states with a Higgs-boson-tagged large-R jet with ≥ 2 b-tags and with the other jet top-quark-tagged with no associated b-tags (*VR*5 and *VR*6) are expected to be dominated by mistagged events and are used to cross-check the mistagging estimates for the Higgs-boson, top-quark, and b-jet tagging schemes. The validation regions defined by one jet that is neither Higgs-boson-tagged nor top-quark-tagged with 1 b-tag and the other jet being top-quark-tagged with ≥ 2 b-tags (*VR*7 and *VR*8) are considered to validate the background modeling involving ≥ 3 b-tags.

5 Background estimation and validation

The two largest contributions to the *SR* and *NR* are multijet events and $t\bar{t}$ production, with smaller contributions arising from events with only one hadronically decaying top quark or from $t\bar{t}$ production in association with a W, Z, or Higgs boson.

The multijet background in all the regions is estimated using a data-driven technique employing sidebands and control regions dominated by multijet events and originally developed to study boosted $t\bar{t}$ production [53, 58, 135]. This background is found to be the largest source of candidate events in the signal region and is determined iteratively, as described in Section 5.1.

The second-largest background in the *SR* consists of events in which a pair of boosted top quarks decay hadronically to produce two top-quark jets. This background is estimated using MC calculations normalized by the event yield in the *NR* after subtracting other backgrounds. As this subtraction requires an estimate of the multijet background, the background-subtracted event yield is determined iteratively, as described in Section 5.2.

The third-largest contribution in the *SR* is from the non-all-hadronic $t\bar{t}$ process where one top quark decayed semileptonically and the other hadronically. In this case, the final-state leptons are not reconstructed or are misidentified and not rejected by the electron and muon veto. The rate of this process, estimated using MC samples, is normalized using the observed $t\bar{t}$ event yield in the *NR*.

Other contributions from SM processes with at least one top-quark jet are estimated using MC samples as described in Section 5.3.

5.1 The data-driven multijet background estimate

The multijet background is estimated by a data-driven method using events from specifically chosen event-tagging states to estimate the multijet background event yields in the signal, normalization, and validation regions. The event-tagging states used are dominated by multijet backgrounds and have small contributions from events with one or more top quarks. Contributions from W/Z+jets are negligible due to a combination of a relatively low cross-section for high-p_{T} hadronically-decaying bosons [136] and the tagging requirements. For a given event-tagging state, the number of events from all MC backgrounds is subtracted from the observed number of events with that event-tagging state. This provides an estimate of the number of multijet events in each event-tagging state. As noted above, the $t\bar{t}$ background subtracted from each region is normalized to the event yield in the *NR* that depends on the multijet estimate in that region. Hence, the multijet background and $t\bar{t}$ yield are calculated iteratively. This procedure is similar to the algorithm used in Ref. [58].

For example, consider the *SR* event-tagging state defined by requiring that the leading jet is top-quark-tagged with 1 b-tag and the second-leading jet is Higgs-boson-tagged with $\geq$2 b-tags. The method uses the numbers of multijet events N_{A}, N_{B}, N_{C}, and N_{D}, after MC background subtraction, in four regions A, B, C, and D. In region A the leading jet is neither top-quark-tagged nor Higgs-boson-tagged with no b-tags and the second-leading jet is neither top-quark-tagged nor Higgs-boson-tagged with no b-tags. In region B the leading jet is neither top-quark-tagged nor Higgs-boson-tagged with no b-tags and the second-leading jet is Higgs-boson-tagged with $\geq$2 b-tags. In region C the leading jet is top-quark-tagged with 1 b-tag and the second-leading jet is neither top-quark-tagged nor Higgs-boson-tagged with no b-tags. In region D, which is one of the *SR* event-tagging states, the leading jet is top-quark-tagged with 1 b-tag and the second-leading jet is Higgs-boson-tagged with $\geq$2 b-tags. If the tagging efficiencies of the two large-R jets are uncorrelated, then the ratio of the numbers of multijet events in two distinct event-tagging states that differ only by the tagging state for one of the large-R jets will be independent of the tagging state of the other large-R jet. In this example, the ratio of N_{D} to N_{C} is equal to the ratio of N_{B} to N_{A} since the ratios

only differ by the tagging state of the leading large-R jet. Hence, the number of multijet events in region D is

$$N_{\mathrm{D}} = \frac{N_{\mathrm{B}} \times N_{\mathrm{C}}}{N_{\mathrm{A}}}.$$

A corresponding method is performed for each of the event-tagging states of the *SR* and *NR*, and for all the validation regions using different event-tagging states to define regions A, B, and C. Since the $t\bar{t}$ background subtraction in regions A, B, and C is normalized to the $t\bar{t}$ event yield in the *NR*, which requires an estimate of the multijet background, the calculation of the multijet background and the $t\bar{t}$ event yield in each region is iterated as described in Section 5.2.

The assumption of uncorrelated jet-tagging states is only approximately true. The level of correlation is determined by examining ratios of the numbers of events with specific event-tagging states that do not overlap with the *SR*, *NR*, or validation regions, shown as the gray event-tagging states in Figure 2. The observed corrections between the jet-tagging states defined by the top-quark, Higgs-boson, and b-tagging criteria are applied to the multijet background estimates for each of the event-tagging states that define the *SR*, *NR*, and the eight validation regions, with the total corrections varying from 1.01 to 1.10 with uncertainties ranging from 0.03 to 0.06. In the calculation of the multijet background for the event-tagging state belonging to the *SR* illustrated above, there are four corrections applied as a product. The multijet estimates are calculated independently for each of the four event-tagging states that make up the *SR* and *NR*, after which they are summed. This provides a fully data-driven multijet background estimate in each region.

For example, to calculate the correlation between the mistagging probabilities when the leading jet is top-quark-tagged and the second-leading jet is Higgs-boson-tagged, the event yields in four regions, E, F, G, and H are considered. In region E the leading jet is neither top-quark-tagged nor Higgs-boson tagged with no b-tags and the second-leading jet is neither top-quark-tagged nor Higgs-boson-tagged with no b-tags. In region F the leading jet is top-quark-tagged with no b-tags and the second-leading jet is neither top-quark-tagged nor Higgs-boson-tagged with no b-tags. In region G the leading jet is neither top-quark-tagged nor Higgs-boson-tagged with no b-tags and the second-leading jet is Higgs-boson-tagged with no b-tags. In region H the leading jet is top-quark-tagged with no b-tags and the second-leading jet is Higgs-boson-tagged with no b-tags. The ratio between the number of events in regions E and F is related to the ratio of events in regions G and H by

$$\frac{N_{\mathrm{E}}}{N_{\mathrm{F}}} = K \frac{N_{\mathrm{G}}}{N_{\mathrm{H}}},$$

where K is the measure of the correlation in mistagging probabilities between the leading jet being top-quark-tagged and the second-leading jet being Higgs-boson-tagged, with both large-R jets having no associated b-tags. The value of K in this example is 0.976 ± 0.004, where the uncertainty is statistical only, and is applied as a correction to the multijet background estimate.

Each correlation is measured in an analogous way using the numbers of events in pairs of event-tagging states. The pairs chosen have MC background contributions less than 8% of the observed event yield, thus reducing the systematic uncertainties arising from the subtraction of the MC background contributions. The multijet background estimate taking into account the tagging correlations is calculated bin-by-bin for each distribution so that the shape of the multijet background distribution is measured as well as the total background event yield.

Since the multijet background depends on the $t\bar{t}$ background subtraction, the two are determined iteratively as described in the next section.

5.2 Top-quark pair yields and multijet backgrounds in the *NR* and *SR*

Previous measurements of the $t\bar{t}$ differential cross-sections for highly boosted top quarks [58] show that the observed cross-section is lower than MC predictions by ∼20%. To avoid the uncertainty this would create in the $t\bar{t}$ background contribution and the multijet estimates in each region, the ratio of the observed rate to the predicted rate of events in the *NR*, α^{norm}, is used to normalize the predicted $t\bar{t}$ background contributions in the *SR*, validation regions, and the event-tagging-states used for the multijet estimate.

The value of α^{norm} is determined after the initial multijet estimate that uses the nominal $t\bar{t}$ prediction by requiring the predicted event yield in the *NR* to match the observed yield. However, the multijet estimate itself is a function of α^{norm}, as the estimation technique described in the previous section requires the subtraction of the $t\bar{t}$ background contribution in the multijet-dominated event-tagging states during its calculation. Thus, both the multijet estimate and α^{norm} are calculated iteratively using

$$\alpha^{\text{norm}}_{n+1} = \frac{N_{\text{Data}} - N_{\text{Multijet}}(\alpha^{\text{norm}}_{n}) - N_{\text{top-related}}}{N_{t\bar{t}\text{MC}}},$$

where α^{norm}_{n} is the value of α^{norm} resulting from the n^{th} iteration, N_{Data} is the observed event yield in the *NR*, $N_{\text{Multijet}}(\alpha^{\text{norm}}_{n})$ is the data-driven multijet background event yield from the n^{th} iteration in the *NR*, $N_{\text{top-related}}$ is the sum of the backgrounds from single-top-quark, $t\bar{t}+W$, $t\bar{t}+Z$, and $t\bar{t}+H$ production that are estimated by MC calculations in the *NR*, and $N_{t\bar{t}\text{MC}}$ is the sum of the $t\bar{t}$ events with all-hadronic and non-all-hadronic decays in the *NR*.

In each iteration of the multijet estimate, $N_{t\bar{t}\text{MC}}$ is scaled by $\alpha^{\text{norm}}_{n+1}$ before subtraction. This calculation converges to subpercent level in four iterations to a value of $\alpha^{\text{norm}} = 0.82 \pm 0.01$, where only statistical uncertainties are considered. This is consistent with cross-section measurements of boosted $t\bar{t}$ production [57]. The $t\bar{t}$ contribution predicted by the MC calculations in the *SR* is scaled by α^{norm}.

The resulting $t\bar{t}$ yield estimates are 8587 ± 1368 events and 174 ± 35 events in the *NR* and *SR*, respectively, where the uncertainties include the systematic uncertainties described in Section 6. This estimate of the $t\bar{t}$ yield in the *NR* is used only for the iterative multijet background estimate.

The multijet yields in the *NR* and *SR* after this iterative calculation are estimated to be 1454 ± 56 and 316 ± 9 events, respectively. The uncertainties in the multijet estimates, including the uncertainties in the tagging correlations, consist of the statistical uncertainties in the event-tagging states used for the calculation and the systematic uncertainties arising from the MC background subtraction, as described in Section 6.

5.3 Other top-quark backgrounds

Single-top-quark production in the Wt final state and the t-channel represent a small contribution to the total background prediction, which is estimated using the Powheg+Pythia8 MC calculation described in Section 3. The s-channel single-top-quark process is not included as an explicit contribution because of its small cross-section and because a part of it is already taken into account in the data-driven multijet estimate.

The uncertainty in the single-top-quark background is increased by 50% to account for the uncertainty in this contribution.

The estimated single-top-quark yields in the $t\bar{t}$ *NR* and *SR* are 120 ± 82 and 8 ± 4 events, respectively.

The backgrounds from production of a top-quark pair in association with a W, Z, or Higgs boson are also estimated using the MC samples described in Section 3. The estimated yields in the *NR* and *SR* are 115 ± 25 events and 9 ± 2 events, respectively.

5.4 Validation of background calculations

Kinematic variables with the ability to distinguish between $t\bar{t}$ and multijet contributions in the *NR* and the validation regions are examined to further validate the background modeling. The potential contribution of T-quark production to these regions is <1%. The distributions of the mass of the leading small-R jet associated with the leading large-R jet events in the *NR* where both large-R jets are top-quark-tagged and have ≥1 b-tags are shown in Figure 3(a). A W-mass peak is observed, which arises when the W-boson decay products are collimated into a small-R jet, along with a low-mass peak arising from light quarks and bottom quarks. A shoulder is seen around the top-quark mass, which arises from a small number of highly boosted top-quark jets where all the decay products of the top quark are clustered into the small-R jet. The observed distribution is well-modeled with a large $t\bar{t}$ contribution and a smaller and featureless multijet distribution. The invariant mass distribution of the leading large-R jet in the same sample, shown in Figure 3(b), confirms the interpretation that this region is dominated by $t\bar{t}$ production.

The distributions of the jet mass for the leading small-R jet associated with the leading large-R jet are shown in Figure 4 for validation regions *VR*1 through *VR*4. The relative sizes of the $t\bar{t}$ and multijet contributions vary between these validation regions, further testing the robustness of their modeling and normalization. There is agreement between the observed and predicted distributions in both normalization and shape.

Further validation of the multijet background estimates is illustrated in Figure 5, where the distributions of the invariant mass of the two leading jets, or dijet system, are shown for the four validation regions dominated by multijet backgrounds. The distributions for events with a top-quark-tagged jet with no b-tags and a Higgs-boson-tagged jet with ≥2 b-tags (*VR*5 and *VR*6) are shown in Figures 5(a) and 5(b), respectively. Distributions for events with a jet with 1 b-tag, but no top-quark or Higgs-boson tag, and another jet with a top-quark tag and ≥2 b-tags (*VR*7 and *VR*8) are shown in Figures 5(c) and 5(d), respectively. There is also agreement between the observed and predicted distributions.

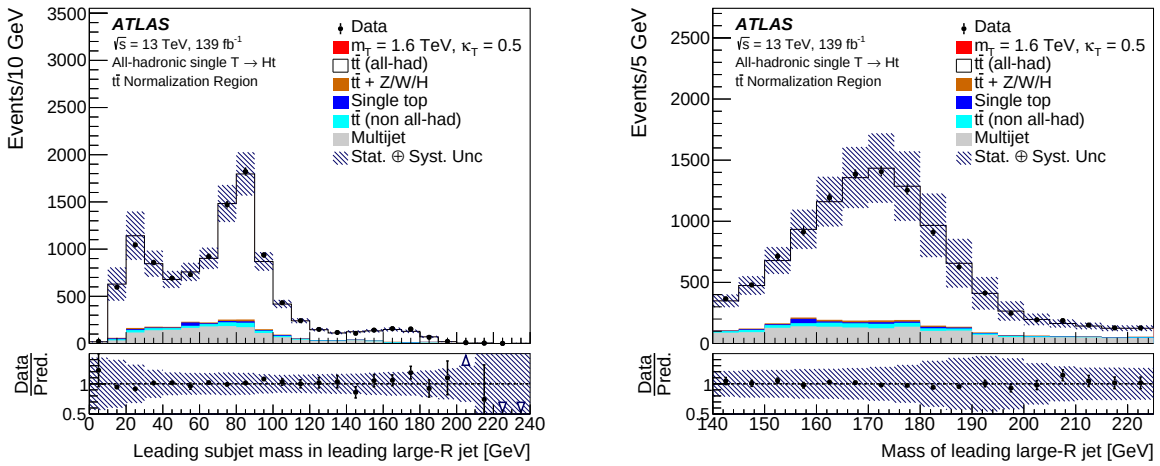

(a) (b)

Figure 3: Invariant mass distributions for (a) the leading small-R jet associated with the leading large-R jet in the $t\bar{t}$ normalization region where both the leading and second-leading large-R jets are top-quark-tagged with at least 1 b-tag, and (b) the leading large-R jet, in the same region. The predicted distributions include the estimated backgrounds and a hypothetical T-quark signal with $m_T = 1.6$ TeV and $\kappa_T = 0.5$. The blue hashed lines correspond to the sum in quadrature of the statistical and systematic uncertainties of the prediction in a given bin. The lower panels show the ratio of the data to the prediction, along with the uncertainty in the ratio. A ratio outside the bounds of the axis is represented by a blue arrow. The last bin includes the event overflows. Contributions to the predicted yield are stacked in the same order as they appear in the legend.

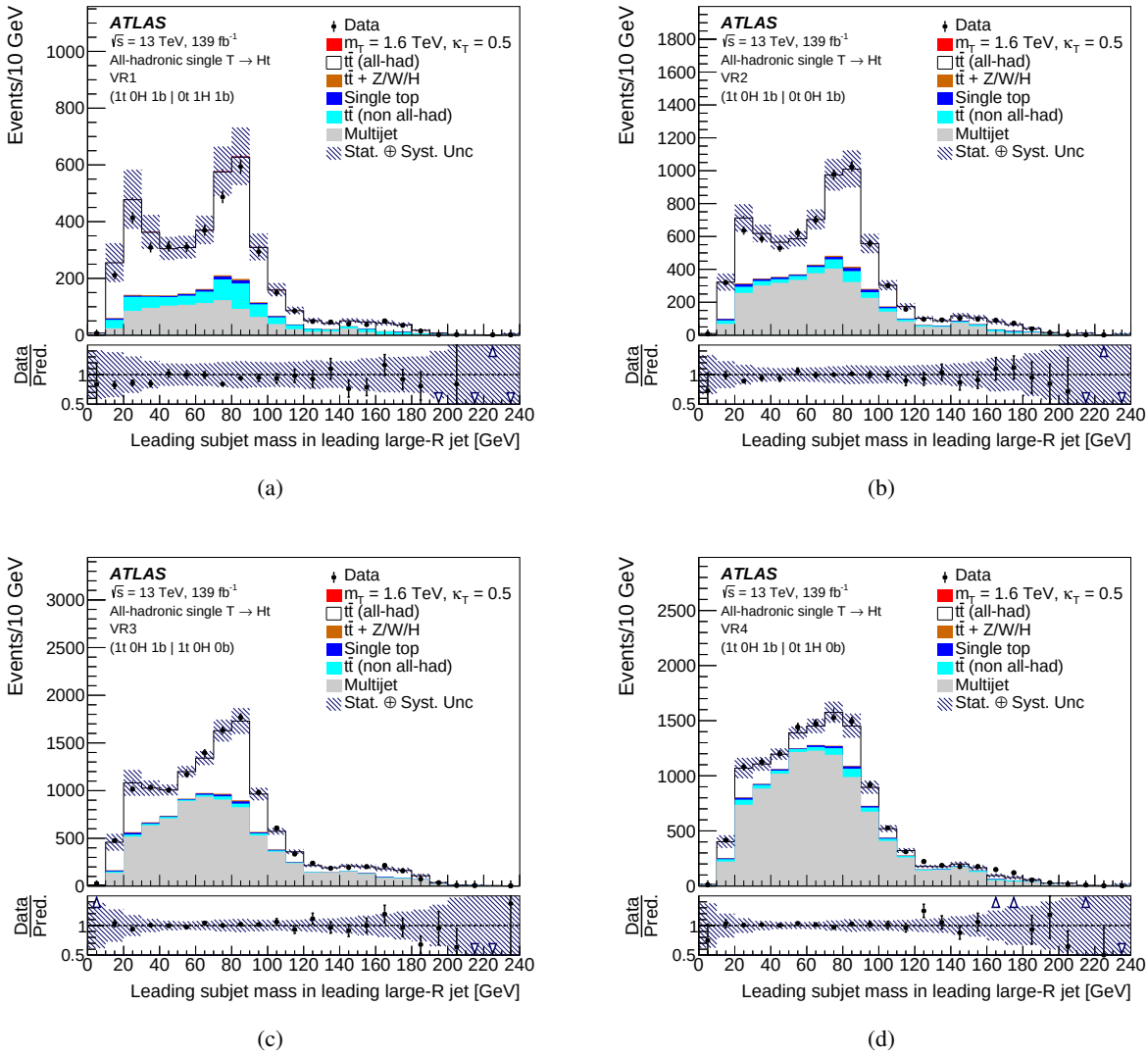

Figure 4: Invariant mass distributions for the leading small-R jet associated with the leading large-R jet for (a) $VR1$ defined by requiring the leading large-R jet be top-quark-tagged with 1 b-tag and the second-leading jet is Higgs-boson-tagged with 1 b-tag, (b) $VR2$ defined by requiring the leading large-R jet be top-quark-tagged with 1 b-tag and the second-leading jet is neither Higgs-boson-tagged nor top-quark-tagged with 1 b-tag, (c) $VR3$ defined by requiring the leading large-R jet be top-quark-tagged with 1 b-tag and the second-leading jet is top-quark-tagged with no b-tag, and (d) $VR4$ defined by requiring the leading large-R jet be top-quark-tagged with 1 b-tag and the second-leading jet is Higgs-boson-tagged with no b-tag. The predicted distribution includes the estimated backgrounds and a hypothetical T-quark signal with $m_T = 1.6$ TeV and $\kappa_T = 0.5$. The blue hashed lines correspond to the sum in quadrature of the statistical and systematic uncertainties of the prediction in a given bin. The lower panels show the ratio of the data to the prediction, along with the uncertainty in the ratio. A ratio outside the bounds of the axis is represented by a blue arrow. The last bin includes the event overflows. Contributions to the predicted yield are stacked in the same order as they appear in the legend.

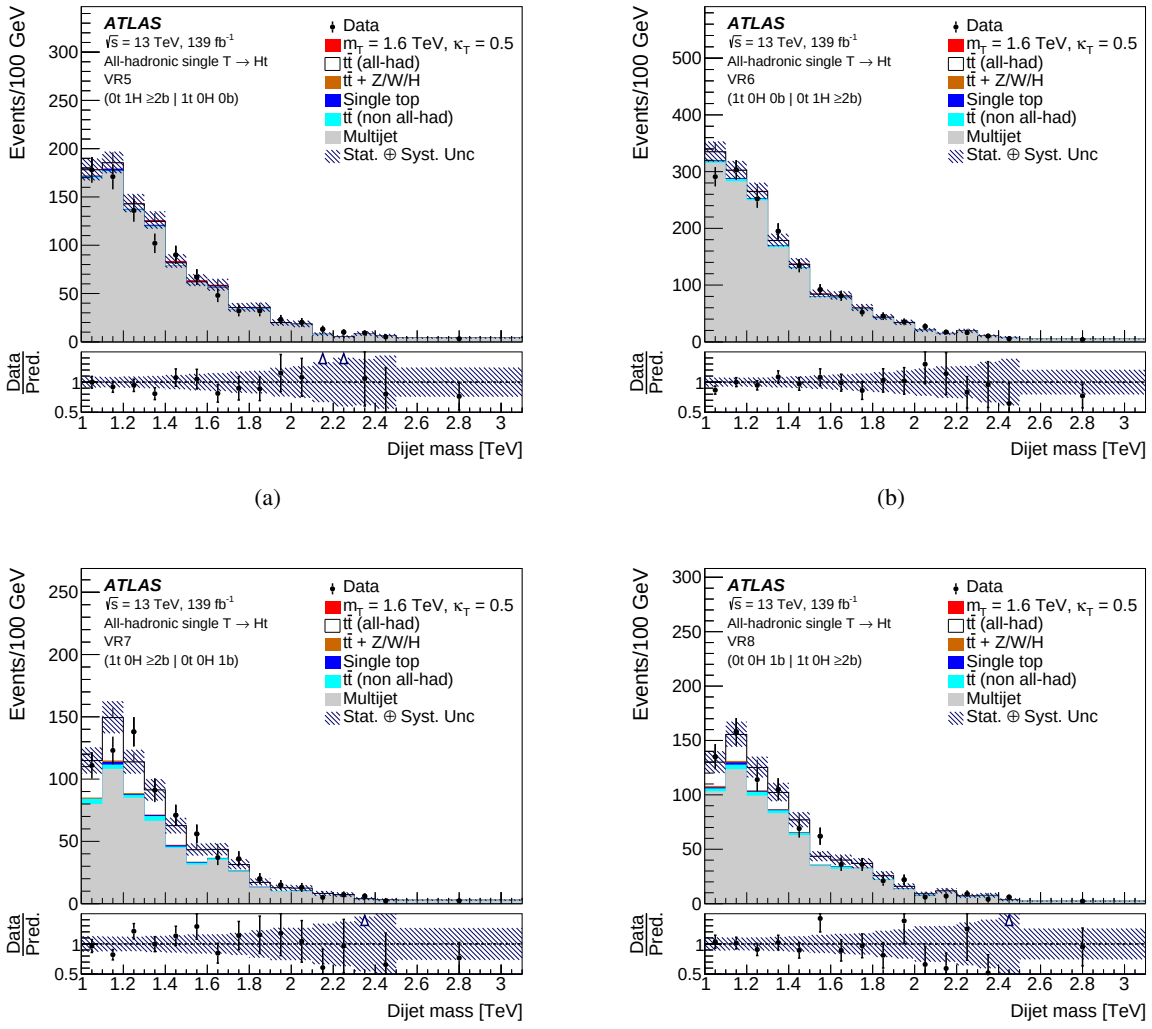

Figure 5: Dijet invariant mass distributions for the two large-R jets in four validation regions: (a) $VR5$ defined by requiring a leading jet Higgs-boson-tagged with ≥ 2 b-tags and second-leading jet top-quark-tagged with no associated b-tag, (b) $VR6$ defined by requiring a leading jet top-quark-tagged with no associated b-tag and second-leading jet Higgs-boson-tagged with ≥ 2 b-tags, (c) $VR7$ defined by requiring a leading jet top-quark-tagged with ≥ 2 b-tags and second-leading jet neither top-quark-tagged nor Higgs-boson-tagged with 1 b-tag, and (d) $VR8$ defined by requiring a leading jet neither top-quark-tagged nor Higgs-boson-tagged with 1 b-tag and second-leading jet top-quark-tagged with ≥ 2 b-tags. The predicted distributions include the estimated backgrounds and a hypothetical T-quark signal with $m_T = 1.6$ TeV and $\kappa_T = 0.5$. The blue hashed lines correspond to the sum in quadrature of the statistical and systematic uncertainties of the prediction in a given bin. The lower panels show the ratio of the data to the prediction, along with the uncertainty in the ratio. A ratio outside the bounds of the axis is represented by a blue arrow. The last bin includes the event overflows. Contributions to the predicted yield are stacked in the same order as they appear in the legend.

6 Systematic uncertainties

Systematic uncertainties that affect the interpretation of the data are estimated using data and MC samples. Variations corresponding to a $+1\sigma$ and -1σ confidence interval are derived for each uncertainty.

These systematic uncertainties are broken down into detector-related and modeling uncertainties. They do not have a significant dependence on the choice of T-quark mass and coupling, so an example of the size of the systematic uncertainties arising from the likelihood fit described in Section 7 (the "post-fit" results) is provided in Table 1 for $m_T = 1.6$ TeV and $\kappa_T = 0.5$.

6.1 Detector-related uncertainties

The most significant detector-related systematic uncertainties arise from the measurements of jet properties and tagging efficiencies.

Uncertainties associated with the large-R jets arise from the jet energy scale (JES), jet mass scale (JMS), jet mass response (JMR), jet energy resolution (JER), and the JVT requirement. The uncertainties in the JES, JMS, and JMR are evaluated by using in situ measurements [125]. The JES is measured in events where a large-R jet recoils against well-defined reference objects (photons, Z bosons, or calibrated small-R jets). The JMS and JMR uncertainties are measured using both a double-ratio method that compares the calorimeter-to-tracker response ratio between data and simulation [125] and a fit to the W-boson mass peak in high-p_{T} lepton+jets $t\bar{t}$ events. The JER uncertainty is measured by studying dijet mass resolution and the effect of energy flow near the jet radius [128]. The JVT uncertainty arises from the correction factors used to match the efficiencies in the MC samples to data.

The efficiency for tagging b-jets is measured in data using dilepton $t\bar{t}$ events [49]. Correction factors are applied to the jets in the MC sample so that the b-jet tagging efficiency as a function of jet p_{T} in MC events matches that in data events. Uncertainties arising in the evaluation of the efficiencies are propagated to the correction factors. The largest source of b-jet tagging uncertainty is the extrapolation of tagging efficiencies to b-jets with $p_{\mathrm{T}} > 300$ GeV, as b-jet tagging calibrations use data with $p_{\mathrm{T}} < 300$ GeV.

The efficiency and rejection power of the DNN top-quark tagger is measured in data and correction factors are applied to MC events to match the measured efficiencies [137]. These corrections take into account the correlations between the tagging efficiencies and other jet observables such as the jet energy and mass. The uncertainties in these corrections are treated as systematic uncertainties.

The efficiency of the τ_{21} requirement used for the Higgs-boson tagger is measured using the calorimeter-to-tracker response double-ratio method [125]. The corresponding uncertainty, which is approximately 2%, is included in the uncertainty of the Higgs-boson-tagger efficiency.

The relative uncertainty in the integrated luminosity is determined to be 1.7% [75], obtained using the LUCID-2 detector [76] for the primary luminosity measurements.

6.2 Modeling and background uncertainties

The most significant modeling uncertainties arise from the MC calculations of the $t\bar{t}$ production process and decay into the all-hadronic final states, the modeling of the non-all-hadronic $t\bar{t}$ background, the cross-sections for processes producing smaller backgrounds involving at least one top quark, and the multijet background estimates.

The $t\bar{t}$ background estimate has systematic uncertainties from initial/final-state radiation (ISR/FSR), the renormalization scale, factorization scale, PDF, parton-shower algorithm, matrix-element calculation, and h_{damp} parameter value. The effects of ISR/FSR, renormalization scale, and factorization scale uncertainties are evaluated using the method described in Section 3. The PDF uncertainties are evaluated by use of the PDF4LHC15 Hessian uncertainties, where the 30 variations are combined into one nuisance parameter. Uncertainties arising from the choice of parton-shower and hadronization algorithms are evaluated by comparing the nominal POWHEG+PYTHIA8 sample with the POWHEG+HERWIG sample. The uncertainty arising from the matrix-element calculation is assessed by comparing the nominal MC sample with the MADGRAPH5_AMC@NLO+PYTHIA8 sample.

Although the non-all-hadronic $t\bar{t}$ background is relatively small in the *SR* and *NR*, a 5% excess of predicted events relative to the data is observed in *VR*1 defined by the event-tagging state with the leading large-*R* jet top-quark-tagged with 1 *b*-tag and the second-leading jet Higgs-boson-tagged with 1 *b*-tag. This validation region is estimated to have a non-all-hadronic $t\bar{t}$ background fraction of approximately 15% and it is possible that the observed excess is due to mismodeling of this background. A conservative uncertainty of 60%, which covers the excess if it is attributed entirely to the non-all-hadronic $t\bar{t}$ background, is applied to the size of this background in the *SR* and *NR*.

The uncertainty in the multijet background estimate is approximately 5%, as described in Section 5.2. The uncertainty in the predicted single-top-quark background estimate is 3.3% while the uncertainty in the predicted $t\bar{t} + W/Z/H$ background estimate is 20%, as described in Section 5.3.

7 Results

The dijet invariant mass formed from the tagged large-*R* jets is interpreted as a combination of the expected SM backgrounds and a *T*-quark signal. The dijet mass in the *SR* is the invariant mass of the Higgs-boson and top-quark candidates while in the *NR* it is the invariant mass of the two top-quark candidates. The dijet invariant mass distributions for the *SR* and *NR* are shown in Figure 6, assuming a *T*-quark signal contribution with $m_T = 1.6$ TeV and $\kappa_T = 0.5$ scaled to the theory cross-section of 41 fb. The overall acceptance times efficiency of *T*-quark detection in the all-hadronc final state is 1.6% for this choice of mass and couplings, taking into account the kinematic requirements and tagging efficiencies. The predicted background rates and shapes are in good agreement with the observed distributions.

The dijet mass is used as a discriminant in the *SR* and *NR* to test for the presence of a *T*-quark signal. Two parameters of interest are defined: σ_{obs}, the observed cross-section for single production of a *T*-quark, and α^{fit}, the *SR* and *NR* $t\bar{t}$ background normalization.

A binned-likelihood fit is performed in which a *T*-quark signal and the background model is fitted to the *SR* dijet mass distribution and simultaneously the *NR* background model is fitted to the *NR* dijet mass distribution. The fit is performed for events with a dijet mass greater than 1 TeV. The fit model in the *SR* is the sum of the background distributions and a *T*-quark signal distribution with a given mass, coupling, and

Table 1: Size of the post-fit uncertainties in the T-quark signal cross-section for a T-quark mass of 1.6 TeV and coupling $\kappa_T = 0.5$. The fitted cross-section is -10 fb and is consistent with zero. The background uncertainty is the sum in quadrature of the systematic uncertainty on the multijet background and the statistical uncertainties on the MC-derived backgrounds. The total uncertainty of 25 fb is the sum in quadrature of the total systematic uncertainty and statistical uncertainty. The uncertainty arising from simultaneously fitting the $t\bar{t}$ normalization factor is included in the total systematic uncertainty. The individual uncertainties do not add up in quadrature to the total uncertainty because of their correlations in the fit.

Category	Uncertainty in $\sigma\ (pp \to T + X \to Ht + X)$ [fb]
Detector Uncertainties	
b-jet tagging	6.2
Top-quark jet tagging	6.0
Jet mass resolution	3.0
Jet mass scale	2.3
Jet energy scale	1.9
Jet energy resolution	1.5
Higgs-boson tagging	1.6
Other detector uncertainties	0.4
Modeling Uncertainties	
Other $t\bar{t}$ modeling uncertainties	5.0
$t\bar{t}$ parton shower and hadronization	2.0
$t\bar{t}$ matrix element	2.4
Background uncertainty	6.7
Signal MC statistical uncertainty	4.9
$t\bar{t}$ normalization (α^{fit})	1.3
Other top-quark-background theory uncertainties	0.5
Total Uncertainties	
Total statistical uncertainty	19
Total systematic uncertainty	15
Total uncertainty	25

signal cross-section σ_{obs}. In the *NR* the very small contribution from the T-quark signal is neglected. The signal cross-section is allowed to take negative values in the fit whereas α^{fit} is constrained to be positive. The fit of the $t\bar{t}$ background in the *NR* and *SR* measures α^{fit} using both regions and thus provides a scaled $t\bar{t}$ background contribution in the *SR*.

The fit incorporates the systematic uncertainties as Gaussian nuisance parameters. Additional bin-by-bin uncertainties are included to account for the statistical uncertainties in the predicted multijet and MC backgrounds. The $t\bar{t}$ contributions to the *NR* and *SR* are fully correlated in the fit. The likelihood is then profiled [138] as a function of each nuisance parameter and used as the test statistic to determine the statistical significance of the fit results.

Figure 7 shows the dijet mass distributions for the *SR* and *NR* after the fit (post-fit) assuming a signal hypothesis with $m_T = 1.6$ TeV and $\kappa_T = 0.5$. The observed and predicted event yields in the *NR* and *SR* are given in Table 2. The fitted value of $\alpha^{\text{fit}} = 0.78 \pm 0.11$ is consistent with the $t\bar{t}$ normalization factor $\alpha^{\text{norm}} = 0.82 \pm 0.01$ determined from the background-subtracted event yield in the *NR* (the uncertainty on α^{norm} is statistical only). There is good agreement between the predicted post-fit signal region background

Table 2: The event yields are shown for the $t\bar{t}$ normalization region and for the signal region after the likelihood fit (post-fit). The requirement of the Ht invariant mass being greater than 1 TeV has been imposed on the signal region. The post-fit yields incorporate the statistical, detector, and modeling uncertainties as well as their correlations.

Region	$t\bar{t}$ Normalization Post-Fit		Ht Signal Region Post-Fit	
$t\bar{t}$ all-hadronic	8347	± 220	147	± 17
$t\bar{t}$ non-all-hadronic	191	± 134	14	± 10
Single top-quark	112	± 70	8	± 4
$t\bar{t}$+$W/Z/H$	117	± 24	9	± 2
Multijet events	1454	± 56	316	± 9
Signal events (m_T = 1.6 TeV, κ_T = 0.5)			−9	± 21
Predicted background	10 221	± 154	494	± 22
Data (139 fb^{-1})	10 231		471	

yield of 494 ± 22 events and the observed yield of 471 events, consistent with no significant excess in data above SM backgrounds over the entire Ht invariant mass distribution as seen in Figure 7(a). The fit of the m_T = 1.6 TeV and κ_T = 0.5 signal hypothesis results in $\sigma(pp \to T + X \to Ht + X) = -10 \pm 25$ fb, further confirming no excess of events at Ht masses around 1.6 TeV.

Similarly, fit results with T-quark cross-sections consistent with zero are obtained for T-quark masses between 1.0 and 2.3 TeV and for κ_T values from 0.1 to 1.6. Based on these fit results, for $1.0 < m_T < 2.3$ TeV there is no significant evidence of a T quark decaying to the Ht final state.

The fit results are used to set 95% CL upper limits on the single-T-quark production cross-section for $1.0 < m_T < 2.3$ TeV and $0.1 < \kappa_T < 1.6$ using the CL_s method [139]. The predicted cross-sections assume a singlet T quark with a $T \to Ht$ branching fraction of 1/4. Figure 8 shows the 95% CL upper limits as a function of m_T for different values of κ_T. The cross-section limits range from ~10 fb to ~200 fb, depending on κ_T. The decrease in sensitivity for masses from 1.0 to 1.2 TeV arises from the change in signal shape due to the p_T requirements on the Higgs-boson and top-quark candidate jets. The p_T requirements shape the distribution to peak at roughly 1.2 TeV, which can be seen in Figures 6 and 7. Figure 9 shows the exclusion limits as a function of m_T and κ_T. Figure 10 shows the observed and expected 95% CL limits on the T-quark mass as a function of the T-quark width-to-mass ratio Γ/m_T and the branching fraction for T-quark decay into a Higgs boson and a top quark.

For the considered mass range of 1.0 to 2.3 TeV the upper limit on allowed values of κ_T rises from a minimum value of 0.3 starting at m_T = 1.1 TeV, up to 1.6 for m_T = 2.3 TeV.

At 95% CL, this analysis excludes T quarks with $\Gamma/m_T \geq 0.05$ for $1.05 < m_T < 1.2$ TeV, with the mass limits rising with Γ/m_T to exclude $m_T < 1.7$ TeV for $\Gamma/m_T \geq 0.5$.

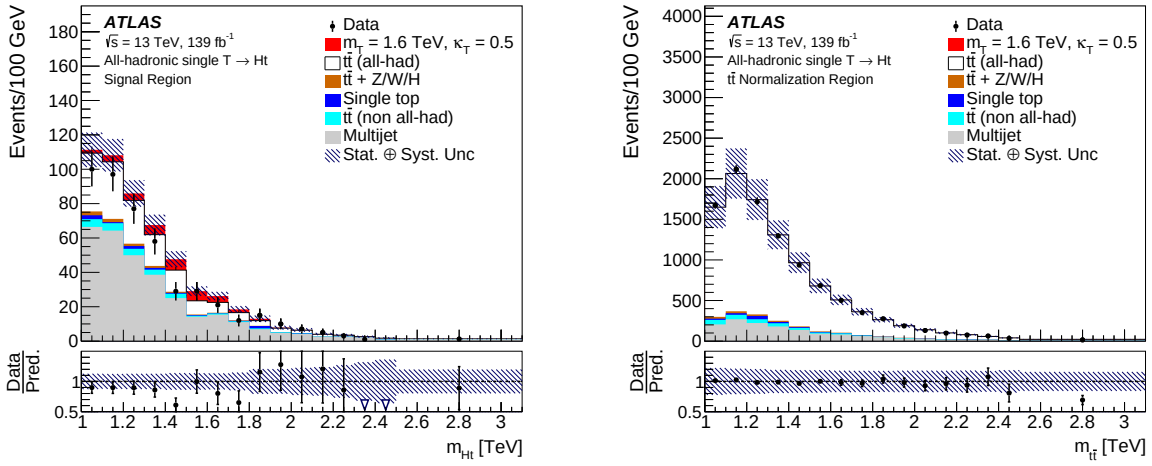

(a) (b)

Figure 6: Dijet invariant mass distributions in (a) the *SR* and (b) the *NR* before the fit of the signal and background model to the data. A T-quark hypothesis with $m_T = 1.6$ TeV and $\kappa_T = 0.5$ is used in these plots. The blue hashed lines correspond to the sum in quadrature of the statistical and systematic uncertainties of the prediction in a given bin. The lower panels show the ratio of the data to the prediction, along with the uncertainty in the ratio. A ratio outside the bounds of the axis is represented by a blue arrow. The last bin includes the event overflows. Contributions to the predicted distributions are stacked in the same order as they appear in the legend.

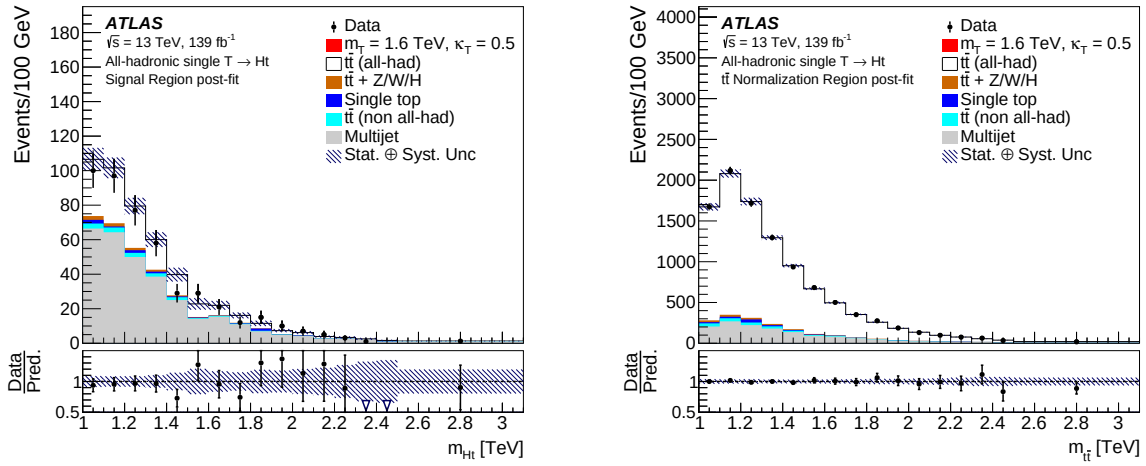

(a) (b)

Figure 7: Dijet invariant mass distributions for (a) the *SR* and (b) the *NR* showing the results of the model when fitted to the data. A T-quark hypothesis with $m_T = 1.6$ TeV and $\kappa_T = 0.5$ is used in the fit. Since the central value of the fitted T-quark cross-section is negative, the predicted *SR* mass distribution shows no contribution from the signal. The blue hashed lines correspond to the sum in quadrature of the statistical and systematic uncertainties of the prediction. The lower panels show the ratio of the data to the prediction, along with the uncertainty in the ratio. A ratio outside the bounds of the axis is represented by a blue arrow. The last bin includes the event overflows. Contributions to the predicted distributions are stacked in the same order as they appear in the legend.

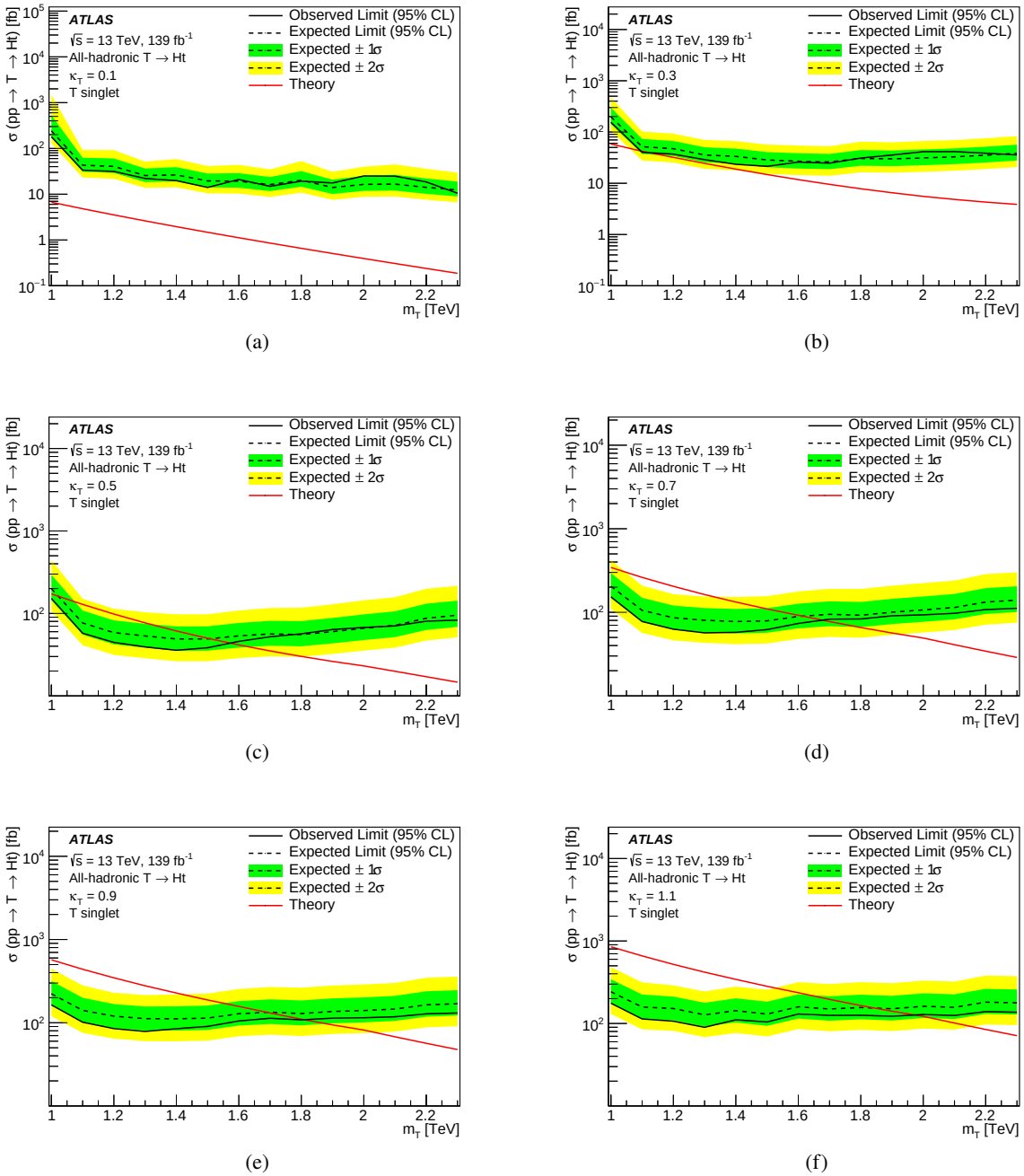

Figure 8: Observed and expected 95% CL upper limits on the single T-quark production cross-section as a function of m_T for values of κ_T ranging from 0.1 to 1.1. The green (yellow) band is the 68% (95%) confidence interval around the median expected limit, as determined using pseudo-experiments. The predicted cross-sections of single T-quark production are shown in red.

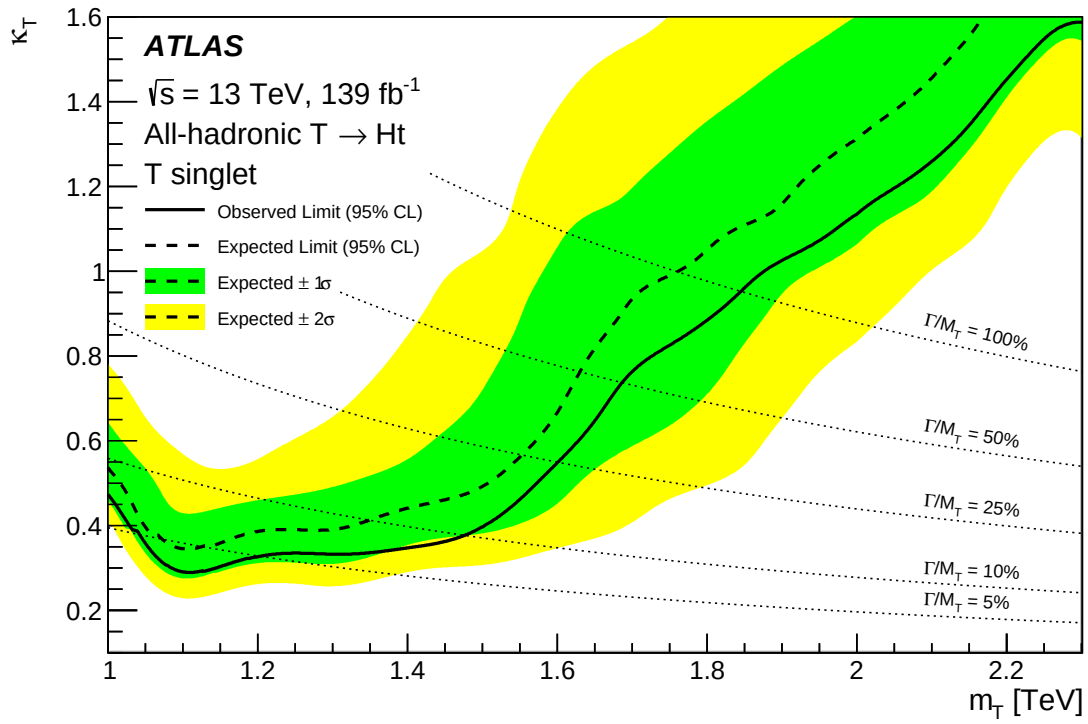

Figure 9: Observed and expected 95% CL upper limits on the single T-quark coupling κ_T as a function of m_T are shown as solid and dashed lines, respectively. The green (yellow) band is the 68% (95%) confidence interval around the median expected limit, as determined using pseudo-experiments. All values of κ_T above the solid line are excluded. The dashed curves represent contours of fixed Γ/m_T.

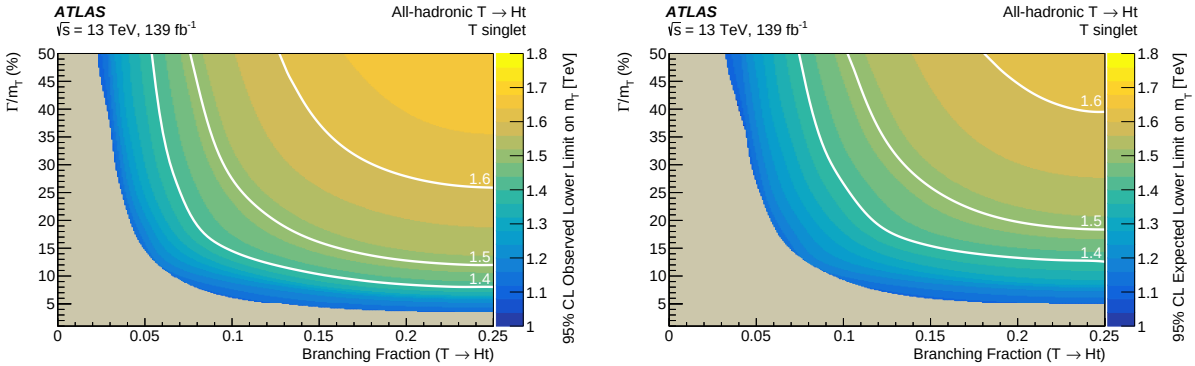

(a) (b)

Figure 10: Observed (a) and expected (b) 95% CL lower limits on the T-quark mass as a function of the T-quark width-to-mass ratio and the branching fraction of the $T \to Ht$ decay (Γ_T is the T-quark width) . The branching fractions ($\mathcal{B}$) for $T \to Ht$ and $T \to Zt$ are kept equal. The branching fraction for $T \to Wb$ is $1 - \mathcal{B}(T \to Ht) - \mathcal{B}(T \to Zt)$. The colour scale on the right side of each plot defines the 95% CL limit on the T-quark mass. Masses below the observed limit are excluded. The dashed white contour lines denote isolines of equal exclusion on the mass in units of TeV.

8 Conclusion

A search is reported for the single production of a vector-like singlet T quark decaying into a Higgs boson and a top quark both of which decay hadronically. The search uses 139 fb^{-1} of 13 TeV proton–proton collision data collected with the ATLAS detector at the LHC. The final states are fully reconstructed by clustering the decay products into two large-R jets. The use of fully hadronic decays allows the direct reconstruction of the T-quark final state, increasing the signal-to-background ratio for the search. The results significantly extend the sensitivity for the production of T quarks decaying fully hadronically. The search sensitivity is further improved by a larger dataset than used previously, tagging techniques with greater background rejection, and a data-driven multijet background estimate that reduces the uncertainty in the background modeling.

The analysis is performed by searching for an excess above SM backgrounds in the Ht invariant mass distribution. This distribution shows no evidence of significant contributions from single T-quark production and is consistent with the expected SM background sources. Therefore, limits are set at 95% C.L. on the production cross-section of a T quark decaying to the Ht final state. These depend on the T-quark mass and coupling to SM particles and range from ~10 fb to ~200 fb, depending on the assumed κ_T value for the couplings. In the resonance mass range between 1.0 and 2.3 TeV, the upper limit on the allowed coupling values rises with m_T from a minimum value of 0.3 for $m_T = 1.1$ TeV to 1.6 for $m_T = 2.3$ TeV. This analysis excludes T quarks with $\Gamma/m_T \geq 0.05$ for $1.05 < m_T < 1.2$ TeV, with the mass limits rising with Γ/m_T to exclude $m_T < 1.7$ TeV for $\Gamma/m_T \geq 0.5$.

These results provide significantly improved mass and coupling limits on vector-like quark models involving a T quark decaying into a Higgs boson and a top quark. The exclusion limits set by this analysis extend the limits set by previous searches.

Acknowledgments

We thank CERN for the very successful operation of the LHC, as well as the support staff from our institutions without whom ATLAS could not be operated efficiently.

We acknowledge the support of ANPCyT, Argentina; YerPhI, Armenia; ARC, Australia; BMWFW and FWF, Austria; ANAS, Azerbaijan; SSTC, Belarus; CNPq and FAPESP, Brazil; NSERC, NRC and CFI, Canada; CERN; ANID, Chile; CAS, MOST and NSFC, China; Minciencias, Colombia; MSMT CR, MPO CR and VSC CR, Czech Republic; DNRF and DNSRC, Denmark; IN2P3-CNRS and CEA-DRF/IRFU, France; SRNSFG, Georgia; BMBF, HGF and MPG, Germany; GSRI, Greece; RGC and Hong Kong SAR, China; ISF and Benoziyo Center, Israel; INFN, Italy; MEXT and JSPS, Japan; CNRST, Morocco; NWO, Netherlands; RCN, Norway; MEiN, Poland; FCT, Portugal; MNE/IFA, Romania; JINR; MES of Russia and NRC KI, Russian Federation; MESTD, Serbia; MSSR, Slovakia; ARRS and MIZŠ, Slovenia; DSI/NRF, South Africa; MICINN, Spain; SRC and Wallenberg Foundation, Sweden; SERI, SNSF and Cantons of Bern and Geneva, Switzerland; MOST, Taiwan; TAEK, Turkey; STFC, United Kingdom; DOE and NSF, United States of America. In addition, individual groups and members have received support from BCKDF, CANARIE, Compute Canada and CRC, Canada; COST, ERC, ERDF, Horizon 2020 and Marie Skłodowska-Curie Actions, European Union; Investissements d'Avenir Labex, Investissements d'Avenir Idex and ANR, France; DFG and AvH Foundation, Germany; Herakleitos, Thales and Aristeia programmes co-financed by EU-ESF and the Greek NSRF, Greece; BSF-NSF and GIF, Israel; Norwegian Financial

Mechanism 2014-2021, Norway; NCN and NAWA, Poland; La Caixa Banking Foundation, CERCA Programme Generalitat de Catalunya and PROMETEO and GenT Programmes Generalitat Valenciana, Spain; Göran Gustafssons Stiftelse, Sweden; The Royal Society and Leverhulme Trust, United Kingdom.

The crucial computing support from all WLCG partners is acknowledged gratefully, in particular from CERN, the ATLAS Tier-1 facilities at TRIUMF (Canada), NDGF (Denmark, Norway, Sweden), CC-IN2P3 (France), KIT/GridKA (Germany), INFN-CNAF (Italy), NL-T1 (Netherlands), PIC (Spain), ASGC (Taiwan), RAL (UK) and BNL (USA), the Tier-2 facilities worldwide and large non-WLCG resource providers. Major contributors of computing resources are listed in Ref. [140].

References

[1] ATLAS Collaboration, *Observation of a new particle in the search for the Standard Model Higgs boson with the ATLAS detector at the LHC*, Phys. Lett. B **716** (2012) 1, arXiv: 1207.7214 [hep-ex].

[2] CMS Collaboration, *Observation of a new boson at a mass of 125 GeV with the CMS experiment at the LHC*, Phys. Lett. B **716** (2012) 30, arXiv: 1207.7235 [hep-ex].

[3] ATLAS Collaboration, *Combined measurements of Higgs boson production and decay using up to 80 fb^{-1} of proton–proton collision data at $\sqrt{s}$ = 13 TeV collected with the ATLAS experiment*, Phys. Rev. D **101** (2020) 012002, arXiv: 1909.02845 [hep-ex].

[4] CMS Collaboration, *Combined measurements of Higgs boson couplings in proton–proton collisions at $\sqrt{s}$ = 13 TeV*, Eur. Phys. J. C **79** (2019) 421, arXiv: 1809.10733 [hep-ex].

[5] CMS Collaboration, *Measurements of properties of the Higgs boson in the four-lepton final state in proton-proton collisions at $\sqrt{s}$ = 13 TeV*, (2019), URL: https://cds.cern.ch/record/2668684.

[6] CMS Collaboration, *Measurement of the inclusive and differential Higgs boson production cross sections in the leptonic WW decay mode at $\sqrt{s}$ = 13 TeV*, JHEP **03** (2021) 003, arXiv: 2007.01984 [hep-ex].

[7] L. Susskind, *Dynamics of spontaneous symmetry breaking in the Weinberg-Salam Theory*, Phys. Rev. D **20** (1979) 2619.

[8] F. del Aguila and M. J. Bowick, *The possibility of new fermions with $\Delta I = 0$ Mass*, Nucl. Phys. B **224** (1983) 107.

[9] J. A. Aguilar-Saavedra, *Identifying top partners at LHC*, JHEP **11** (2009) 030, arXiv: 0907.3155 [hep-ph].

[10] N. Arkani-Hamed, A. G. Cohen, E. Katz, and A. E. Nelson, *The Littlest Higgs*, JHEP **07** (2002) 034, arXiv: hep-ph/0206021.

[11] M. Schmaltz and D. Tucker-Smith, *Little Higgs Theories*, Ann. Rev. Nucl. Part. Sci. **55** (2005) 229, arXiv: hep-ph/0502182.

[12] D. B. Kaplan, H. Georgi, and S. Dimopoulos, *Composite Higgs scalars*, Phys. Lett. B **136** (1984) 187.

[13] K. Agashe, R. Contino, and A. Pomarol, *The minimal composite Higgs model*, Nucl. Phys. B **719** (2005) 165, arXiv: hep-ph/0412089.

[14] C. T. Hill and E. H. Simmons, *Strong dynamics and electroweak symmetry breaking*, Phys. Rept. **381** (2003) 235, [Erratum: Phys. Rept. **390** (2004) 553], arXiv: hep-ph/0203079.

[15] J. A. Aguilar-Saavedra, *Mixing with vector-like quarks: constraints and expectations*, EPJ Web of Conferences **60** (2013) 16012, arXiv: 1306.4432 [hep-ph].

[16] J. A. Aguilar-Saavedra, R. Benbrik, S. Heinemeyer, and M. Pérez-Victoria, *Handbook of vectorlike quarks: Mixing and single production*, Phys. Rev. D **88** (2013) 094010, arXiv: 1306.0572 [hep-ph].

[17] A. Atre, M. Carena, T. Han, and J. Santiago, *Heavy quarks above the top at the Tevatron*, Phys. Rev. D **79** (2009) 054018, arXiv: 0806.3966 [hep-ph].

[18] A. Atre et al., *Model-independent searches for new quarks at the LHC*, JHEP **08** (2011) 080, arXiv: 1102.1987 [hep-ph].

[19] CMS Collaboration, *Search for a Vectorlike Quark with Charge 2/3 in $t + Z$ Events from pp Collisions at $\sqrt{s} = 7$ TeV*, Phys. Rev. Lett. **107** (2011) 271802, arXiv: 1109.4985 [hep-ex].

[20] CMS Collaboration, *Search for pair produced fourth-generation up-type quarks in pp collisions at $\sqrt{s} = 7$ TeV with a lepton in the final state*, Phys. Lett. B **718** (2012) 307, arXiv: 1209.0471 [hep-ex].

[21] ATLAS Collaboration, *Search for Pair Production of a New b' Quark that Decays into a Z Boson and a Bottom Quark with the ATLAS Detector*, Phys. Rev. Lett. **109** (2012) 071801, arXiv: 1204.1265 [hep-ex].

[22] CMS Collaboration, *Search for vectorlike charge 2/3 T quarks in proton–proton collisions at $\sqrt{(s)} = 8$ TeV*, Phys. Rev. D **93** (2016) 012003, arXiv: 1509.04177 [hep-ex].

[23] CMS Collaboration, *Search for pair-produced vectorlike B quarks in proton–proton collisions at $\sqrt{s} = 8$ TeV*, Phys. Rev. D **93** (2016) 112009, arXiv: 1507.07129 [hep-ex].

[24] CMS Collaboration, *Inclusive search for a vector-like T quark with charge $\frac{2}{3}$ in pp collisions at $\sqrt{s} = 8$ TeV*, Phys. Lett. B **729** (2014) 149, arXiv: 1311.7667 [hep-ex].

[25] CMS Collaboration, *Search for vector-like T quarks decaying to top quarks and Higgs bosons in the all-hadronic channel using jet substructure*, JHEP **06** (2015) 080, arXiv: 1503.01952 [hep-ex].

[26] ATLAS Collaboration, *Search for pair production of a new heavy quark that decays into a W boson and a light quark in pp collisions at $\sqrt{s} = 8$ TeV with the ATLAS detector*, Phys. Rev. D **92** (2015) 112007, arXiv: 1509.04261 [hep-ex].

[27] ATLAS Collaboration, *Search for production of vector-like quark pairs and of four top quarks in the lepton-plus-jets final state in pp collisions at $\sqrt{s} = 8$ TeV with the ATLAS detector*, JHEP **08** (2015) 105, arXiv: 1505.04306 [hep-ex].

[28] ATLAS Collaboration, *Search for pair production of vector-like top quarks in events with one lepton, jets, and missing transverse momentum in $\sqrt{s} = 13$ TeV pp collisions with the ATLAS detector*, JHEP **08** (2017) 052, arXiv: 1705.10751 [hep-ex].

[29] CMS Collaboration, *Search for pair production of vector-like T and B quarks in single-lepton final states using boosted jet substructure techniques at $\sqrt{s} = 13$ TeV*, JHEP **11** (2017) 085, arXiv: 1706.03408 [hep-ex].

[30] CMS Collaboration, *Search for pair production of vector-like quarks in the $bW\bar{b}W$ channel from proton–proton collisions at $\sqrt{s} = 13$ TeV*, Phys. Lett. B **779** (2018) 82, arXiv: 1710.01539 [hep-ex].

[31] CMS Collaboration,
Search for vector-like T and B quark pairs in final states with leptons at $\sqrt{s} = 13$ *TeV*,
JHEP **08** (2018) 177, arXiv: 1805.04758 [hep-ex].

[32] CMS Collaboration, *Search for vector-like quarks in events with two oppositely charged leptons and jets in proton–proton collisions at* $\sqrt{s} = 13$ *TeV*, Eur. Phys. J. C **79** (2019) 364,
arXiv: 1812.09768 [hep-ex].

[33] ATLAS Collaboration,
Search for pair production of heavy vector-like quarks decaying to high-p_T *W bosons and b quarks in the lepton-plus-jets final state in pp collisions at* $\sqrt{s} = 13$ *TeV with the ATLAS detector*,
JHEP **10** (2017) 141, arXiv: 1707.03347 [hep-ex].

[34] ATLAS Collaboration, *Search for pair production of up-type vector-like quarks and for four-top-quark events in final states with multiple b-jets with the ATLAS detector*,
JHEP **07** (2018) 089, arXiv: 1803.09678 [hep-ex].

[35] ATLAS Collaboration,
Search for pair production of heavy vector-like quarks decaying into high-p_T *W bosons and top quarks in the lepton-plus-jets final state in pp collisions at* $\sqrt{s} = 13$ *TeV with the ATLAS detector*,
JHEP **08** (2018) 048, arXiv: 1806.01762 [hep-ex].

[36] CMS Collaboration,
Search for pair production of vectorlike quarks in the fully hadronic final state,
Phys. Rev. D **100** (2019) 072001, arXiv: 1906.11903 [hep-ex].

[37] ATLAS Collaboration, *Search for single production of vector-like quarks decaying into Wb in pp collisions at* $\sqrt{s} = 8$ *TeV with the ATLAS detector*, Eur. Phys. J. C **76** (2016) 442,
arXiv: 1602.05606 [hep-ex].

[38] ATLAS Collaboration, *Search for the production of single vector-like and excited quarks in the Wt final state in pp collisions at* $\sqrt{s} = 8$ *TeV with the ATLAS detector*, JHEP **02** (2016) 110,
arXiv: 1510.02664 [hep-ex].

[39] CMS Collaboration, *Search for single production of a heavy vector-like T quark decaying to a Higgs boson and a top quark with a lepton and jets in the final state*, Phys. Lett. B **771** (2017) 80,
arXiv: 1612.00999 [hep-ex].

[40] CMS Collaboration, *Search for single production of vector-like quarks decaying to a Z boson and a top or a bottom quark in proton–proton collisions at* $\sqrt{s} = 13$ *TeV*, JHEP **05** (2017) 029,
arXiv: 1701.07409 [hep-ex].

[41] CMS Collaboration, *Search for electroweak production of a vector-like quark decaying to a top quark and a Higgs boson using boosted topologies in fully hadronic final states*,
JHEP **04** (2017) 136, arXiv: 1612.05336 [hep-ex].

[42] CMS Collaboration,
Search for a heavy resonance decaying to a top quark and a vector-like top quark at $\sqrt{s} = 13$ *TeV*,
JHEP **09** (2017) 053, arXiv: 1703.06352 [hep-ex].

[43] ATLAS Collaboration, *Combination of the searches for pair-produced vector-like partners of the third-generation quarks at* $\sqrt{s} = 13$ *TeV with the ATLAS detector*,
Phys. Rev. Lett. **121** (2018) 211801, arXiv: 1808.02343 [hep-ex].

[44] CMS Collaboration, *Search for single production of a vector-like T quark decaying to a Z boson and a top quark in proton–proton collisions at* $\sqrt{s} = 13$ *TeV*, Phys. Lett. B **781** (2018) 574, arXiv: 1708.01062 [hep-ex].

[45] CMS Collaboration, *Search for single production of vector-like quarks decaying to a top quark and a W boson in proton–proton collisions at* $\sqrt{s} = 13$ *TeV*, Eur. Phys. J. C **79** (2019) 90, arXiv: 1809.08597 [hep-ex].

[46] CMS Collaboration, *Search for electroweak production of a vector-like T quark using fully hadronic final states*, JHEP **01** (2020) 036, arXiv: 1909.04721 [hep-ex].

[47] M. Buchkremer, G. Cacciapaglia, A. Deandrea, and L. Panizzi, *Model-independent framework for searches of top partners*, Nucl. Phys. B **876** (2013) 376, arXiv: 1305.4172 [hep-ph].

[48] ATLAS Collaboration, *Performance of top-quark and W-boson tagging with ATLAS in Run 2 of the LHC*, Eur. Phys. J. C **79** (2019) 375, arXiv: 1808.07858 [hep-ex].

[49] ATLAS Collaboration, *ATLAS b-jet identification performance and efficiency measurement with* $t\bar{t}$ *events in* pp *collisions at* $\sqrt{s} = 13$ *TeV*, Eur. Phys. J. C **79** (2019) 970, arXiv: 1907.05120 [hep-ex].

[50] ATLAS Collaboration, *Measurements of top quark pair relative differential cross-sections with ATLAS in* pp *collisions at* $\sqrt{s} = 7$ *TeV*, Eur. Phys. J. C **73** (2013) 2261, arXiv: 1207.5644 [hep-ex].

[51] ATLAS Collaboration, *Measurements of normalized differential cross-sections for* $t\bar{t}$ *production in* pp *collisions at* $\sqrt{s} = 7$ *TeV using the ATLAS detector*, Phys. Rev. D **90** (2014) 072004, arXiv: 1407.0371 [hep-ex].

[52] ATLAS Collaboration, *Differential top-antitop cross-section measurements as a function of observables constructed from final-state particles using* pp *collisions at* $\sqrt{s} = 7$ *TeV in the ATLAS detector*, JHEP **06** (2015) 100, arXiv: 1502.05923 [hep-ex].

[53] ATLAS Collaboration, *Measurement of the differential cross-section of highly boosted top quarks as a function of their transverse momentum in* $\sqrt{s} = 8$ *TeV proton–proton collisions using the ATLAS detector*, Phys. Rev. D **93** (2016) 032009, arXiv: 1510.03818 [hep-ex].

[54] ATLAS Collaboration, *Measurements of top-quark pair differential cross-sections in the lepton+jets channel in* pp *collisions at* $\sqrt{s} = 8$ *TeV using the ATLAS detector*, Eur. Phys. J. C **76** (2016) 538, arXiv: 1511.04716 [hep-ex].

[55] ATLAS Collaboration, *Measurement of top quark pair differential cross sections in the dilepton channel in* pp *collisions at* $\sqrt{s} = 7$ *and* 8 *TeV with ATLAS*, Phys. Rev. D **94** (2016) 092003, arXiv: 1607.07281 [hep-ex].

[56] ATLAS Collaboration, *Measurements of top-quark pair differential cross-sections in the* $e\mu$ *channel in* pp *collisions at* $\sqrt{s} = 13$ *TeV using the ATLAS detector*, Eur. Phys. J. C **77** (2017) 292, arXiv: 1612.05220 [hep-ex].

[57] ATLAS Collaboration, *Measurements of top-quark pair differential cross-sections in the lepton+jets channel in pp collisions at $\sqrt{s}$ = 13 TeV using the ATLAS detector*, JHEP **11** (2017) 191, arXiv: 1708.00727 [hep-ex].

[58] ATLAS Collaboration, *Measurements of $t\bar{t}$ differential cross-sections of highly boosted top quarks decaying to all-hadronic final states in pp collisions at $\sqrt{s}$ = 13 TeV using the ATLAS detector*, Phys. Rev. D **98** (2018) 012003, arXiv: 1801.02052 [hep-ex].

[59] CMS Collaboration, *Measurement of differential top-quark-pair production cross sections in pp colisions at $\sqrt{s}$ = 7 TeV*, Eur. Phys. J. C **73** (2013) 2339, arXiv: 1211.2220 [hep-ex].

[60] CMS Collaboration, *Measurement of the semileptonic $t\bar{t}+\gamma$ production cross section in pp collisions at $\sqrt{s}$ = 8 TeV*, JHEP **10** (2017) 006, arXiv: 1706.08128 [hep-ex].

[61] CMS Collaboration, *Measurement of the differential cross section for top quark pair production in pp collisions at $\sqrt{s}$ = 8 TeV*, Eur. Phys. J. C **75** (2015) 542, arXiv: 1505.04480 [hep-ex].

[62] CMS Collaboration, *Measurement of the integrated and differential $t\bar{t}$ production cross sections for high-p_T top quarks in pp collisions at $\sqrt{s}$ = 8 TeV*, Phys. Rev. D **94** (2016) 072002, arXiv: 1605.00116 [hep-ex].

[63] CMS Collaboration, *Measurement of differential cross sections for top quark pair production using the lepton+jets final state in proton–proton collisions at* 13 *TeV*, Phys. Rev. D **95** (2017) 092001, arXiv: 1610.04191 [hep-ex].

[64] CMS Collaboration, *Measurement of double-differential cross sections for top quark pair production in pp collisions at $\sqrt{s}$ = 8 TeV and impact on parton distribution functions*, Eur. Phys. J. C **77** (2017) 459, arXiv: 1703.01630 [hep-ex].

[65] CMS Collaboration, *Measurement of normalized differential $t\bar{t}$ cross sections in the dilepton channel from pp collisions at $\sqrt{s}$ = 13 TeV*, JHEP **04** (2018) 060, arXiv: 1708.07638 [hep-ex].

[66] CMS Collaboration, *Measurements of differential cross sections of top quark pair production as a function of kinematic event variables in proton–proton collisions at $\sqrt{s}$ = 13 TeV*, JHEP **06** (2018) 002, arXiv: 1803.03991 [hep-ex].

[67] CMS Collaboration, *Measurement of differential cross sections for the production of top quark pairs and of additional jets in lepton+jets events from pp collisions at $\sqrt{s}$ = 13 TeV*, Phys. Rev. D **97** (2018) 112003, arXiv: 1803.08856 [hep-ex].

[68] CMS Collaboration, *Measurement of $t\bar{t}$ normalised multi-differential cross sections in pp collisions at $\sqrt{s}$ = 13 TeV, and simultaneous determination of the strong coupling strength, top quark pole mass, and parton distribution functions*, Eur. Phys. J. C **80** (2020) 658, arXiv: 1904.05237 [hep-ex].

[69] CMS Collaboration, *Measurement of differential $t\bar{t}$ production cross sections using top quarks at large transverse momenta in pp collisions at $\sqrt{s}$ = 13 TeV*, Phys. Rev. D **103** (2021) 052008, arXiv: 2008.07860 [hep-ex].

[70] ATLAS Collaboration, *The ATLAS Experiment at the CERN Large Hadron Collider*, JINST **3** (2008) S08003.

[71] ATLAS Collaboration, *ATLAS Insertable B-Layer Technical Design Report*, ATLAS-TDR-19 (2010), URL: https://cds.cern.ch/record/1291633, ATLAS Insertable B-Layer Technical Design Report Addendum, ATLAS-TDR-19-ADD-1 (2012), URL: http://cds.cern.ch/record/1451888.

[72] B. Abbott et al., *Production and integration of the ATLAS Insertable B-Layer*, JINST **13** (2018) T05008, arXiv: 1803.00844 [physics.ins-det].

[73] ATLAS Collaboration, *Performance of the ATLAS trigger system in 2015*, Eur. Phys. J. C **77** (2017) 317, arXiv: 1611.09661 [hep-ex].

[74] ATLAS Collaboration, *The ATLAS Collaboration Software and Firmware*, ATL-SOFT-PUB-2021-001, 2021, URL: https://cds.cern.ch/record/2767187.

[75] ATLAS Collaboration, *Luminosity determination in pp collisions at $\sqrt{s} = 13$ TeV using the ATLAS detector at the LHC*, ATLAS-CONF-2019-021, 2019, URL: https://cds.cern.ch/record/2677054.

[76] G. Avoni et al., *The new LUCID-2 detector for luminosity measurement and monitoring in ATLAS*, JINST **13** (2018) P07017.

[77] M. Cacciari, G. P. Salam, and G. Soyez, *The anti-k_t jet clustering algorithm*, JHEP 04 (2008) 063, arXiv: 0802.1189 [hep-ph].

[78] M. Cacciari, G. P. Salam, and G. Soyez, *FastJet User Manual*, Eur. Phys. J. C **72** (2012) 1896, arXiv: 1111.6097 [hep-ph].

[79] J. Alwall, M. Herquet, F. Maltoni, O. Mattelaer, and T. Stelzer, *MadGraph 5 : going beyond*, JHEP **06** (2011) 128, arXiv: 1106.0522 [hep-ph].

[80] R. D. Ball et al., *Parton distributions for the LHC run II*, JHEP **04** (2015) 040, arXiv: 1410.8849 [hep-ph].

[81] G. Cacciapaglia et al., *Next-to-leading-order predictions for single vector-like quark production at the LHC*, Physics Letters B **793** (2019) 206, arXiv: 1811.05055.

[82] A. Roy, N. Nikiforou, N. Castro, and T. Andeen, *Novel interpretation strategy for searches of singly produced vectorlike quarks at the LHC*, Physical Review D **101** (2020), arXiv: 2003.00640.

[83] S. Frixione, P. Nason, and G. Ridolfi, *A positive-weight next-to-leading-order Monte Carlo for heavy flavour hadroproduction*, JHEP **09** (2007) 126, arXiv: 0707.3088 [hep-ph].

[84] P. Nason, *A new method for combining NLO QCD with shower Monte Carlo algorithms*, JHEP **11** (2004) 040, arXiv: hep-ph/0409146.

[85] S. Frixione, P. Nason, and C. Oleari, *Matching NLO QCD computations with parton shower simulations: the POWHEG method*, JHEP **11** (2007) 070, arXiv: 0709.2092 [hep-ph].

[86] S. Alioli, P. Nason, C. Oleari, and E. Re, *A general framework for implementing NLO calculations in shower Monte Carlo programs: the POWHEG BOX*, JHEP **06** (2010) 043, arXiv: 1002.2581 [hep-ph].

[87] ATLAS Collaboration, *Studies on top-quark Monte Carlo modelling for Top2016*, ATL-PHYS-PUB-2016-020, 2016, URL: https://cds.cern.ch/record/2216168.

[88] T. Sojstrand et al., *An Introduction to PYTHIA 8.2*, Comput. Phys. Commun. **191** (2015) 159, arXiv: 1410.3012 [hep-ph].

[89] ATLAS Collaboration, *ATLAS Pythia 8 tunes to 7 TeV data*, ATL-PHYS-PUB-2014-021, 2014, URL: https://cds.cern.ch/record/1966419.

[90] R. D. Ball et al., *Parton distributions with LHC data*, Nucl. Phys. B **867** (2013) 244, arXiv: 1207.1303 [hep-ph].

[91] D. J. Lange, *The EvtGen particle decay simulation package*, Nucl. Instrum. Meth. A **462** (2001) 152.

[92] M. Beneke, P. Falgari, S. Klein, and C. Schwinn, *Hadronic top-quark pair production with NNLL threshold resummation*, Nucl. Phys. B **855** (2012) 695, arXiv: 1109.1536 [hep-ph].

[93] M. Cacciari, M. Czakon, M. Mangano, A. Mitov, and P. Nason, *Top-pair production at hadron colliders with next-to-next-to-leading logarithmic soft-gluon resummation*, Phys. Lett. **B710** (2012) 612, arXiv: 1111.5869 [hep-ph].

[94] P. Baernreuther, M. Czakon, and A. Mitov, *Percent Level Precision Physics at the Tevatron: First Genuine NNLO QCD Corrections to $q\bar{q} \to t\bar{t} + X$*, Phys. Rev. Lett. **109** (2012) 132001, arXiv: 1204.5201 [hep-ph].

[95] M. Czakon and A. Mitov, *NNLO corrections to top-pair production at hadron colliders: the all-fermionic scattering channels*, JHEP **12** (2012) 054, arXiv: 1207.0236 [hep-ph].

[96] M. Czakon and A. Mitov, *NNLO corrections to top pair production at hadron colliders: the quark-gluon reaction*, JHEP **01** (2013) 080, arXiv: 1210.6832 [hep-ph].

[97] M. Czakon, P. Fiedler, and A. Mitov, *Total Top-Quark Pair-Production Cross Section at Hadron Colliders Through $O(\alpha_S^4)$*, Phys. Rev. Lett. **110** (2013) 252004, arXiv: 1303.6254 [hep-ph].

[98] M. Czakon and A. Mitov, *Top++: A program for the calculation of the top-pair cross-section at hadron colliders*, Comput. Phys. Commun. **185** (2014) 2930, arXiv: 1112.5675 [hep-ph].

[99] J. Butterworth et al., *PDF4LHC recommendations for LHC Run II*, J. Phys. G **43** (2016) 023001, arXiv: 1510.03865 [hep-ph].

[100] A. D. Martin, W. J. Stirling, R. S. Thorne, and G. Watt, *Parton distributions for the LHC*, Eur. Phys. J. C **63** (2009) 189, arXiv: 0901.0002 [hep-ph].

[101] A. D. Martin, W. J. Stirling, R. S. Thorne, and G. Watt, *Uncertainties on alpha(S) in global PDF analyses and implications for predicted hadronic cross sections*, Eur. Phys. J. C **64** (2009) 653, arXiv: 0905.3531 [hep-ph].

[102] H.-L. Lai et al., *New parton distributions for collider physics*, Phys. Rev. D **82** (2010) 074024, arXiv: 1007.2241 [hep-ph].

[103] J. Gao, M. Guzzi, J. Huston, H.-L. Lai, Z. Li, et al., *CT10 next-to-next-to-leading order global analysis of QCD*, Phys. Rev. D **89** (2014) 033009, arXiv: 1302.6246 [hep-ph].

[104] M. Bähr et al., *Herwig++ physics and manual*, Eur. Phys. J. C **58** (2008) 639, arXiv: 0803.0883 [hep-ph].

[105] J. Bellm et al., *Herwig 7.0/Herwig++ 3.0 release note*, Eur. Phys. J. C **76** (2016) 196, arXiv: 1512.01178 [hep-ph].

[106] J. Bellm et al., *Herwig 7.1 Release Note*, (2017), arXiv: 1705.06919 [hep-ph].

[107] L. Harland-Lang, A. Martin, P. Motylinski, and R. Thorne,
Parton distributions in the LHC era: MMHT 2014 PDFs, Eur. Phys. J. C **75** (2015) 204, arXiv: 1412.3989 [hep-ph].

[108] E. Re,
Single-top Wt-channel production matched with parton showers using the POWHEG method, Eur. Phys. J. C **71** (2011) 1547, arXiv: 1009.2450 [hep-ph].

[109] S. Frixione, E. Laenen, P. Motylinski, C. White, and B. R. Webber,
Single-top hadroproduction in association with a W boson, JHEP **07** (2008) 029, arXiv: 0805.3067 [hep-ph].

[110] N. Kidonakis,
Two-loop soft anomalous dimensions for single top quark associated production with a W^- or H^-, Phys. Rev. D **82** (2010) 054018, arXiv: 1005.4451 [hep-ph].

[111] N. Kidonakis, "Top Quark Production," *Proceedings, Helmholtz International Summer School on Physics of Heavy Quarks and Hadrons (HQ 2013)* (JINR, Dubna, Russia, July 15–28, 2013) 139, arXiv: 1311.0283 [hep-ph].

[112] R. Frederix, E. Re, and P. Torrielli,
Single-top t-channel hadroproduction in the four-flavour scheme with POWHEG and aMC@NLO, JHEP **09** (2012) 130, arXiv: 1207.5391 [hep-ph].

[113] M. Aliev, H. Lacker, U. Langenfeld, S. Moch, P. Uwer, et al.,
HATHOR: HAdronic Top and Heavy quarks crOss section calculatoR, Comput. Phys. Commun. **182** (2011) 1034, arXiv: 1007.1327 [hep-ph].

[114] P. Kant et al., *HatHor for single top-quark production: Updated predictions and uncertainty estimates for single top-quark production in hadronic collisions*, Comput. Phys. Commun. **191** (2015) 74, arXiv: 1406.4403 [hep-ph].

[115] H. B. Hartanto, B. Jäger, L. Reina, and D. Wackeroth,
Higgs boson production in association with top quarks in the POWHEG BOX, Phys. Rev. D **91** (2015) 094003, arXiv: 1501.04498 [hep-ph].

[116] D. de Florian et al.,
Handbook of LHC Higgs Cross Sections: 4. Deciphering the Nature of the Higgs Sector, (2016), arXiv: 1610.07922 [hep-ph].

[117] T. Sjöstrand, S. Mrenna, and P. Z. Skands, *A brief introduction to PYTHIA 8.1*, Comput. Phys. Commun. **178** (2008) 852, arXiv: 0710.3820 [hep-ph].

[118] ATLAS Collaboration, *The Pythia 8 A3 tune description of ATLAS minimum bias and inelastic measurements incorporating the Donnachie–Landshoff diffractive model*, ATL-PHYS-PUB-2016-017, 2016, URL: https://cds.cern.ch/record/2206965.

[119] S. Agostinelli et al., *GEANT4: a simulation toolkit*, Nucl. Instrum. Meth. Phys. A **506** (2003) 250.

[120] ATLAS Collaboration, *The ATLAS Simulation Infrastructure*, Eur. Phys. J. C **70** (2010) 823, arXiv: 1005.4568 [physics.ins-det].

[121] ATLAS Collaboration, *Electron and photon performance measurements with the ATLAS detector using the 2015–2017 LHC proton–proton collision data*, JINST **14** (2019) P12006, arXiv: 1908.00005 [hep-ex].

[122] ATLAS Collaboration, *Muon reconstruction and identification efficiency in ATLAS using the full Run 2 pp collision data set at* $\sqrt{s}$ = 13 *TeV*, Eur. Phys. J. C **81** (2020) 578, arXiv: 2012.00578 [hep-ex].

[123] ATLAS Collaboration, *Muon reconstruction performance of the ATLAS detector in proton–proton collision data at* $\sqrt{s}$ = 13 *TeV*, Eur. Phys. J. C **76** (2016) 292, arXiv: 1603.05598 [hep-ex].

[124] D. Krohn, J. Thaler, and L.-T. Wang, *Jets with variable R*, JHEP **06** (2009) 059, arXiv: 0903.0392 [hep-ph].

[125] ATLAS Collaboration, *In situ calibration of large-radius jet energy and mass in* 13 *TeV proton–proton collisions with the ATLAS detector*, Eur. Phys. J. C **79** (2019) 135, arXiv: 1807.09477 [hep-ex].

[126] ATLAS Collaboration, *Jet reconstruction and performance using particle flow with the ATLAS Detector*, Eur. Phys. J. C **77** (2017) 466, arXiv: 1703.10485 [hep-ex].

[127] ATLAS Collaboration, *Performance of pile-up mitigation techniques for jets in pp collisions at* $\sqrt{s}$ = 8 *TeV using the ATLAS detector*, Eur. Phys. J. C **76** (2016) 581, arXiv: 1510.03823 [hep-ex].

[128] ATLAS Collaboration, *Jet energy scale and resolution measured in proton–proton collisions at* $\sqrt{s}$ = 13 *TeV with the ATLAS detector*, Eur. Phys. J. C **81** (2020) 689, arXiv: 2007.02645 [hep-ex].

[129] ATLAS Collaboration, *Optimisation of large-radius jet reconstruction for the ATLAS detector in* 13 *TeV proton–proton collisions*, Eur. Phys. J. C **81** (2020) 334, arXiv: 2009.04986 [hep-ex].

[130] ATLAS Collaboration, *Measurement of the ATLAS Detector Jet Mass Response using Forward Folding with* 80 fb^{-1} *of* $\sqrt{s}$ = 13 *TeV pp data*, ATLAS-CONF-2020-022, 2020, URL: https://cds.cern.ch/record/2724442.

[131] ATLAS Collaboration, *Performance of jet substructure techniques for large-R jets in proton–proton collisions at* $\sqrt{s}$ = 7 *TeV using the ATLAS detector*, JHEP **09** (2013) 076, arXiv: 1306.4945 [hep-ex].

[132] J. Thaler and K. V. Tilburg, *Identifying boosted objects with N-subjettiness*, JHEP **03** (2011) 015, arXiv: 1011.2268 [hep-ph].

[133] J. Thaler and K. V. Tilburg, *Maximizing boosted top identification by minimizing N-subjettiness*, JHEP **02** (2012) 093, arXiv: 1108.2701 [hep-ph].

[134] ATLAS Collaboration, *Vertex Reconstruction Performance of the ATLAS Detector at* $\sqrt{s}$ = 13 *TeV*, ATL-PHYS-PUB-2015-026, 2015, URL: https://cds.cern.ch/record/2037717.

[135] ATLAS Collaboration, *Search for resonances decaying into top-quark pairs using fully hadronic decays in pp collisions with ATLAS at* $\sqrt{s}$ = 7 *TeV*, JHEP **01** (2013) 116, arXiv: 1211.2202 [hep-ex].

[136] ATLAS Collaboration, *Measurements of* W^+W^- + ≥ 1 *jet production cross-sections in pp collisions at* $\sqrt{s}$ = 13 *TeV with the ATLAS detector*, JHEP **06** (2021) 003, arXiv: 2103.10319 [hep-ex].

[137] ATLAS Collaboration, *Boosted hadronic vector boson and top quark tagging with ATLAS using Run 2 data*, ATL-PHYS-PUB-2020-017, 2020, URL: https://cds.cern.ch/record/2724149.

[138] G. Bohm and G. Zech, *Introduction to statistics and data analysis for physicists*, http://www-library.desy.de/preparch/books/vstatmp_engl.pdf, Hamburg: Verl. Dt. Elektronen-Synchrotron, 2010 336, ISBN: 978-3-935702-41-6.

[139] G. Cowan, K. Cranmer, E. Gross, and O. Vitells, *Asymptotic formulae for likelihood-based tests of new physics*, Eur. Phys. J. C **71** (2011), ISSN: 1434-6052, URL: http://dx.doi.org/10.1140/epjc/s10052-011-1554-0.

[140] ATLAS Collaboration, *ATLAS Computing Acknowledgements*, ATL-SOFT-PUB-2021-003, URL: https://cds.cern.ch/record/2776662.

The ATLAS Collaboration

G. Aad[100], B. Abbott[126], D.C. Abbott[101], A. Abed Abud[36], K. Abeling[53], D.K. Abhayasinghe[93], S.H. Abidi[29], A. Aboulhorma[35e], H. Abramowicz[158], H. Abreu[157], Y. Abulaiti[123], A.C. Abusleme Hoffman[144a], B.S. Acharya[66a,66b,m], B. Achkar[53], L. Adam[98], C. Adam Bourdarios[4], L. Adamczyk[83a], L. Adamek[163], S.V. Addepalli[26], J. Adelman[118], A. Adiguzel[21c], S. Adorni[54], T. Adye[141], A.A. Affolder[143], Y. Afik[36], M.N. Agaras[13], J. Agarwala[70a,70b], A. Aggarwal[98], C. Agheorghiesei[27c], J.A. Aguilar-Saavedra[137f,137a,w], A. Ahmad[36], F. Ahmadov[79], W.S. Ahmed[102], X. Ai[46], G. Aielli[73a,73b], I. Aizenberg[176], M. Akbiyik[98], T.P.A. Åkesson[96], A.V. Akimov[109], K. Al Khoury[39], G.L. Alberghi[23b], J. Albert[172], P. Albicocco[51], M.J. Alconada Verzini[88], S. Alderweireldt[50], M. Aleksa[36], I.N. Aleksandrov[79], C. Alexa[27b], T. Alexopoulos[10], A. Alfonsi[117], F. Alfonsi[23b], M. Alhroob[126], B. Ali[139], S. Ali[155], M. Aliev[162], G. Alimonti[68a], C. Allaire[36], B.M.M. Allbrooke[153], P.P. Allport[20], A. Aloisio[69a,69b], F. Alonso[88], C. Alpigiani[145], E. Alunno Camelia[73a,73b], M. Alvarez Estevez[97], M.G. Alviggi[69a,69b], Y. Amaral Coutinho[80b], A. Ambler[102], L. Ambroz[132], C. Amelung[36], D. Amidei[104], S.P. Amor Dos Santos[137a], S. Amoroso[46], K.R. Amos[170], C.S. Amrouche[54], V. Ananiev[131], C. Anastopoulos[146], N. Andari[142], T. Andeen[11], J.K. Anders[19], S.Y. Andrean[45a,45b], A. Andreazza[68a,68b], S. Angelidakis[9], A. Angerami[39], A.V. Anisenkov[119b,119a], A. Annovi[71a], C. Antel[54], M.T. Anthony[146], E. Antipov[127], M. Antonelli[51], D.J.A. Antrim[17], F. Anulli[72a], M. Aoki[81], J.A. Aparisi Pozo[170], M.A. Aparo[153], L. Aperio Bella[46], C. Appelt[18], N. Aranzabal[36], V. Araujo Ferraz[80a], C. Arcangeletti[51], A.T.H. Arce[49], E. Arena[90], J-F. Arguin[108], S. Argyropoulos[52], J.-H. Arling[46], A.J. Armbruster[36], O. Arnaez[163], H. Arnold[117], Z.P. Arrubarrena Tame[112], G. Artoni[132], H. Asada[114], K. Asai[124], S. Asai[160], N.A. Asbah[59], E.M. Asimakopoulou[168], J. Assahsah[35d], K. Assamagan[29], R. Astalos[28a], R.J. Atkin[33a], M. Atkinson[169], N.B. Atlay[18], H. Atmani[60b], P.A. Atmasiddha[104], K. Augsten[139], S. Auricchio[69a,69b], V.A. Austrup[178], G. Avner[157], G. Avolio[36], M.K. Ayoub[14c], G. Azuelos[108,ad], D. Babal[28a], H. Bachacou[142], K. Bachas[159], A. Bachiu[34], F. Backman[45a,45b], A. Badea[59], P. Bagnaia[72a,72b], M. Bahmani[18], A.J. Bailey[170], V.R. Bailey[169], J.T. Baines[141], C. Bakalis[10], O.K. Baker[179], P.J. Bakker[117], E. Bakos[15], D. Bakshi Gupta[8], S. Balaji[154], R. Balasubramanian[117], E.M. Baldin[119b,119a], P. Balek[140], E. Ballabene[68a,68b], F. Balli[142], L.M. Baltes[61a], W.K. Balunas[32], J. Balz[98], E. Banas[84], M. Bandieramonte[136], A. Bandyopadhyay[24], S. Bansal[24], L. Barak[158], E.L. Barberio[103], D. Barberis[55b,55a], M. Barbero[100], G. Barbour[94], K.N. Barends[33a], T. Barillari[113], M-S. Barisits[36], J. Barkeloo[129], T. Barklow[150], R.M. Barnett[17], P. Baron[128], A. Baroncelli[60a], G. Barone[29], A.J. Barr[132], L. Barranco Navarro[45a,45b], F. Barreiro[97], J. Barreiro Guimarães da Costa[14a], U. Barron[158], S. Barsov[135], F. Bartels[61a], R. Bartoldus[150], G. Bartolini[100], A.E. Barton[89], P. Bartos[28a], A. Basalaev[46], A. Basan[98], M. Baselga[47], I. Bashta[74a,74b], A. Bassalat[64,aa], M.J. Basso[163], C.R. Basson[99], R.L. Bates[57], S. Batlamous[35e], J.R. Batley[32], B. Batool[148], M. Battaglia[143], M. Bauce[72a,72b], F. Bauer[142,*], P. Bauer[24], A. Bayirli[21a], J.B. Beacham[49], T. Beau[133], P.H. Beauchemin[166], F. Becherer[52], P. Bechtle[24], H.P. Beck[19,o], K. Becker[174], C. Becot[46], A.J. Beddall[21d], V.A. Bednyakov[79], C.P. Bee[152], L.J. Beemster[15], T.A. Beermann[36], M. Begalli[80b], M. Begel[29], A. Behera[152], J.K. Behr[46], C. Beirao Da Cruz E Silva[36], J.F. Beirer[53,36], F. Beisiegel[24], M. Belfkir[122b], G. Bella[158], L. Bellagamba[23b], A. Bellerive[34], P. Bellos[20], K. Beloborodov[119b,119a], K. Belotskiy[110], N.L. Belyaev[110], D. Benchekroun[35a], Y. Benhammou[158], D.P. Benjamin[29], M. Benoit[29], J.R. Bensinger[26], S. Bentvelsen[117], L. Beresford[36], M. Beretta[51], D. Berge[18], E. Bergeaas Kuutmann[168], N. Berger[4], B. Bergmann[139], J. Beringer[17], S. Berlendis[7], G. Bernardi[5], C. Bernius[150], F.U. Bernlochner[24], T. Berry[93], P. Berta[140], I.A. Bertram[89], O. Bessidskaia Bylund[178], S. Bethke[113], A. Betti[42], A.J. Bevan[92], S. Bhatta[152], D.S. Bhattacharya[173], P. Bhattarai[26], V.S. Bhopatkar[6], R. Bi[136], R. Bi[29], R.M. Bianchi[136], O. Biebel[112], R. Bielski[129], N.V. Biesuz[71a,71b], M. Biglietti[74a], T.R.V. Billoud[139], M. Bindi[53], A. Bingul[21b], C. Bini[72a,72b], S. Biondi[23b,23a], A. Biondini[90], C.J. Birch-sykes[99], G.A. Bird[20,141], M. Birman[176],

T. Bisanz[36], J.P. Biswal[2], D. Biswas[177,i], A. Bitadze[99], K. Bjørke[131], I. Bloch[46], C. Blocker[26], A. Blue[57], U. Blumenschein[92], J. Blumenthal[98], G.J. Bobbink[117], V.S. Bobrovnikov[119b,119a], M. Boehler[52], D. Bogavac[13], A.G. Bogdanchikov[119b,119a], C. Bohm[45a], V. Boisvert[93], P. Bokan[46], T. Bold[83a], M. Bomben[5], M. Bona[92], M. Boonekamp[142], C.D. Booth[93], A.G. Borbély[57], H.M. Borecka-Bielska[108], L.S. Borgna[94], G. Borissov[89], D. Bortoletto[132], D. Boscherini[23b], M. Bosman[13], J.D. Bossio Sola[36], K. Bouaouda[35a], J. Boudreau[136], E.V. Bouhova-Thacker[89], D. Boumediene[38], R. Bouquet[5], A. Boveia[125], J. Boyd[36], D. Boye[29], I.R. Boyko[79], J. Bracinik[20], N. Brahimi[60d,60c], G. Brandt[178], O. Brandt[32], F. Braren[46], B. Brau[101], J.E. Brau[129], W.D. Breaden Madden[57], K. Brendlinger[46], R. Brener[176], L. Brenner[36], R. Brenner[168], S. Bressler[176], B. Brickwedde[98], D. Britton[57], D. Britzger[113], I. Brock[24], G. Brooijmans[39], W.K. Brooks[144f], E. Brost[29], P.A. Bruckman de Renstrom[84], B. Brüers[46], D. Bruncko[28b], A. Bruni[23b], G. Bruni[23b], M. Bruschi[23b], N. Bruscino[72a,72b], L. Bryngemark[150], T. Buanes[16], Q. Buat[145], P. Buchholz[148], A.G. Buckley[57], I.A. Budagov[79], M.K. Bugge[131], O. Bulekov[110], B.A. Bullard[59], S. Burdin[90], C.D. Burgard[46], A.M. Burger[38], B. Burghgrave[8], J.T.P. Burr[32], C.D. Burton[11], J.C. Burzynski[149], E.L. Busch[39], V. Büscher[98], P.J. Bussey[57], J.M. Butler[25], C.M. Buttar[57], J.M. Butterworth[94], W. Buttinger[141], C.J. Buxo Vazquez[105], A.R. Buzykaev[119b,119a], G. Cabras[23b], S. Cabrera Urbán[170], D. Caforio[56], H. Cai[136], Y. Cai[14a], V.M.M. Cairo[36], O. Cakir[3a], N. Calace[36], P. Calafiura[17], G. Calderini[133], P. Calfayan[65], G. Callea[57], L.P. Caloba[80b], D. Calvet[38], S. Calvet[38], T.P. Calvet[100], M. Calvetti[71a,71b], R. Camacho Toro[133], S. Camarda[36], D. Camarero Munoz[97], P. Camarri[73a,73b], M.T. Camerlingo[74a,74b], D. Cameron[131], C. Camincher[172], M. Campanelli[94], A. Camplani[40], V. Canale[69a,69b], A. Canesse[102], M. Cano Bret[77], J. Cantero[97], Y. Cao[169], F. Capocasa[26], M. Capua[41b,41a], A. Carbone[68a,68b], R. Cardarelli[73a], J.C.J. Cardenas[8], F. Cardillo[170], G. Carducci[41b,41a], T. Carli[36], G. Carlino[69a], B.T. Carlson[136], E.M. Carlson[172,164a], L. Carminati[68a,68b], M. Carnesale[72a,72b], S. Caron[116], E. Carquin[144f], S. Carrá[46], G. Carratta[23b,23a], J.W.S. Carter[163], T.M. Carter[50], D. Casadei[33c], M.P. Casado[13,f], A.F. Casha[163], E.G. Castiglia[179], F.L. Castillo[61a], L. Castillo Garcia[13], V. Castillo Gimenez[170], N.F. Castro[137a,137e], A. Catinaccio[36], J.R. Catmore[131], V. Cavaliere[29], N. Cavalli[23b,23a], V. Cavasinni[71a,71b], E. Celebi[21a], F. Celli[132], M.S. Centonze[67a,67b], K. Cerny[128], A.S. Cerqueira[80a], A. Cerri[153], L. Cerrito[73a,73b], F. Cerutti[17], A. Cervelli[23b], S.A. Cetin[21d], Z. Chadi[35a], D. Chakraborty[118], M. Chala[137f], J. Chan[177], W.S. Chan[117], W.Y. Chan[90], J.D. Chapman[32], B. Chargeishvili[156b], D.G. Charlton[20], T.P. Charman[92], M. Chatterjee[19], S. Chekanov[6], S.V. Chekulaev[164a], G.A. Chelkov[79,y], A. Chen[104], B. Chen[158], B. Chen[172], C. Chen[60a], H. Chen[14c], H. Chen[29], J. Chen[60c], J. Chen[26], S. Chen[134], S.J. Chen[14c], X. Chen[60c], X. Chen[14b], Y. Chen[60a], C.L. Cheng[177], H.C. Cheng[62a], A. Cheplakov[79], E. Cheremushkina[46], E. Cherepanova[79], R. Cherkaoui El Moursli[35e], E. Cheu[7], K. Cheung[63], L. Chevalier[142], V. Chiarella[51], G. Chiarelli[71a], G. Chiodini[67a], A.S. Chisholm[20], A. Chitan[27b], Y.H. Chiu[172], M.V. Chizhov[79], K. Choi[11], A.R. Chomont[72a,72b], Y. Chou[101], Y.S. Chow[117], T. Chowdhury[33g], L.D. Christopher[33g], M.C. Chu[62a], X. Chu[14a,14d], J. Chudoba[138], J.J. Chwastowski[84], D. Cieri[113], K.M. Ciesla[84], V. Cindro[91], A. Ciocio[17], F. Cirotto[69a,69b], Z.H. Citron[176,j], M. Citterio[68a], D.A. Ciubotaru[27b], B.M. Ciungu[163], A. Clark[54], P.J. Clark[50], J.M. Clavijo Columbie[46], S.E. Clawson[99], C. Clement[45a,45b], L. Clissa[23b,23a], Y. Coadou[100], M. Cobal[66a,66c], A. Coccaro[55b], R.F. Coelho Barrue[137a], R. Coelho Lopes De Sa[101], S. Coelli[68a], H. Cohen[158], A.E.C. Coimbra[36], B. Cole[39], J. Collot[58], P. Conde Muiño[137a,137g], S.H. Connell[33c], I.A. Connelly[57], E.I. Conroy[132], F. Conventi[69a,ae], H.G. Cooke[20], A.M. Cooper-Sarkar[132], F. Cormier[171], L.D. Corpe[36], M. Corradi[72a,72b], E.E. Corrigan[96], F. Corriveau[102,u], M.J. Costa[170], F. Costanza[4], D. Costanzo[146], B.M. Cote[125], G. Cowan[93], J.W. Cowley[32], K. Cranmer[123], S. Crépé-Renaudin[58], F. Crescioli[133], M. Cristinziani[148], M. Cristoforetti[75a,75b], V. Croft[166], G. Crosetti[41b,41a], A. Cueto[36], T. Cuhadar Donszelmann[167], H. Cui[14a,14d], Z. Cui[7], A.R. Cukierman[150], W.R. Cunningham[57], F. Curcio[41b,41a], P. Czodrowski[36], M.M. Czurylo[61b], M.J. Da Cunha Sargedas De Sousa[60a], J.V. Da Fonseca Pinto[80b], C. Da Via[99], W. Dabrowski[83a], T. Dado[47], S. Dahbi[33g], T. Dai[104],

C. Dallapiccola[101], M. Dam[40], G. D'amen[29], V. D'Amico[74a,74b], J. Damp[98], J.R. Dandoy[134], M.F. Daneri[30], M. Danninger[149], V. Dao[36], G. Darbo[55b], S. Darmora[6], A. Dattagupta[129], S. D'Auria[68a,68b], C. David[164b], T. Davidek[140], D.R. Davis[49], B. Davis-Purcell[34], I. Dawson[92], K. De[8], R. De Asmundis[69a], M. De Beurs[117], S. De Castro[23b,23a], N. De Groot[116], P. de Jong[117], H. De la Torre[105], A. De Maria[14c], A. De Salvo[72a], U. De Sanctis[73a,73b], M. De Santis[73a,73b], A. De Santo[153], J.B. De Vivie De Regie[58], D.V. Dedovich[79], J. Degens[117], A.M. Deiana[42], J. Del Peso[97], F. Del Rio[61a], F. Deliot[142], C.M. Delitzsch[47], M. Della Pietra[69a,69b], D. Della Volpe[54], A. Dell'Acqua[36], L. Dell'Asta[68a,68b], M. Delmastro[4], P.A. Delsart[58], S. Demers[179], M. Demichev[79], S.P. Denisov[120], L. D'Eramo[118], D. Derendarz[84], F. Derue[133], P. Dervan[90], K. Desch[24], K. Dette[163], C. Deutsch[24], P.O. Deviveiros[36], F.A. Di Bello[72a,72b], A. Di Ciaccio[73a,73b], L. Di Ciaccio[4], A. Di Domenico[72a,72b], C. Di Donato[69a,69b], A. Di Girolamo[36], G. Di Gregorio[71a,71b], A. Di Luca[75a,75b], B. Di Micco[74a,74b], R. Di Nardo[74a,74b], C. Diaconu[100], F.A. Dias[117], T. Dias Do Vale[149], M.A. Diaz[144a], F.G. Diaz Capriles[24], M. Didenko[170], E.B. Diehl[104], S. Díez Cornell[46], C. Diez Pardos[148], C. Dimitriadi[24,168], A. Dimitrievska[17], W. Ding[14b], J. Dingfelder[24], I-M. Dinu[27b], S.J. Dittmeier[61b], F. Dittus[36], F. Djama[100], T. Djobava[156b], J.I. Djuvsland[16], D. Dodsworth[26], C. Doglioni[99,96], J. Dolejsi[140], Z. Dolezal[140], M. Donadelli[80c], B. Dong[60c], J. Donini[38], A. D'onofrio[14c], M. D'Onofrio[90], J. Dopke[141], A. Doria[69a], M.T. Dova[88], A.T. Doyle[57], E. Drechsler[149], E. Dreyer[176], A.S. Drobac[166], D. Du[60a], T.A. du Pree[117], F. Dubinin[109], M. Dubovsky[28a], E. Duchovni[176], G. Duckeck[112], O.A. Ducu[36,27b], D. Duda[113], A. Dudarev[36], M. D'uffizi[99], L. Duflot[64], M. Dührssen[36], C. Dülsen[178], A.E. Dumitriu[27b], M. Dunford[61a], S. Dungs[47], K. Dunne[45a,45b], A. Duperrin[100], H. Duran Yildiz[3a], M. Düren[56], A. Durglishvili[156b], B. Dutta[46], G.I. Dyckes[17], M. Dyndal[83a], S. Dysch[99], B.S. Dziedzic[84], B. Eckerova[28a], M.G. Eggleston[49], E. Egidio Purcino De Souza[80b], L.F. Ehrke[54], G. Eigen[16], K. Einsweiler[17], T. Ekelof[168], Y. El Ghazali[35b], H. El Jarrari[35e,155], A. El Moussaouy[35a], V. Ellajosyula[168], M. Ellert[168], F. Ellinghaus[178], A.A. Elliot[92], N. Ellis[36], J. Elmsheuser[29], M. Elsing[36], D. Emeliyanov[141], A. Emerman[39], Y. Enari[160], I. Ene[17], J. Erdmann[47], A. Ereditato[19], P.A. Erland[84], M. Errenst[178], M. Escalier[64], C. Escobar[170], E. Etzion[158], G. Evans[137a], H. Evans[65], M.O. Evans[153], A. Ezhilov[135], S. Ezzarqtouni[35a], F. Fabbri[57], L. Fabbri[23b,23a], G. Facini[174], V. Fadeyev[143], R.M. Fakhrutdinov[120], S. Falciano[72a], P.J. Falke[24], S. Falke[36], J. Faltova[140], Y. Fan[14a], Y. Fang[14a], G. Fanourakis[44], M. Fanti[68a,68b], M. Faraj[60c], A. Farbin[8], A. Farilla[74a], T. Farooque[105], S.M. Farrington[50], F. Fassi[35e], D. Fassouliotis[9], M. Faucci Giannelli[73a,73b], W.J. Fawcett[32], L. Fayard[64], O.L. Fedin[135,n], G. Fedotov[135], M. Feickert[169], L. Feligioni[100], A. Fell[146], D.E. Fellers[129], C. Feng[60b], M. Feng[14b], M.J. Fenton[167], A.B. Fenyuk[120], S.W. Ferguson[43], J.A. Fernandez Pretel[52], J. Ferrando[46], A. Ferrari[168], P. Ferrari[117], R. Ferrari[70a], D. Ferrere[54], C. Ferretti[104], F. Fiedler[98], A. Filipčič[91], E.K. Filmer[1], F. Filthaut[116], M.C.N. Fiolhais[137a,137c,a], L. Fiorini[170], F. Fischer[148], W.C. Fisher[105], T. Fitschen[20,64], I. Fleck[148], P. Fleischmann[104], T. Flick[178], L. Flores[134], M. Flores[33d], L.R. Flores Castillo[62a], F.M. Follega[75a,75b], N. Fomin[16], J.H. Foo[163], B.C. Forland[65], A. Formica[142], A.C. Forti[99], E. Fortin[100], A.W. Fortman[59], M.G. Foti[17], L. Fountas[9], D. Fournier[64], H. Fox[89], P. Francavilla[71a,71b], S. Francescato[59], M. Franchini[23b,23a], S. Franchino[61a], D. Francis[36], L. Franco[4], L. Franconi[19], M. Franklin[59], G. Frattari[72a,72b], A.C. Freegard[92], P.M. Freeman[20], W.S. Freund[80b], E.M. Freundlich[47], D. Froidevaux[36], J.A. Frost[132], Y. Fu[60a], M. Fujimoto[124], E. Fullana Torregrosa[170], J. Fuster[170], A. Gabrielli[23b,23a], A. Gabrielli[36], P. Gadow[46], G. Gagliardi[55b,55a], L.G. Gagnon[17], G.E. Gallardo[132], E.J. Gallas[132], B.J. Gallop[141], R. Gamboa Goni[92], K.K. Gan[125], S. Ganguly[160], J. Gao[60a], Y. Gao[50], F.M. Garay Walls[144a,144b], B. Garcia[29], C. García[170], J.E. García Navarro[170], J.A. García Pascual[14a], M. Garcia-Sciveres[17], R.W. Gardner[37], D. Garg[77], R.B. Garg[150], S. Gargiulo[52], C.A. Garner[163], V. Garonne[29], S.J. Gasiorowski[145], P. Gaspar[80b], G. Gaudio[70a], P. Gauzzi[72a,72b], I.L. Gavrilenko[109], A. Gavrilyuk[121], C. Gay[171], G. Gaycken[46], E.N. Gazis[10], A.A. Geanta[27b], C.M. Gee[143], J. Geisen[96], M. Geisen[98], C. Gemme[55b], M.H. Genest[58], S. Gentile[72a,72b], S. George[93], W.F. George[20], T. Geralis[44], L.O. Gerlach[53], P. Gessinger-Befurt[36], M. Ghasemi Bostanabad[172], A. Ghosal[148], A. Ghosh[167], A. Ghosh[7],

B. Giacobbe[23b], S. Giagu[72a,72b], N. Giangiacomi[163], P. Giannetti[71a], A. Giannini[60a], S.M. Gibson[93], M. Gignac[143], D.T. Gil[83b], B.J. Gilbert[39], D. Gillberg[34], G. Gilles[117], N.E.K. Gillwald[46], L. Ginabat[133], D.M. Gingrich[2,ad], M.P. Giordani[66a,66c], P.F. Giraud[142], G. Giugliarelli[66a,66c], D. Giugni[68a], F. Giuli[73a,73b], I. Gkialas[9,g], P. Gkountoumis[10], L.K. Gladilin[111], C. Glasman[97], G.R. Gledhill[129], M. Glisic[129], I. Gnesi[41b,c], Y. Go[29], M. Goblirsch-Kolb[26], D. Godin[108], S. Goldfarb[103], T. Golling[54], M.G.D. Gololo[33g], D. Golubkov[120], J.P. Gombas[105], A. Gomes[137a,137b], A.J. Gomez Delegido[170], R. Goncalves Gama[53], R. Gonçalo[137a,137c], G. Gonella[129], L. Gonella[20], A. Gongadze[79], F. Gonnella[20], J.L. Gonski[39], S. González de la Hoz[170], S. Gonzalez Fernandez[13], R. Gonzalez Lopez[90], C. Gonzalez Renteria[17], R. Gonzalez Suarez[168], S. Gonzalez-Sevilla[54], G.R. Gonzalvo Rodriguez[170], R.Y. González Andana[50], L. Goossens[36], N.A. Gorasia[20], P.A. Gorbounov[121], H.A. Gordon[29], B. Gorini[36], E. Gorini[67a,67b], A. Gorišek[91], A.T. Goshaw[49], M.I. Gostkin[79], C.A. Gottardo[116], M. Gouighri[35b], V. Goumarre[46], A.G. Goussiou[145], N. Govender[33c], C. Goy[4], I. Grabowska-Bold[83a], K. Graham[34], E. Gramstad[131], S. Grancagnolo[18], M. Grandi[153], V. Gratchev[135], P.M. Gravila[27f], F.G. Gravili[67a,67b], H.M. Gray[17], C. Grefe[24], I.M. Gregor[46], P. Grenier[150], K. Grevtsov[46], C. Grieco[13], A.A. Grillo[143], K. Grimm[31,k], S. Grinstein[13,s], J.-F. Grivaz[64], S. Groh[98], E. Gross[176], J. Grosse-Knetter[53], C. Grud[104], A. Grummer[115], J.C. Grundy[132], L. Guan[104], W. Guan[177], C. Gubbels[171], J.G.R. Guerrero Rojas[170], F. Guescini[113], D. Guest[18], R. Gugel[98], A. Guida[46], T. Guillemin[4], S. Guindon[36], F. Guo[14a], J. Guo[60c], L. Guo[64], Y. Guo[104], R. Gupta[46], S. Gurbuz[24], G. Gustavino[36], M. Guth[54], P. Gutierrez[126], L.F. Gutierrez Zagazeta[134], C. Gutschow[94], C. Guyot[142], C. Gwenlan[132], C.B. Gwilliam[90], E.S. Haaland[131], A. Haas[123], M. Habedank[46], C. Haber[17], H.K. Hadavand[8], A. Hadef[98], S. Hadzic[113], M. Haleem[173], J. Haley[127], J.J. Hall[146], G.D. Hallewell[100], L. Halser[19], K. Hamano[172], H. Hamdaoui[35e], M. Hamer[24], G.N. Hamity[50], J. Han[60b], K. Han[60a], L. Han[14c], L. Han[60a], S. Han[17], Y.F. Han[163], K. Hanagaki[81,q], M. Hance[143], D.A. Hangal[39], M.D. Hank[37], R. Hankache[99], E. Hansen[96], J.B. Hansen[40], J.D. Hansen[40], P.H. Hansen[40], K. Hara[165], D. Harada[54], T. Harenberg[178], S. Harkusha[106], Y.T. Harris[132], P.F. Harrison[174], N.M. Hartman[150], N.M. Hartmann[112], Y. Hasegawa[147], A. Hasib[50], S. Haug[19], R. Hauser[105], M. Havranek[139], C.M. Hawkes[20], R.J. Hawkings[36], S. Hayashida[114], D. Hayden[105], C. Hayes[104], R.L. Hayes[171], C.P. Hays[132], J.M. Hays[92], H.S. Hayward[90], F. He[60a], Y. He[161], Y. He[133], M.P. Heath[50], V. Hedberg[96], A.L. Heggelund[131], N.D. Hehir[92], C. Heidegger[52], K.K. Heidegger[52], W.D. Heidorn[78], J. Heilman[34], S. Heim[46], T. Heim[17], B. Heinemann[46,ab], J.G. Heinlein[134], J.J. Heinrich[129], L. Heinrich[36], J. Hejbal[138], L. Helary[46], A. Held[123], C.M. Helling[143], S. Hellman[45a,45b], C. Helsens[36], R.C.W. Henderson[89], L. Henkelmann[32], A.M. Henriques Correia[36], H. Herde[150], Y. Hernández Jiménez[152], H. Herr[98], M.G. Herrmann[112], T. Herrmann[48], G. Herten[52], R. Hertenberger[112], L. Hervas[36], N.P. Hessey[164a], H. Hibi[82], E. Higón-Rodriguez[170], S.J. Hillier[20], I. Hinchliffe[17], F. Hinterkeuser[24], M. Hirose[130], S. Hirose[165], D. Hirschbuehl[178], B. Hiti[91], O. Hladik[138], J. Hobbs[152], R. Hobincu[27e], N. Hod[176], M.C. Hodgkinson[146], B.H. Hodkinson[32], A. Hoecker[36], J. Hofer[46], D. Hohn[52], T. Holm[24], M. Holzbock[113], L.B.A.H. Hommels[32], B.P. Honan[99], J. Hong[60c], T.M. Hong[136], Y. Hong[53], J.C. Honig[52], A. Hönle[113], B.H. Hooberman[169], W.H. Hopkins[6], Y. Horii[114], L.A. Horyn[37], S. Hou[155], J. Howarth[57], J. Hoya[88], M. Hrabovsky[128], A. Hrynevich[107], T. Hryn'ova[4], P.J. Hsu[63], S.-C. Hsu[145], Q. Hu[39], S. Hu[60c], Y.F. Hu[14a,14d,af], D.P. Huang[94], X. Huang[14c], Y. Huang[60a], Y. Huang[14a], Z. Hubacek[139], M. Huebner[24], F. Huegging[24], T.B. Huffman[132], M. Huhtinen[36], S.K. Huiberts[16], R. Hulsken[58], N. Huseynov[12,x], J. Huston[105], J. Huth[59], R. Hyneman[150], S. Hyrych[28a], G. Iacobucci[54], G. Iakovidis[29], I. Ibragimov[148], L. Iconomidou-Fayard[64], P. Iengo[36], R. Iguchi[160], T. Iizawa[54], Y. Ikegami[81], A. Ilg[19], N. Ilic[163], H. Imam[35a], T. Ingebretsen Carlson[45a,45b], G. Introzzi[70a,70b], M. Iodice[74a], V. Ippolito[72a,72b], M. Ishino[160], W. Islam[177], C. Issever[18,46], S. Istin[21a,ag], H. Ito[175], J.M. Iturbe Ponce[62a], R. Iuppa[75a,75b], A. Ivina[176], J.M. Izen[43], V. Izzo[69a], P. Jacka[138], P. Jackson[1], R.M. Jacobs[46], B.P. Jaeger[149], C.S. Jagfeld[112], G. Jäkel[178], K. Jakobs[52], T. Jakoubek[176], J. Jamieson[57], K.W. Janas[83a], G. Jarlskog[96], A.E. Jaspan[90], T. Javůrek[36], M. Javurkova[101], F. Jeanneau[142], L. Jeanty[129], J. Jejelava[156a,v], P. Jenni[52,d], S. Jézéquel[4],

J. Jia[152], X. Jia[59], Z. Jia[14c], Y. Jiang[60a], S. Jiggins[50], J. Jimenez Pena[113], S. Jin[14c], A. Jinaru[27b], O. Jinnouchi[161], H. Jivan[33g], P. Johansson[146], K.A. Johns[7], C.A. Johnson[65], D.M. Jones[32], E. Jones[174], R.W.L. Jones[89], T.J. Jones[90], J. Jovicevic[15], X. Ju[17], J.J. Junggeburth[36], A. Juste Rozas[13,s], S. Kabana[144e], A. Kaczmarska[84], M. Kado[72a,72b], H. Kagan[125], M. Kagan[150], A. Kahn[39], A. Kahn[134], C. Kahra[98], T. Kaji[175], E. Kajomovitz[157], N. Kakati[176], C.W. Kalderon[29], A. Kamenshchikov[163], N.J. Kang[143], Y. Kano[114], D. Kar[33g], K. Karava[132], M.J. Kareem[164b], E. Karentzos[52], I. Karkanias[159], S.N. Karpov[79], Z.M. Karpova[79], V. Kartvelishvili[89], A.N. Karyukhin[120], E. Kasimi[159], C. Kato[60d], J. Katzy[46], S. Kaur[34], K. Kawade[147], K. Kawagoe[87], T. Kawaguchi[114], T. Kawamoto[142], G. Kawamura[53], E.F. Kay[172], F.I. Kaya[166], S. Kazakos[13], V.F. Kazanin[119b,119a], Y. Ke[152], J.M. Keaveney[33a], R. Keeler[172], G.V. Kehris[59], J.S. Keller[34], A.S. Kelly[94], D. Kelsey[153], J.J. Kempster[20], J. Kendrick[20], K.E. Kennedy[39], O. Kepka[138], S. Kersten[178], B.P. Kerševan[91], S. Ketabchi Haghighat[163], M. Khandoga[133], A. Khanov[127], A.G. Kharlamov[119b,119a], T. Kharlamova[119b,119a], E.E. Khoda[145], T.J. Khoo[18], G. Khoriauli[173], E. Khramov[79], J. Khubua[156b], M. Kiehn[36], A. Kilgallon[129], E. Kim[161], Y.K. Kim[37], N. Kimura[94], A. Kirchhoff[53], D. Kirchmeier[48], C. Kirfel[24], J. Kirk[141], A.E. Kiryunin[113], T. Kishimoto[160], D.P. Kisliuk[163], C. Kitsaki[10], O. Kivernyk[24], M. Klassen[61a], C. Klein[34], L. Klein[173], M.H. Klein[104], M. Klein[90], U. Klein[90], P. Klimek[36], A. Klimentov[29], F. Klimpel[113], T. Klingl[24], T. Klioutchnikova[36], F.F. Klitzner[112], P. Kluit[117], S. Kluth[113], E. Kneringer[76], T.M. Knight[163], A. Knue[52], D. Kobayashi[87], R. Kobayashi[85], M. Kocian[150], T. Kodama[160], P. Kodys[140], D.M. Koeck[153], P.T. Koenig[24], T. Koffas[34], N.M. Köhler[36], M. Kolb[142], I. Koletsou[4], T. Komarek[128], K. Köneke[52], A.X.Y. Kong[1], T. Kono[124], N. Konstantinidis[94], B. Konya[96], R. Kopeliansky[65], S. Koperny[83a], K. Korcyl[84], K. Kordas[159], G. Koren[158], A. Korn[94], S. Korn[53], I. Korolkov[13], N. Korotkova[111], B. Kortman[117], O. Kortner[113], S. Kortner[113], W.H. Kostecka[118], V.V. Kostyukhin[148,162], A. Kotsokechagia[64], A. Kotwal[49], A. Koulouris[36], A. Kourkoumeli-Charalampidi[70a,70b], C. Kourkoumelis[9], E. Kourlitis[6], O. Kovanda[153], R. Kowalewski[172], W. Kozanecki[142], A.S. Kozhin[120], V.A. Kramarenko[111], G. Kramberger[91], P. Kramer[98], M.W. Krasny[133], A. Krasznahorkay[36], J.A. Kremer[98], J. Kretzschmar[90], K. Kreul[18], P. Krieger[163], F. Krieter[112], S. Krishnamurthy[101], A. Krishnan[61b], M. Krivos[140], K. Krizka[17], K. Kroeninger[47], H. Kroha[113], J. Kroll[138], J. Kroll[134], K.S. Krowpman[105], U. Kruchonak[79], H. Krüger[24], N. Krumnack[78], M.C. Kruse[49], J.A. Krzysiak[84], A. Kubota[161], O. Kuchinskaia[162], S. Kuday[3a], D. Kuechler[46], J.T. Kuechler[46], S. Kuehn[36], T. Kuhl[46], V. Kukhtin[79], Y. Kulchitsky[106,x], S. Kuleshov[144d,144b], M. Kumar[33g], N. Kumari[100], M. Kuna[58], A. Kupco[138], T. Kupfer[47], O. Kuprash[52], H. Kurashige[82], L.L. Kurchaninov[164a], Y.A. Kurochkin[106], A. Kurova[110], E.S. Kuwertz[36], M. Kuze[161], A.K. Kvam[145], J. Kvita[128], T. Kwan[102], K.W. Kwok[62a], C. Lacasta[170], F. Lacava[72a,72b], H. Lacker[18], D. Lacour[133], N.N. Lad[94], E. Ladygin[79], B. Laforge[133], T. Lagouri[144e], S. Lai[53], I.K. Lakomiec[83a], N. Lalloue[58], J.E. Lambert[126], S. Lammers[65], W. Lampl[7], C. Lampoudis[159], E. Lançon[29], U. Landgraf[52], M.P.J. Landon[92], V.S. Lang[52], J.C. Lange[53], R.J. Langenberg[101], A.J. Lankford[167], F. Lanni[29], K. Lantzsch[24], A. Lanza[70a], A. Lapertosa[55b,55a], J.F. Laporte[142], T. Lari[68a], F. Lasagni Manghi[23b], M. Lassnig[36], V. Latonova[138], T.S. Lau[62a], A. Laudrain[98], A. Laurier[34], M. Lavorgna[69a,69b], S.D. Lawlor[93], Z. Lawrence[99], M. Lazzaroni[68a,68b], B. Le[99], B. Leban[91], A. Lebedev[78], M. LeBlanc[36], T. LeCompte[150], F. Ledroit-Guillon[58], A.C.A. Lee[94], G.R. Lee[16], L. Lee[59], S.C. Lee[155], L.L. Leeuw[33c], B. Lefebvre[164a], H.P. Lefebvre[93], M. Lefebvre[172], C. Leggett[17], K. Lehmann[149], G. Lehmann Miotto[36], W.A. Leight[101], A. Leisos[159,r], M.A.L. Leite[80c], C.E. Leitgeb[46], R. Leitner[140], K.J.C. Leney[42], T. Lenz[24], S. Leone[71a], C. Leonidopoulos[50], A. Leopold[151], C. Leroy[108], R. Les[105], C.G. Lester[32], M. Levchenko[135], J. Levêque[4], D. Levin[104], L.J. Levinson[176], D.J. Lewis[20], B. Li[14b], B. Li[60b], C. Li[60a], C-Q. Li[60c,60d], H. Li[60a], H. Li[60b], H. Li[60b], J. Li[60c], K. Li[145], L. Li[60c], M. Li[14a,14d], Q.Y. Li[60a], S. Li[60d,60c,b], T. Li[60b], X. Li[46], Z. Li[60b], Z. Li[132], Z. Li[102], Z. Li[90], Z. Liang[14a], M. Liberatore[46], B. Liberti[73a], K. Lie[62c], J. Lieber Marin[80b], K. Lin[105], R.A. Linck[65], R.E. Lindley[7], J.H. Lindon[2], A. Linss[46], E. Lipeles[134], A. Lipniacka[16], T.M. Liss[169,ac], A. Lister[171], J.D. Little[4], B. Liu[14a], B.X. Liu[149], D. Liu[60d,60c], J.B. Liu[60a], J.K.K. Liu[32],

K. Liu[60d,60c], M. Liu[60a], M.Y. Liu[60a], P. Liu[14a], Q. Liu[60d,145,60c], X. Liu[60a], Y. Liu[46], Y. Liu[14c,14d], Y.L. Liu[104], Y.W. Liu[60a], M. Livan[70a,70b], J. Llorente Merino[149], S.L. Lloyd[92], E.M. Lobodzinska[46], P. Loch[7], S. Loffredo[73a,73b], T. Lohse[18], K. Lohwasser[146], M. Lokajicek[138], J.D. Long[169], I. Longarini[72a,72b], L. Longo[67a,67b], R. Longo[169], I. Lopez Paz[36], A. Lopez Solis[46], J. Lorenz[112], N. Lorenzo Martinez[4], A.M. Lory[112], A. Lösle[52], X. Lou[45a,45b], X. Lou[14a], A. Lounis[64], J. Love[6], P.A. Love[89], J.J. Lozano Bahilo[170], G. Lu[14a], M. Lu[77], S. Lu[134], Y.J. Lu[63], H.J. Lubatti[145], C. Luci[72a,72b], F.L. Lucio Alves[14c], A. Lucotte[58], F. Luehring[65], I. Luise[152], O. Lundberg[151], B. Lund-Jensen[151], N.A. Luongo[129], M.S. Lutz[158], D. Lynn[29], H. Lyons[90], R. Lysak[138], E. Lytken[96], F. Lyu[14a], V. Lyubushkin[79], T. Lyubushkina[79], H. Ma[29], L.L. Ma[60b], Y. Ma[94], D.M. Mac Donell[172], G. Maccarrone[51], J.C. MacDonald[146], R. Madar[38], W.F. Mader[48], J. Maeda[82], T. Maeno[29], M. Maerker[48], V. Magerl[52], J. Magro[66a,66c], D.J. Mahon[39], C. Maidantchik[80b], A. Maio[137a,137b,137d], K. Maj[83a], O. Majersky[28a], S. Majewski[129], N. Makovec[64], V. Maksimovic[15], B. Malaescu[133], Pa. Malecki[84], V.P. Maleev[135], F. Malek[58], D. Malito[41b,41a], U. Mallik[77], C. Malone[32], S. Maltezos[10], S. Malyukov[79], J. Mamuzic[170], G. Mancini[51], J.P. Mandalia[92], I. Mandić[91], L. Manhaes de Andrade Filho[80a], I.M. Maniatis[159], M. Manisha[142], J. Manjarres Ramos[48], D.C. Mankad[176], K.H. Mankinen[96], A. Mann[112], A. Manousos[76], B. Mansoulie[142], S. Manzoni[36], A. Marantis[159,r], G. Marchiori[5], M. Marcisovsky[138], L. Marcoccia[73a,73b], C. Marcon[96], M. Marinescu[20], M. Marjanovic[126], Z. Marshall[17], S. Marti-Garcia[170], T.A. Martin[174], V.J. Martin[50], B. Martin dit Latour[16], L. Martinelli[72a,72b], M. Martinez[13,s], P. Martinez Agullo[170], V.I. Martinez Outschoorn[101], P. Martinez Suarez[13], S. Martin-Haugh[141], V.S. Martoiu[27b], A.C. Martyniuk[94], A. Marzin[36], S.R. Maschek[113], L. Masetti[98], T. Mashimo[160], J. Masik[99], A.L. Maslennikov[119b,119a], L. Massa[23b], P. Massarotti[69a,69b], P. Mastrandrea[71a,71b], A. Mastroberardino[41b,41a], T. Masubuchi[160], T. Mathisen[168], A. Matic[112], N. Matsuzawa[160], J. Maurer[27b], B. Maček[91], D.A. Maximov[119b,119a], R. Mazini[155], I. Maznas[159], M. Mazza[105], S.M. Mazza[143], C. Mc Ginn[29], J.P. Mc Gowan[102], S.P. Mc Kee[104], T.G. McCarthy[113], W.P. McCormack[17], E.F. McDonald[103], A.E. McDougall[117], J.A. Mcfayden[153], G. Mchedlidze[156b], M.A. McKay[42], R.P. Mckenzie[33g], D.J. Mclaughlin[94], K.D. McLean[172], S.J. McMahon[141], P.C. McNamara[103], R.A. McPherson[172,u], J.E. Mdhluli[33g], S. Meehan[36], T. Megy[38], S. Mehlhase[112], A. Mehta[90], B. Meirose[43], D. Melini[157], B.R. Mellado Garcia[33g], A.H. Melo[53], F. Meloni[46], A. Melzer[24], E.D. Mendes Gouveia[137a], A.M. Mendes Jacques Da Costa[20], H.Y. Meng[163], L. Meng[89], S. Menke[113], M. Mentink[36], E. Meoni[41b,41a], C. Merlassino[132], L. Merola[69a,69b], C. Meroni[68a], G. Merz[104], O. Meshkov[109,111], J.K.R. Meshreki[148], J. Metcalfe[6], A.S. Mete[6], C. Meyer[65], J-P. Meyer[142], M. Michetti[18], R.P. Middleton[141], L. Mijović[50], G. Mikenberg[176], M. Mikestikova[138], M. Mikuž[91], H. Mildner[146], A. Milic[163], C.D. Milke[42], D.W. Miller[37], L.S. Miller[34], A. Milov[176], D.A. Milstead[45a,45b], T. Min[14c], A.A. Minaenko[120], I.A. Minashvili[156b], L. Mince[57], A.I. Mincer[123], B. Mindur[83a], M. Mineev[79], Y. Minegishi[160], Y. Mino[85], L.M. Mir[13], M. Miralles Lopez[170], M. Mironova[132], T. Mitani[175], A. Mitra[174], V.A. Mitsou[170], O. Miu[163], P.S. Miyagawa[92], Y. Miyazaki[87], A. Mizukami[81], J.U. Mjörnmark[96], T. Mkrtchyan[61a], M. Mlynarikova[118], T. Moa[45a,45b], S. Mobius[53], K. Mochizuki[108], P. Moder[46], P. Mogg[112], A.F. Mohammed[14a], S. Mohapatra[39], G. Mokgatitswane[33g], B. Mondal[148], S. Mondal[139], K. Mönig[46], E. Monnier[100], L. Monsonis Romero[170], J. Montejo Berlingen[36], M. Montella[125], F. Monticelli[88], N. Morange[64], A.L. Moreira De Carvalho[137a], M. Moreno Llácer[170], C. Moreno Martinez[13], P. Morettini[55b], S. Morgenstern[174], D. Mori[149], M. Morii[59], M. Morinaga[160], V. Morisbak[131], A.K. Morley[36], L. Morvaj[36], P. Moschovakos[36], B. Moser[117], M. Mosidze[156b], T. Moskalets[52], P. Moskvitina[116], J. Moss[31,l], E.J.W. Moyse[101], S. Muanza[100], J. Mueller[136], R. Mueller[19], D. Muenstermann[89], G.A. Mullier[96], J.J. Mullin[134], D.P. Mungo[68a,68b], J.L. Munoz Martinez[13], F.J. Munoz Sanchez[99], M. Murin[99], W.J. Murray[174,141], A. Murrone[68a,68b], J.M. Muse[126], M. Muškinja[17], C. Mwewa[29], A.G. Myagkov[120,y], A.J. Myers[8], A.A. Myers[136], G. Myers[65], M. Myska[139], B.P. Nachman[17], O. Nackenhorst[47], A.Nag Nag[48], K. Nagai[132], K. Nagano[81], J.L. Nagle[29], E. Nagy[100], A.M. Nairz[36], Y. Nakahama[81], K. Nakamura[81],

H. Nanjo[130], R. Narayan[42], E.A. Narayanan[115], I. Naryshkin[135], M. Naseri[34], C. Nass[24], G. Navarro[22a], J. Navarro-Gonzalez[170], R. Nayak[158], P.Y. Nechaeva[109], F. Nechansky[46], T.J. Neep[20], A. Negri[70a,70b], M. Negrini[23b], C. Nellist[116], C. Nelson[102], K. Nelson[104], S. Nemecek[138], M. Nessi[36,e], M.S. Neubauer[169], F. Neuhaus[98], J. Neundorf[46], R. Newhouse[171], P.R. Newman[20], C.W. Ng[136], Y.S. Ng[18], Y.W.Y. Ng[167], B. Ngair[35e], H.D.N. Nguyen[108], R.B. Nickerson[132], R. Nicolaidou[142], D.S. Nielsen[40], J. Nielsen[143], M. Niemeyer[53], N. Nikiforou[11], V. Nikolaenko[120,y], I. Nikolic-Audit[133], K. Nikolopoulos[20], P. Nilsson[29], H.R. Nindhito[54], A. Nisati[72a], N. Nishu[2], R. Nisius[113], S.J. Noacco Rosende[88], T. Nobe[160], D.L. Noel[32], Y. Noguchi[85], I. Nomidis[133], M.A. Nomura[29], M.B. Norfolk[146], R.R.B. Norisam[94], J. Novak[91], T. Novak[46], O. Novgorodova[48], L. Novotny[139], R. Novotny[115], L. Nozka[128], K. Ntekas[167], E. Nurse[94], F.G. Oakham[34,ad], J. Ocariz[133], A. Ochi[82], I. Ochoa[137a], J.P. Ochoa-Ricoux[144a], S. Oda[87], S. Oerdek[168], A. Ogrodnik[83a], A. Oh[99], C.C. Ohm[151], H. Oide[161], R. Oishi[160], M.L. Ojeda[46], Y. Okazaki[85], M.W. O'Keefe[90], Y. Okumura[160], A. Olariu[27b], L.F. Oleiro Seabra[137a], S.A. Olivares Pino[144e], D. Oliveira Damazio[29], D. Oliveira Goncalves[80a], J.L. Oliver[167], M.J.R. Olsson[167], A. Olszewski[84], J. Olszowska[84], Ö.O. Öncel[52], D.C. O'Neil[149], A.P. O'neill[19], A. Onofre[137a,137e], P.U.E. Onyisi[11], R.G. Oreamuno Madriz[118], M.J. Oreglia[37], G.E. Orellana[88], D. Orestano[74a,74b], N. Orlando[13], R.S. Orr[163], V. O'Shea[57], R. Ospanov[60a], G. Otero y Garzon[30], H. Otono[87], P.S. Ott[61a], G.J. Ottino[17], M. Ouchrif[35d], J. Ouellette[29], F. Ould-Saada[131], M. Owen[57], R.E. Owen[141], K.Y. Oyulmaz[21a], V.E. Ozcan[21a], N. Ozturk[8], S. Ozturk[21d], J. Pacalt[128], H.A. Pacey[32], K. Pachal[49], A. Pacheco Pages[13], C. Padilla Aranda[13], S. Pagan Griso[17], G. Palacino[65], S. Palazzo[50], S. Palestini[36], M. Palka[83b], J. Pan[179], D.K. Panchal[11], C.E. Pandini[117], J.G. Panduro Vazquez[93], P. Pani[46], G. Panizzo[66a,66c], L. Paolozzi[54], C. Papadatos[108], S. Parajuli[42], A. Paramonov[6], C. Paraskevopoulos[10], D. Paredes Hernandez[62b], B. Parida[176], T.H. Park[163], A.J. Parker[31], M.A. Parker[32], F. Parodi[55b,55a], E.W. Parrish[118], V.A. Parrish[50], J.A. Parsons[39], U. Parzefall[52], B. Pascual Dias[108], L. Pascual Dominguez[158], V.R. Pascuzzi[17], F. Pasquali[117], E. Pasqualucci[72a], S. Passaggio[55b], F. Pastore[93], P. Pasuwan[45a,45b], J.R. Pater[99], A. Pathak[177], J. Patton[90], T. Pauly[36], J. Pearkes[150], M. Pedersen[131], R. Pedro[137a], S.V. Peleganchuk[119b,119a], O. Penc[138], C. Peng[62b], H. Peng[60a], M. Penzin[162], B.S. Peralva[80a], A.P. Pereira Peixoto[58], L. Pereira Sanchez[45a,45b], D.V. Perepelitsa[29], E. Perez Codina[164a], M. Perganti[10], L. Perini[68a,68b], H. Pernegger[36], S. Perrella[36], A. Perrevoort[116], O. Perrin[38], K. Peters[46], R.F.Y. Peters[99], B.A. Petersen[36], T.C. Petersen[40], E. Petit[100], V. Petousis[139], C. Petridou[159], A. Petrukhin[148], M. Pettee[17], N.E. Pettersson[36], K. Petukhova[140], A. Peyaud[142], R. Pezoa[144f], L. Pezzotti[36], G. Pezzullo[179], T. Pham[103], P.W. Phillips[141], M.W. Phipps[169], G. Piacquadio[152], E. Pianori[17], F. Piazza[68a,68b], R. Piegaia[30], D. Pietreanu[27b], A.D. Pilkington[99], M. Pinamonti[66a,66c], J.L. Pinfold[2], C. Pitman Donaldson[94], D.A. Pizzi[34], L. Pizzimento[73a,73b], A. Pizzini[117], M.-A. Pleier[29], V. Plesanovs[52], V. Pleskot[140], E. Plotnikova[79], G. Poddar[4], R. Poettgen[96], R. Poggi[54], L. Poggioli[133], I. Pogrebnyak[105], D. Pohl[24], I. Pokharel[53], S. Polacek[140], G. Polesello[70a], A. Poley[149,164a], R. Polifka[139], A. Polini[23b], C.S. Pollard[132], Z.B. Pollock[125], V. Polychronakos[29], D. Ponomarenko[110], L. Pontecorvo[36], S. Popa[27a], G.A. Popeneciu[27d], D.M. Portillo Quintero[164a], S. Pospisil[139], P. Postolache[27c], K. Potamianos[132], I.N. Potrap[79], C.J. Potter[32], H. Potti[1], T. Poulsen[46], J. Poveda[170], G. Pownall[46], M.E. Pozo Astigarraga[36], A. Prades Ibanez[170], P. Pralavorio[100], M.M. Prapa[44], D. Price[99], M. Primavera[67a], M.A. Principe Martin[97], M.L. Proffitt[145], N. Proklova[110], K. Prokofiev[62c], F. Prokoshin[79], G. Proto[73a,73b], S. Protopopescu[29], J. Proudfoot[6], M. Przybycien[83a], D. Pudzha[135], P. Puzo[64], D. Pyatiizbyantseva[110], J. Qian[104], Y. Qin[99], T. Qiu[92], A. Quadt[53], M. Queitsch-Maitland[24], G. Rabanal Bolanos[59], D. Rafanoharana[52], F. Ragusa[68a,68b], J.A. Raine[54], S. Rajagopalan[29], K. Ran[14a,14d], V. Raskina[133], D.F. Rassloff[61a], S. Rave[98], B. Ravina[57], I. Ravinovich[176], M. Raymond[36], A.L. Read[131], N.P. Readioff[146], D.M. Rebuzzi[70a,70b], G. Redlinger[29], K. Reeves[43], D. Reikher[158], A. Reiss[98], A. Rej[148], C. Rembser[36], A. Renardi[46], M. Renda[27b], M.B. Rendel[113], A.G. Rennie[57], S. Resconi[68a], M. Ressegotti[55b,55a], E.D. Resseguie[17], S. Rettie[94], B. Reynolds[125], E. Reynolds[17], M. Rezaei Estabragh[178], O.L. Rezanova[119b,119a], P. Reznicek[140], E. Ricci[75a,75b], R. Richter[113],

S. Richter[45a,45b], E. Richter-Was[83b], M. Ridel[133], P. Rieck[123], P. Riedler[36], M. Rijssenbeek[152], A. Rimoldi[70a,70b], M. Rimoldi[46], L. Rinaldi[23b,23a], T.T. Rinn[169], M.P. Rinnagel[112], G. Ripellino[151], I. Riu[13], P. Rivadeneira[46], J.C. Rivera Vergara[172], F. Rizatdinova[127], E. Rizvi[92], C. Rizzi[54], B.A. Roberts[174], B.R. Roberts[17], S.H. Robertson[102,u], M. Robin[46], D. Robinson[32], C.M. Robles Gajardo[144f], M. Robles Manzano[98], A. Robson[57], A. Rocchi[73a,73b], C. Roda[71a,71b], S. Rodriguez Bosca[61a], Y. Rodriguez Garcia[22a], A. Rodriguez Rodriguez[52], A.M. Rodríguez Vera[164b], S. Roe[36], J.T. Roemer[167], A.R. Roepe[126], J. Roggel[178], O. Røhne[131], R.A. Rojas[172], B. Roland[52], C.P.A. Roland[65], J. Roloff[29], A. Romaniouk[110], M. Romano[23b], A.C. Romero Hernandez[169], N. Rompotis[90], M. Ronzani[123], L. Roos[133], S. Rosati[72a], B.J. Rosser[134], E. Rossi[4], E. Rossi[69a,69b], L.P. Rossi[55b], L. Rossini[46], R. Rosten[125], M. Rotaru[27b], B. Rottler[52], D. Rousseau[64], D. Rousso[32], G. Rovelli[70a,70b], A. Roy[169], A. Rozanov[100], Y. Rozen[157], X. Ruan[33g], A.J. Ruby[90], T.A. Ruggeri[1], F. Rühr[52], A. Ruiz-Martinez[170], A. Rummler[36], Z. Rurikova[52], N.A. Rusakovich[79], H.L. Russell[172], L. Rustige[38], J.P. Rutherfoord[7], E.M. Rüttinger[146], K. Rybacki[89], M. Rybar[140], E.B. Rye[131], A. Ryzhov[120], J.A. Sabater Iglesias[54], P. Sabatini[170], L. Sabetta[72a,72b], H.F-W. Sadrozinski[143], R. Sadykov[79], F. Safai Tehrani[72a], B. Safarzadeh Samani[153], M. Safdari[150], S. Saha[102], M. Sahinsoy[113], A. Sahu[178], M. Saimpert[142], M. Saito[160], T. Saito[160], D. Salamani[36], G. Salamanna[74a,74b], A. Salnikov[150], J. Salt[170], A. Salvador Salas[13], D. Salvatore[41b,41a], F. Salvatore[153], A. Salzburger[36], D. Sammel[52], D. Sampsonidis[159], D. Sampsonidou[60d,60c], J. Sánchez[170], A. Sanchez Pineda[4], V. Sanchez Sebastian[170], H. Sandaker[131], C.O. Sander[46], I.G. Sanderswood[89], J.A. Sandesara[101], M. Sandhoff[178], C. Sandoval[22b], D.P.C. Sankey[141], A. Sansoni[51], C. Santoni[38], H. Santos[137a,137b], S.N. Santpur[17], A. Santra[176], K.A. Saoucha[146], A. Sapronov[79], J.G. Saraiva[137a,137d], J. Sardain[100], O. Sasaki[81], K. Sato[165], C. Sauer[61b], F. Sauerburger[52], E. Sauvan[4], P. Savard[163,ad], R. Sawada[160], C. Sawyer[141], L. Sawyer[95], I. Sayago Galvan[170], C. Sbarra[23b], A. Sbrizzi[23b,23a], T. Scanlon[94], J. Schaarschmidt[145], P. Schacht[113], D. Schaefer[37], U. Schäfer[98], A.C. Schaffer[64], D. Schaile[112], R.D. Schamberger[152], E. Schanet[112], C. Scharf[18], N. Scharmberg[99], V.A. Schegelsky[135], D. Scheirich[140], F. Schenck[18], M. Schernau[167], C. Scheulen[53], C. Schiavi[55b,55a], Z.M. Schillaci[26], E.J. Schioppa[67a,67b], M. Schioppa[41b,41a], B. Schlag[98], K.E. Schleicher[52], S. Schlenker[36], K. Schmieden[98], C. Schmitt[98], S. Schmitt[46], L. Schoeffel[142], A. Schoening[61b], P.G. Scholer[52], E. Schopf[132], M. Schott[98], J. Schovancova[36], S. Schramm[54], F. Schroeder[178], H-C. Schultz-Coulon[61a], M. Schumacher[52], B.A. Schumm[143], Ph. Schune[142], A. Schwartzman[150], T.A. Schwarz[104], Ph. Schwemling[142], R. Schwienhorst[105], A. Sciandra[143], G. Sciolla[26], F. Scuri[71a], F. Scutti[103], C.D. Sebastiani[90], K. Sedlaczek[47], P. Seema[18], S.C. Seidel[115], A. Seiden[143], B.D. Seidlitz[29], T. Seiss[37], C. Seitz[46], J.M. Seixas[80b], G. Sekhniaidze[69a], S.J. Sekula[42], L. Selem[4], N. Semprini-Cesari[23b,23a], S. Sen[49], V. Senthilkumar[170], L. Serin[64], L. Serkin[66a,66b], M. Sessa[74a,74b], H. Severini[126], S. Sevova[150], F. Sforza[55b,55a], A. Sfyrla[54], E. Shabalina[53], R. Shaheen[151], J.D. Shahinian[134], N.W. Shaikh[45a,45b], D. Shaked Renous[176], L.Y. Shan[14a], M. Shapiro[17], A. Sharma[36], A.S. Sharma[1], S. Sharma[46], P.B. Shatalov[121], K. Shaw[153], S.M. Shaw[99], P. Sherwood[94], L. Shi[94], C.O. Shimmin[179], Y. Shimogama[175], J.D. Shinner[93], I.P.J. Shipsey[132], S. Shirabe[54], M. Shiyakova[79], J. Shlomi[176], M.J. Shochet[37], J. Shojaii[103], D.R. Shope[151], S. Shrestha[125], E.M. Shrif[33g], M.J. Shroff[172], P. Sicho[138], A.M. Sickles[169], E. Sideras Haddad[33g], O. Sidiropoulou[36], A. Sidoti[23b], F. Siegert[48], Dj. Sijacki[15], F. Sili[88], J.M. Silva[20], M.V. Silva Oliveira[36], S.B. Silverstein[45a], S. Simion[64], R. Simoniello[36], E.L. Simpson[57], N.D. Simpson[96], S. Simsek[21d], S. Sindhu[53], P. Sinervo[163], V. Sinetckii[111], S. Singh[149], S. Singh[163], S. Sinha[46], S. Sinha[33g], M. Sioli[23b,23a], I. Siral[129], S.Yu. Sivoklokov[111], J. Sjölin[45a,45b], A. Skaf[53], E. Skorda[96], P. Skubic[126], M. Slawinska[84], V. Smakhtin[176], B.H. Smart[141], J. Smiesko[140], S.Yu. Smirnov[110], Y. Smirnov[110], L.N. Smirnova[111,p], O. Smirnova[96], E.A. Smith[37], H.A. Smith[132], R. Smith[150], M. Smizanska[89], K. Smolek[139], A. Smykiewicz[84], A.A. Snesarev[109], H.L. Snoek[117], S. Snyder[29], R. Sobie[172,u], A. Soffer[158], C.A. Solans Sanchez[36], E.Yu. Soldatov[110], U. Soldevila[170], A.A. Solodkov[120], S. Solomon[52], A. Soloshenko[79], K. Solovieva[52], O.V. Solovyanov[120], V. Solovyev[135], P. Sommer[146], H. Son[166],

A. Sonay[13], W.Y. Song[164b], A. Sopczak[139], A.L. Sopio[94], F. Sopkova[28b], V. Sothilingam[61a], S. Sottocornola[70a,70b], R. Soualah[122c], A.M. Soukharev[119b,119a], Z. Soumaimi[35e], D. South[46], S. Spagnolo[67a,67b], M. Spalla[113], M. Spangenberg[174], F. Spanò[93], D. Sperlich[52], G. Spigo[36], M. Spina[153], S. Spinali[89], D.P. Spiteri[57], M. Spousta[140], E.J. Staats[34], A. Stabile[68a,68b], B.L. Stamas[118], R. Stamen[61a], M. Stamenkovic[117], A. Stampekis[20], M. Standke[24], E. Stanecka[84], B. Stanislaus[17], M.M. Stanitzki[46], M. Stankaityte[132], B. Stapf[46], E.A. Starchenko[120], G.H. Stark[143], J. Stark[100], D.M. Starko[164b], P. Staroba[138], P. Starovoitov[61a], S. Stärz[102], R. Staszewski[84], G. Stavropoulos[44], J. Steentoft[168], P. Steinberg[29], A.L. Steinhebel[129], B. Stelzer[149,164a], H.J. Stelzer[136], O. Stelzer-Chilton[164a], H. Stenzel[56], T.J. Stevenson[153], G.A. Stewart[36], M.C. Stockton[36], G. Stoicea[27b], M. Stolarski[137a], S. Stonjek[113], A. Straessner[48], J. Strandberg[151], S. Strandberg[45a,45b], M. Strauss[126], T. Strebler[100], P. Strizenec[28b], R. Ströhmer[173], D.M. Strom[129], L.R. Strom[46], R. Stroynowski[42], A. Strubig[45a,45b], S.A. Stucci[29], B. Stugu[16], J. Stupak[126], N.A. Styles[46], D. Su[150], S. Su[60a], W. Su[60d,145,60c], X. Su[60a,64], K. Sugizaki[160], V.V. Sulin[109], M.J. Sullivan[90], D.M.S. Sultan[75a,75b], L. Sultanaliyeva[109], S. Sultansoy[3b], T. Sumida[85], S. Sun[104], S. Sun[177], O. Sunneborn Gudnadottir[168], M.R. Sutton[153], M. Svatos[138], M. Swiatlowski[164a], T. Swirski[173], I. Sykora[28a], M. Sykora[140], T. Sykora[140], D. Ta[98], K. Tackmann[46,t], A. Taffard[167], R. Tafirout[164a], R.H.M. Taibah[133], R. Takashima[86], K. Takeda[82], E.P. Takeva[50], Y. Takubo[81], M. Talby[100], A.A. Talyshev[119b,119a], K.C. Tam[62b], N.M. Tamir[158], A. Tanaka[160], J. Tanaka[160], R. Tanaka[64], J. Tang[60c], Z. Tao[171], S. Tapia Araya[78], S. Tapprogge[98], A. Tarek Abouelfadl Mohamed[105], S. Tarem[157], K. Tariq[60b], G. Tarna[27b], G.F. Tartarelli[68a], P. Tas[140], M. Tasevsky[138], E. Tassi[41b,41a], G. Tateno[160], Y. Tayalati[35e], G.N. Taylor[103], W. Taylor[164b], H. Teagle[90], A.S. Tee[177], R. Teixeira De Lima[150], P. Teixeira-Dias[93], J.J. Teoh[163], K. Terashi[160], J. Terron[97], S. Terzo[13], M. Testa[51], R.J. Teuscher[163,u], N. Themistokleous[50], T. Theveneaux-Pelzer[18], O. Thielmann[178], D.W. Thomas[93], J.P. Thomas[20], E.A. Thompson[46], P.D. Thompson[20], E. Thomson[134], E.J. Thorpe[92], Y. Tian[53], V.O. Tikhomirov[109,z], Yu.A. Tikhonov[119b,119a], S. Timoshenko[110], E.X.L. Ting[1], P. Tipton[179], S. Tisserant[100], S.H. Tlou[33g], A. Tnourji[38], K. Todome[23b,23a], S. Todorova-Nova[140], S. Todt[48], M. Togawa[81], J. Tojo[87], S. Tokár[28a], K. Tokushuku[81], R. Tombs[32], M. Tomoto[81,114], L. Tompkins[150], P. Tornambe[101], E. Torrence[129], H. Torres[48], E. Torró Pastor[170], M. Toscani[30], C. Tosciri[37], D.R. Tovey[146], A. Traeet[16], I.S. Trandafir[27b], C.J. Treado[123], T. Trefzger[173], A. Tricoli[29], I.M. Trigger[164a], S. Trincaz-Duvoid[133], D.A. Trischuk[171], W. Trischuk[163], B. Trocmé[58], A. Trofymov[64], C. Troncon[68a], F. Trovato[153], L. Truong[33c], M. Trzebinski[84], A. Trzupek[84], F. Tsai[152], M. Tsai[104], A. Tsiamis[159], P.V. Tsiareshka[106], A. Tsirigotis[159,r], V. Tsiskaridze[152], E.G. Tskhadadze[156a], M. Tsopoulou[159], Y. Tsujikawa[85], I.I. Tsukerman[121], V. Tsulaia[17], S. Tsuno[81], O. Tsur[157], D. Tsybychev[152], Y. Tu[62b], A. Tudorache[27b], V. Tudorache[27b], A.N. Tuna[36], S. Turchikhin[79], I. Turk Cakir[3a], R. Turra[68a], P.M. Tuts[39], S. Tzamarias[159], P. Tzanis[10], E. Tzovara[98], K. Uchida[160], F. Ukegawa[165], P.A. Ulloa Poblete[144c], G. Unal[36], M. Unal[11], A. Undrus[29], G. Unel[167], K. Uno[160], J. Urban[28b], P. Urquijo[103], G. Usai[8], R. Ushioda[161], M. Usman[108], Z. Uysal[21b], V. Vacek[139], B. Vachon[102], K.O.H. Vadla[131], T. Vafeiadis[36], C. Valderanis[112], E. Valdes Santurio[45a,45b], M. Valente[164a], S. Valentinetti[23b,23a], A. Valero[170], A. Vallier[100], J.A. Valls Ferrer[170], T.R. Van Daalen[145], P. Van Gemmeren[6], S. Van Stroud[94], I. Van Vulpen[117], M. Vanadia[73a,73b], W. Vandelli[36], M. Vandenbroucke[142], E.R. Vandewall[127], D. Vannicola[158], L. Vannoli[55b,55a], R. Vari[72a], E.W. Varnes[7], C. Varni[17], T. Varol[155], D. Varouchas[64], K.E. Varvell[154], M.E. Vasile[27b], L. Vaslin[38], G.A. Vasquez[172], F. Vazeille[38], D. Vazquez Furelos[13], T. Vazquez Schroeder[36], J. Veatch[53], V. Vecchio[99], M.J. Veen[117], I. Veliscek[132], L.M. Veloce[163], F. Veloso[137a,137c], S. Veneziano[72a], A. Ventura[67a,67b], A. Verbytskyi[113], M. Verducci[71a,71b], C. Vergis[24], M. Verissimo De Araujo[80b], W. Verkerke[117], J.C. Vermeulen[117], C. Vernieri[150], P.J. Verschuuren[93], M. Vessella[101], M.L. Vesterbacka[123], M.C. Vetterli[149,ad], A. Vgenopoulos[159], N. Viaux Maira[144f], T. Vickey[146], O.E. Vickey Boeriu[146], G.H.A. Viehhauser[132], L. Vigani[61b], M. Villa[23b,23a], M. Villaplana Perez[170], E.M. Villhauer[50], E. Vilucchi[51], M.G. Vincter[34], G.S. Virdee[20], A. Vishwakarma[50], C. Vittori[23b,23a], I. Vivarelli[153], V. Vladimirov[174], E. Voevodina[113],

M. Vogel[178], P. Vokac[139], J. Von Ahnen[46], E. Von Toerne[24], B. Vormwald[36], V. Vorobel[140], K. Vorobev[110], M. Vos[170], J.H. Vossebeld[90], M. Vozak[117], L. Vozdecky[92], N. Vranjes[15], M. Vranjes Milosavljevic[15], V. Vrba[139,*], M. Vreeswijk[117], N.K. Vu[100], R. Vuillermet[36], O.V. Vujinovic[98], I. Vukotic[37], S. Wada[165], C. Wagner[101], W. Wagner[178], S. Wahdan[178], H. Wahlberg[88], R. Wakasa[165], M. Wakida[114], V.M. Walbrecht[113], J. Walder[141], R. Walker[112], W. Walkowiak[148], A.M. Wang[59], A.Z. Wang[177], C. Wang[60a], C. Wang[60c], H. Wang[17], J. Wang[62a], P. Wang[42], R.-J. Wang[98], R. Wang[59], R. Wang[6], S.M. Wang[155], S. Wang[60b], T. Wang[60a], W.T. Wang[77], W.X. Wang[60a], X. Wang[14c], X. Wang[169], X. Wang[60c], Y. Wang[60d], Z. Wang[104], Z. Wang[60d,49,60c], Z. Wang[104], A. Warburton[102], R.J. Ward[20], N. Warrack[57], A.T. Watson[20], M.F. Watson[20], G. Watts[145], B.M. Waugh[94], A.F. Webb[11], C. Weber[29], M.S. Weber[19], S.A. Weber[34], S.M. Weber[61a], C. Wei[60a], Y. Wei[132], A.R. Weidberg[132], J. Weingarten[47], M. Weirich[98], C. Weiser[52], T. Wenaus[29], B. Wendland[47], T. Wengler[36], N.S. Wenke[113], N. Wermes[24], M. Wessels[61a], K. Whalen[129], A.M. Wharton[89], A.S. White[59], A. White[8], M.J. White[1], D. Whiteson[167], L. Wickremasinghe[130], W. Wiedenmann[177], C. Wiel[48], M. Wielers[141], N. Wieseotte[98], C. Wiglesworth[40], L.A.M. Wiik-Fuchs[52], D.J. Wilbern[126], H.G. Wilkens[36], D.M. Williams[39], H.H. Williams[134], S. Williams[32], S. Willocq[101], P.J. Windischhofer[132], F. Winklmeier[129], B.T. Winter[52], M. Wittgen[150], M. Wobisch[95], A. Wolf[98], R. Wölker[132], J. Wollrath[167], M.W. Wolter[84], H. Wolters[137a,137c], V.W.S. Wong[171], A.F. Wongel[46], S.D. Worm[46], B.K. Wosiek[84], K.W. Woźniak[84], K. Wraight[57], J. Wu[14a,14d], S.L. Wu[177], X. Wu[54], Y. Wu[60a], Z. Wu[142,60a], J. Wuerzinger[132], T.R. Wyatt[99], B.M. Wynne[50], S. Xella[40], L. Xia[14c], M. Xia[14b], J. Xiang[62c], X. Xiao[104], M. Xie[60a], X. Xie[60a], I. Xiotidis[153], D. Xu[14a], H. Xu[60a], H. Xu[60a], L. Xu[60a], R. Xu[134], T. Xu[60a], W. Xu[104], Y. Xu[14b], Z. Xu[60b], Z. Xu[150], B. Yabsley[154], S. Yacoob[33a], N. Yamaguchi[87], Y. Yamaguchi[161], H. Yamauchi[165], T. Yamazaki[17], Y. Yamazaki[82], J. Yan[60c], S. Yan[132], Z. Yan[25], H.J. Yang[60c,60d], H.T. Yang[17], S. Yang[60a], T. Yang[62c], X. Yang[60a], X. Yang[14a], Y. Yang[42], Z. Yang[104,60a], W-M. Yao[17], Y.C. Yap[46], H. Ye[14c], J. Ye[42], S. Ye[29], X. Ye[60a], I. Yeletskikh[79], M.R. Yexley[89], P. Yin[39], K. Yorita[175], C.J.S. Young[52], C. Young[150], M. Yuan[104], R. Yuan[60b,h], X. Yue[61a], M. Zaazoua[35e], B. Zabinski[84], G. Zacharis[10], E. Zaid[50], A.M. Zaitsev[120,y], T. Zakareishvili[156b], N. Zakharchuk[34], S. Zambito[36], D. Zanzi[52], O. Zaplatilek[139], S.V. Zeißner[47], C. Zeitnitz[178], J.C. Zeng[169], D.T. Zenger Jr[26], O. Zenin[120], T. Ženiš[28a], S. Zenz[92], S. Zerradi[35a], D. Zerwas[64], B. Zhang[14c], D.F. Zhang[146], G. Zhang[14b], J. Zhang[6], K. Zhang[14a], L. Zhang[14c], M. Zhang[169], R. Zhang[177], S. Zhang[104], X. Zhang[60c], X. Zhang[60b], Z. Zhang[64], H. Zhao[145], P. Zhao[49], T. Zhao[60b], Y. Zhao[143], Z. Zhao[60a], A. Zhemchugov[79], Z. Zheng[150], D. Zhong[169], B. Zhou[104], C. Zhou[177], H. Zhou[7], N. Zhou[60c], Y. Zhou[7], C.G. Zhu[60b], C. Zhu[14a,14d], H.L. Zhu[60a], H. Zhu[14a], J. Zhu[104], Y. Zhu[60a], X. Zhuang[14a], K. Zhukov[109], V. Zhulanov[119b,119a], D. Zieminska[65], N.I. Zimine[79], S. Zimmermann[52,*], J. Zinsser[61b], M. Ziolkowski[148], L. Živković[15], A. Zoccoli[23b,23a], K. Zoch[54], T.G. Zorbas[146], O. Zormpa[44], W. Zou[39], L. Zwalinski[36].

[1]Department of Physics, University of Adelaide, Adelaide; Australia.
[2]Department of Physics, University of Alberta, Edmonton AB; Canada.
[3(a)]Department of Physics, Ankara University, Ankara;[(b)]Division of Physics, TOBB University of Economics and Technology, Ankara; Turkey.
[4]LAPP, Univ. Savoie Mont Blanc, CNRS/IN2P3, Annecy ; France.
[5]Université de Paris, CNRS/IN2P3, AstroParticule et Cosmologie, Paris; France.
[6]High Energy Physics Division, Argonne National Laboratory, Argonne IL; United States of America.
[7]Department of Physics, University of Arizona, Tucson AZ; United States of America.
[8]Department of Physics, University of Texas at Arlington, Arlington TX; United States of America.
[9]Physics Department, National and Kapodistrian University of Athens, Athens; Greece.
[10]Physics Department, National Technical University of Athens, Zografou; Greece.
[11]Department of Physics, University of Texas at Austin, Austin TX; United States of America.

[12]Institute of Physics, Azerbaijan Academy of Sciences, Baku; Azerbaijan.
[13]Institut de Física d'Altes Energies (IFAE), Barcelona Institute of Science and Technology, Barcelona; Spain.
[14(a)]Institute of High Energy Physics, Chinese Academy of Sciences, Beijing;[(b)]Physics Department, Tsinghua University, Beijing;[(c)]Department of Physics, Nanjing University, Nanjing;[(d)]University of Chinese Academy of Science (UCAS), Beijing; China.
[15]Institute of Physics, University of Belgrade, Belgrade; Serbia.
[16]Department for Physics and Technology, University of Bergen, Bergen; Norway.
[17]Physics Division, Lawrence Berkeley National Laboratory and University of California, Berkeley CA; United States of America.
[18]Institut für Physik, Humboldt Universität zu Berlin, Berlin; Germany.
[19]Albert Einstein Center for Fundamental Physics and Laboratory for High Energy Physics, University of Bern, Bern; Switzerland.
[20]School of Physics and Astronomy, University of Birmingham, Birmingham; United Kingdom.
[21(a)]Department of Physics, Bogazici University, Istanbul;[(b)]Department of Physics Engineering, Gaziantep University, Gaziantep;[(c)]Department of Physics, Istanbul University, Istanbul;[(d)]Istinye University, Sariyer, Istanbul; Turkey.
[22(a)]Facultad de Ciencias y Centro de Investigaciónes, Universidad Antonio Nariño, Bogotá;[(b)]Departamento de Física, Universidad Nacional de Colombia, Bogotá; Colombia.
[23(a)]Dipartimento di Fisica e Astronomia A. Righi, Università di Bologna, Bologna;[(b)]INFN Sezione di Bologna; Italy.
[24]Physikalisches Institut, Universität Bonn, Bonn; Germany.
[25]Department of Physics, Boston University, Boston MA; United States of America.
[26]Department of Physics, Brandeis University, Waltham MA; United States of America.
[27(a)]Transilvania University of Brasov, Brasov;[(b)]Horia Hulubei National Institute of Physics and Nuclear Engineering, Bucharest;[(c)]Department of Physics, Alexandru Ioan Cuza University of Iasi, Iasi;[(d)]National Institute for Research and Development of Isotopic and Molecular Technologies, Physics Department, Cluj-Napoca;[(e)]University Politehnica Bucharest, Bucharest;[(f)]West University in Timisoara, Timisoara; Romania.
[28(a)]Faculty of Mathematics, Physics and Informatics, Comenius University, Bratislava;[(b)]Department of Subnuclear Physics, Institute of Experimental Physics of the Slovak Academy of Sciences, Kosice; Slovak Republic.
[29]Physics Department, Brookhaven National Laboratory, Upton NY; United States of America.
[30]Departamento de Física (FCEN) and IFIBA, Universidad de Buenos Aires and CONICET, Buenos Aires; Argentina.
[31]California State University, CA; United States of America.
[32]Cavendish Laboratory, University of Cambridge, Cambridge; United Kingdom.
[33(a)]Department of Physics, University of Cape Town, Cape Town;[(b)]iThemba Labs, Western Cape;[(c)]Department of Mechanical Engineering Science, University of Johannesburg, Johannesburg;[(d)]National Institute of Physics, University of the Philippines Diliman (Philippines);[(e)]University of South Africa, Department of Physics, Pretoria;[(f)]University of Zululand, KwaDlangezwa;[(g)]School of Physics, University of the Witwatersrand, Johannesburg; South Africa.
[34]Department of Physics, Carleton University, Ottawa ON; Canada.
[35(a)]Faculté des Sciences Ain Chock, Réseau Universitaire de Physique des Hautes Energies - Université Hassan II, Casablanca;[(b)]Faculté des Sciences, Université Ibn-Tofail, Kénitra;[(c)]Faculté des Sciences Semlalia, Université Cadi Ayyad, LPHEA-Marrakech;[(d)]LPMR, Faculté des Sciences, Université Mohamed Premier, Oujda;[(e)]Faculté des sciences, Université Mohammed V, Rabat;[(f)]Mohammed VI

Polytechnic University, Ben Guerir; Morocco.
[36]CERN, Geneva; Switzerland.
[37]Enrico Fermi Institute, University of Chicago, Chicago IL; United States of America.
[38]LPC, Université Clermont Auvergne, CNRS/IN2P3, Clermont-Ferrand; France.
[39]Nevis Laboratory, Columbia University, Irvington NY; United States of America.
[40]Niels Bohr Institute, University of Copenhagen, Copenhagen; Denmark.
[41(a)]Dipartimento di Fisica, Università della Calabria, Rende;[(b)]INFN Gruppo Collegato di Cosenza, Laboratori Nazionali di Frascati; Italy.
[42]Physics Department, Southern Methodist University, Dallas TX; United States of America.
[43]Physics Department, University of Texas at Dallas, Richardson TX; United States of America.
[44]National Centre for Scientific Research "Demokritos", Agia Paraskevi; Greece.
[45(a)]Department of Physics, Stockholm University;[(b)]Oskar Klein Centre, Stockholm; Sweden.
[46]Deutsches Elektronen-Synchrotron DESY, Hamburg and Zeuthen; Germany.
[47]Fakultät Physik , Technische Universität Dortmund, Dortmund; Germany.
[48]Institut für Kern- und Teilchenphysik, Technische Universität Dresden, Dresden; Germany.
[49]Department of Physics, Duke University, Durham NC; United States of America.
[50]SUPA - School of Physics and Astronomy, University of Edinburgh, Edinburgh; United Kingdom.
[51]INFN e Laboratori Nazionali di Frascati, Frascati; Italy.
[52]Physikalisches Institut, Albert-Ludwigs-Universität Freiburg, Freiburg; Germany.
[53]II. Physikalisches Institut, Georg-August-Universität Göttingen, Göttingen; Germany.
[54]Département de Physique Nucléaire et Corpusculaire, Université de Genève, Genève; Switzerland.
[55(a)]Dipartimento di Fisica, Università di Genova, Genova;[(b)]INFN Sezione di Genova; Italy.
[56]II. Physikalisches Institut, Justus-Liebig-Universität Giessen, Giessen; Germany.
[57]SUPA - School of Physics and Astronomy, University of Glasgow, Glasgow; United Kingdom.
[58]LPSC, Université Grenoble Alpes, CNRS/IN2P3, Grenoble INP, Grenoble; France.
[59]Laboratory for Particle Physics and Cosmology, Harvard University, Cambridge MA; United States of America.
[60(a)]Department of Modern Physics and State Key Laboratory of Particle Detection and Electronics, University of Science and Technology of China, Hefei;[(b)]Institute of Frontier and Interdisciplinary Science and Key Laboratory of Particle Physics and Particle Irradiation (MOE), Shandong University, Qingdao;[(c)]School of Physics and Astronomy, Shanghai Jiao Tong University, Key Laboratory for Particle Astrophysics and Cosmology (MOE), SKLPPC, Shanghai;[(d)]Tsung-Dao Lee Institute, Shanghai; China.
[61(a)]Kirchhoff-Institut für Physik, Ruprecht-Karls-Universität Heidelberg, Heidelberg;[(b)]Physikalisches Institut, Ruprecht-Karls-Universität Heidelberg, Heidelberg; Germany.
[62(a)]Department of Physics, Chinese University of Hong Kong, Shatin, N.T., Hong Kong;[(b)]Department of Physics, University of Hong Kong, Hong Kong;[(c)]Department of Physics and Institute for Advanced Study, Hong Kong University of Science and Technology, Clear Water Bay, Kowloon, Hong Kong; China.
[63]Department of Physics, National Tsing Hua University, Hsinchu; Taiwan.
[64]IJCLab, Université Paris-Saclay, CNRS/IN2P3, 91405, Orsay; France.
[65]Department of Physics, Indiana University, Bloomington IN; United States of America.
[66(a)]INFN Gruppo Collegato di Udine, Sezione di Trieste, Udine;[(b)]ICTP, Trieste;[(c)]Dipartimento Politecnico di Ingegneria e Architettura, Università di Udine, Udine; Italy.
[67(a)]INFN Sezione di Lecce;[(b)]Dipartimento di Matematica e Fisica, Università del Salento, Lecce; Italy.
[68(a)]INFN Sezione di Milano;[(b)]Dipartimento di Fisica, Università di Milano, Milano; Italy.
[69(a)]INFN Sezione di Napoli;[(b)]Dipartimento di Fisica, Università di Napoli, Napoli; Italy.
[70(a)]INFN Sezione di Pavia;[(b)]Dipartimento di Fisica, Università di Pavia, Pavia; Italy.
[71(a)]INFN Sezione di Pisa;[(b)]Dipartimento di Fisica E. Fermi, Università di Pisa, Pisa; Italy.

[72(a)]INFN Sezione di Roma;[(b)]Dipartimento di Fisica, Sapienza Università di Roma, Roma; Italy.
[73(a)]INFN Sezione di Roma Tor Vergata;[(b)]Dipartimento di Fisica, Università di Roma Tor Vergata, Roma; Italy.
[74(a)]INFN Sezione di Roma Tre;[(b)]Dipartimento di Matematica e Fisica, Università Roma Tre, Roma; Italy.
[75(a)]INFN-TIFPA;[(b)]Università degli Studi di Trento, Trento; Italy.
[76]Institut für Astro- und Teilchenphysik, Leopold-Franzens-Universität, Innsbruck; Austria.
[77]University of Iowa, Iowa City IA; United States of America.
[78]Department of Physics and Astronomy, Iowa State University, Ames IA; United States of America.
[79]Joint Institute for Nuclear Research, Dubna; Russia.
[80(a)]Departamento de Engenharia Elétrica, Universidade Federal de Juiz de Fora (UFJF), Juiz de Fora;[(b)]Universidade Federal do Rio De Janeiro COPPE/EE/IF, Rio de Janeiro;[(c)]Instituto de Física, Universidade de São Paulo, São Paulo;[(d)]Rio de Janeiro State University, Rio de Janeiro; Brazil.
[81]KEK, High Energy Accelerator Research Organization, Tsukuba; Japan.
[82]Graduate School of Science, Kobe University, Kobe; Japan.
[83(a)]AGH University of Science and Technology, Faculty of Physics and Applied Computer Science, Krakow;[(b)]Marian Smoluchowski Institute of Physics, Jagiellonian University, Krakow; Poland.
[84]Institute of Nuclear Physics Polish Academy of Sciences, Krakow; Poland.
[85]Faculty of Science, Kyoto University, Kyoto; Japan.
[86]Kyoto University of Education, Kyoto; Japan.
[87]Research Center for Advanced Particle Physics and Department of Physics, Kyushu University, Fukuoka ; Japan.
[88]Instituto de Física La Plata, Universidad Nacional de La Plata and CONICET, La Plata; Argentina.
[89]Physics Department, Lancaster University, Lancaster; United Kingdom.
[90]Oliver Lodge Laboratory, University of Liverpool, Liverpool; United Kingdom.
[91]Department of Experimental Particle Physics, Jožef Stefan Institute and Department of Physics, University of Ljubljana, Ljubljana; Slovenia.
[92]School of Physics and Astronomy, Queen Mary University of London, London; United Kingdom.
[93]Department of Physics, Royal Holloway University of London, Egham; United Kingdom.
[94]Department of Physics and Astronomy, University College London, London; United Kingdom.
[95]Louisiana Tech University, Ruston LA; United States of America.
[96]Fysiska institutionen, Lunds universitet, Lund; Sweden.
[97]Departamento de Física Teorica C-15 and CIAFF, Universidad Autónoma de Madrid, Madrid; Spain.
[98]Institut für Physik, Universität Mainz, Mainz; Germany.
[99]School of Physics and Astronomy, University of Manchester, Manchester; United Kingdom.
[100]CPPM, Aix-Marseille Université, CNRS/IN2P3, Marseille; France.
[101]Department of Physics, University of Massachusetts, Amherst MA; United States of America.
[102]Department of Physics, McGill University, Montreal QC; Canada.
[103]School of Physics, University of Melbourne, Victoria; Australia.
[104]Department of Physics, University of Michigan, Ann Arbor MI; United States of America.
[105]Department of Physics and Astronomy, Michigan State University, East Lansing MI; United States of America.
[106]B.I. Stepanov Institute of Physics, National Academy of Sciences of Belarus, Minsk; Belarus.
[107]Research Institute for Nuclear Problems of Byelorussian State University, Minsk; Belarus.
[108]Group of Particle Physics, University of Montreal, Montreal QC; Canada.
[109]P.N. Lebedev Physical Institute of the Russian Academy of Sciences, Moscow; Russia.
[110]National Research Nuclear University MEPhI, Moscow; Russia.

[111]D.V. Skobeltsyn Institute of Nuclear Physics, M.V. Lomonosov Moscow State University, Moscow; Russia.
[112]Fakultät für Physik, Ludwig-Maximilians-Universität München, München; Germany.
[113]Max-Planck-Institut für Physik (Werner-Heisenberg-Institut), München; Germany.
[114]Graduate School of Science and Kobayashi-Maskawa Institute, Nagoya University, Nagoya; Japan.
[115]Department of Physics and Astronomy, University of New Mexico, Albuquerque NM; United States of America.
[116]Institute for Mathematics, Astrophysics and Particle Physics, Radboud University/Nikhef, Nijmegen; Netherlands.
[117]Nikhef National Institute for Subatomic Physics and University of Amsterdam, Amsterdam; Netherlands.
[118]Department of Physics, Northern Illinois University, DeKalb IL; United States of America.
[119(a)]Budker Institute of Nuclear Physics and NSU, SB RAS, Novosibirsk;[(b)]Novosibirsk State University Novosibirsk; Russia.
[120]Institute for High Energy Physics of the National Research Centre Kurchatov Institute, Protvino; Russia.
[121]Institute for Theoretical and Experimental Physics named by A.I. Alikhanov of National Research Centre "Kurchatov Institute", Moscow; Russia.
[122(a)]New York University Abu Dhabi, Abu Dhabi;[(b)]United Arab Emirates University, Al Ain;[(c)]University of Sharjah, Sharjah; United Arab Emirates.
[123]Department of Physics, New York University, New York NY; United States of America.
[124]Ochanomizu University, Otsuka, Bunkyo-ku, Tokyo; Japan.
[125]Ohio State University, Columbus OH; United States of America.
[126]Homer L. Dodge Department of Physics and Astronomy, University of Oklahoma, Norman OK; United States of America.
[127]Department of Physics, Oklahoma State University, Stillwater OK; United States of America.
[128]Palacký University, Joint Laboratory of Optics, Olomouc; Czech Republic.
[129]Institute for Fundamental Science, University of Oregon, Eugene, OR; United States of America.
[130]Graduate School of Science, Osaka University, Osaka; Japan.
[131]Department of Physics, University of Oslo, Oslo; Norway.
[132]Department of Physics, Oxford University, Oxford; United Kingdom.
[133]LPNHE, Sorbonne Université, Université de Paris, CNRS/IN2P3, Paris; France.
[134]Department of Physics, University of Pennsylvania, Philadelphia PA; United States of America.
[135]Konstantinov Nuclear Physics Institute of National Research Centre "Kurchatov Institute", PNPI, St. Petersburg; Russia.
[136]Department of Physics and Astronomy, University of Pittsburgh, Pittsburgh PA; United States of America.
[137(a)]Laboratório de Instrumentação e Física Experimental de Partículas - LIP, Lisboa;[(b)]Departamento de Física, Faculdade de Ciências, Universidade de Lisboa, Lisboa;[(c)]Departamento de Física, Universidade de Coimbra, Coimbra;[(d)]Centro de Física Nuclear da Universidade de Lisboa, Lisboa;[(e)]Departamento de Física, Universidade do Minho, Braga;[(f)]Departamento de Física Teórica y del Cosmos, Universidad de Granada, Granada (Spain);[(g)]Instituto Superior Técnico, Universidade de Lisboa, Lisboa; Portugal.
[138]Institute of Physics of the Czech Academy of Sciences, Prague; Czech Republic.
[139]Czech Technical University in Prague, Prague; Czech Republic.
[140]Charles University, Faculty of Mathematics and Physics, Prague; Czech Republic.
[141]Particle Physics Department, Rutherford Appleton Laboratory, Didcot; United Kingdom.
[142]IRFU, CEA, Université Paris-Saclay, Gif-sur-Yvette; France.
[143]Santa Cruz Institute for Particle Physics, University of California Santa Cruz, Santa Cruz CA; United

States of America.
[144(a)]Departamento de Física, Pontificia Universidad Católica de Chile, Santiago;[(b)]Millennium Institute for Subatomic physics at high energy frontier (SAPHIR), Santiago;[(c)]Instituto de Investigación Multidisciplinario en Ciencia y Tecnología, y Departamento de Física, Universidad de La Serena;[(d)]Universidad Andres Bello, Department of Physics, Santiago;[(e)]Instituto de Alta Investigación, Universidad de Tarapacá, Arica;[(f)]Departamento de Física, Universidad Técnica Federico Santa María, Valparaíso; Chile.
[145]Department of Physics, University of Washington, Seattle WA; United States of America.
[146]Department of Physics and Astronomy, University of Sheffield, Sheffield; United Kingdom.
[147]Department of Physics, Shinshu University, Nagano; Japan.
[148]Department Physik, Universität Siegen, Siegen; Germany.
[149]Department of Physics, Simon Fraser University, Burnaby BC; Canada.
[150]SLAC National Accelerator Laboratory, Stanford CA; United States of America.
[151]Department of Physics, Royal Institute of Technology, Stockholm; Sweden.
[152]Departments of Physics and Astronomy, Stony Brook University, Stony Brook NY; United States of America.
[153]Department of Physics and Astronomy, University of Sussex, Brighton; United Kingdom.
[154]School of Physics, University of Sydney, Sydney; Australia.
[155]Institute of Physics, Academia Sinica, Taipei; Taiwan.
[156(a)]E. Andronikashvili Institute of Physics, Iv. Javakhishvili Tbilisi State University, Tbilisi;[(b)]High Energy Physics Institute, Tbilisi State University, Tbilisi; Georgia.
[157]Department of Physics, Technion, Israel Institute of Technology, Haifa; Israel.
[158]Raymond and Beverly Sackler School of Physics and Astronomy, Tel Aviv University, Tel Aviv; Israel.
[159]Department of Physics, Aristotle University of Thessaloniki, Thessaloniki; Greece.
[160]International Center for Elementary Particle Physics and Department of Physics, University of Tokyo, Tokyo; Japan.
[161]Department of Physics, Tokyo Institute of Technology, Tokyo; Japan.
[162]Tomsk State University, Tomsk; Russia.
[163]Department of Physics, University of Toronto, Toronto ON; Canada.
[164(a)]TRIUMF, Vancouver BC;[(b)]Department of Physics and Astronomy, York University, Toronto ON; Canada.
[165]Division of Physics and Tomonaga Center for the History of the Universe, Faculty of Pure and Applied Sciences, University of Tsukuba, Tsukuba; Japan.
[166]Department of Physics and Astronomy, Tufts University, Medford MA; United States of America.
[167]Department of Physics and Astronomy, University of California Irvine, Irvine CA; United States of America.
[168]Department of Physics and Astronomy, University of Uppsala, Uppsala; Sweden.
[169]Department of Physics, University of Illinois, Urbana IL; United States of America.
[170]Instituto de Física Corpuscular (IFIC), Centro Mixto Universidad de Valencia - CSIC, Valencia; Spain.
[171]Department of Physics, University of British Columbia, Vancouver BC; Canada.
[172]Department of Physics and Astronomy, University of Victoria, Victoria BC; Canada.
[173]Fakultät für Physik und Astronomie, Julius-Maximilians-Universität Würzburg, Würzburg; Germany.
[174]Department of Physics, University of Warwick, Coventry; United Kingdom.
[175]Waseda University, Tokyo; Japan.
[176]Department of Particle Physics and Astrophysics, Weizmann Institute of Science, Rehovot; Israel.
[177]Department of Physics, University of Wisconsin, Madison WI; United States of America.
[178]Fakultät für Mathematik und Naturwissenschaften, Fachgruppe Physik, Bergische Universität

Wuppertal, Wuppertal; Germany.
[179]Department of Physics, Yale University, New Haven CT; United States of America.
[a] Also at Borough of Manhattan Community College, City University of New York, New York NY; United States of America.
[b] Also at Center for High Energy Physics, Peking University; China.
[c] Also at Centro Studi e Ricerche Enrico Fermi; Italy.
[d] Also at CERN, Geneva; Switzerland.
[e] Also at Département de Physique Nucléaire et Corpusculaire, Université de Genève, Genève; Switzerland.
[f] Also at Departament de Fisica de la Universitat Autonoma de Barcelona, Barcelona; Spain.
[g] Also at Department of Financial and Management Engineering, University of the Aegean, Chios; Greece.
[h] Also at Department of Physics and Astronomy, Michigan State University, East Lansing MI; United States of America.
[i] Also at Department of Physics and Astronomy, University of Louisville, Louisville, KY; United States of America.
[j] Also at Department of Physics, Ben Gurion University of the Negev, Beer Sheva; Israel.
[k] Also at Department of Physics, California State University, East Bay; United States of America.
[l] Also at Department of Physics, California State University, Sacramento; United States of America.
[m] Also at Department of Physics, King's College London, London; United Kingdom.
[n] Also at Department of Physics, St. Petersburg State Polytechnical University, St. Petersburg; Russia.
[o] Also at Department of Physics, University of Fribourg, Fribourg; Switzerland.
[p] Also at Faculty of Physics, M.V. Lomonosov Moscow State University, Moscow; Russia.
[q] Also at Graduate School of Science, Osaka University, Osaka; Japan.
[r] Also at Hellenic Open University, Patras; Greece.
[s] Also at Institucio Catalana de Recerca i Estudis Avancats, ICREA, Barcelona; Spain.
[t] Also at Institut für Experimentalphysik, Universität Hamburg, Hamburg; Germany.
[u] Also at Institute of Particle Physics (IPP); Canada.
[v] Also at Institute of Theoretical Physics, Ilia State University, Tbilisi; Georgia.
[w] Also at Instituto de Fisica Teorica, IFT-UAM/CSIC, Madrid; Spain.
[x] Also at Joint Institute for Nuclear Research, Dubna; Russia.
[y] Also at Moscow Institute of Physics and Technology State University, Dolgoprudny; Russia.
[z] Also at National Research Nuclear University MEPhI, Moscow; Russia.
[aa] Also at Physics Department, An-Najah National University, Nablus; Palestine.
[ab] Also at Physikalisches Institut, Albert-Ludwigs-Universität Freiburg, Freiburg; Germany.
[ac] Also at The City College of New York, New York NY; United States of America.
[ad] Also at TRIUMF, Vancouver BC; Canada.
[ae] Also at Universita di Napoli Parthenope, Napoli; Italy.
[af] Also at University of Chinese Academy of Sciences (UCAS), Beijing; China.
[ag] Also at Yeditepe University, Physics Department, Istanbul; Turkey.
[*] Deceased